Structures of three MORN repeat proteins and a re-evaluation of the proposed lipid-binding properties of MORN repeats.

Sara Sajko*[,1], Irina Grishkovskaya*[,1], Julius Kostan*[,1], Melissa Graewert[2], Kim Setiawan[3], Linda Trübestein[1], Korbinian Niedermüller[3], Charlotte Gehin[4], Antonio Sponga[1], Martin Puchinger[1], Anne-Claude Gavin[4], Thomas Leonard[1], Dimitri Svergun[2], Terry K. Smith[5], Brooke Morriswood[3,$], Kristina Djinovic-Carugo[1,6,$]

* Equal contribution

$ Authors for correspondence:
Brooke Morriswood (brooke.morriswood@uni-wuerzburg.de)
Kristina Djinovic-Carugo (kristina.djinovic@univie.ac.at)

Affiliations:

[1]Department of Structural and Computational Biology, Max Perutz Labs, University of Vienna, Campus Vienna Biocenter 5, A-1030 Vienna, Austria

[2]European Molecular Biology Laboratory, Hamburg Unit, c/o DESY, Notkestrasse 85, 22607 Hamburg, Germany

[3]Department of Cell and Developmental Biology, Biocenter, University of Würzburg, 97074 Würzburg, Germany

[4]European Molecular Biology Laboratory, Meyerhofstraße 1, 69117 Heidelberg, Germany

[5]School of Biology, BSRC, University of St. Andrews, North Haugh, St. Andrews, Fife KY16 9ST, UK

[6]Department of Biochemistry, Faculty of Chemistry and Chemical Technology, University of Ljubljana, Večna pot 113, SI-1000 Ljubljana, Slovenia

Keywords: MORN repeat, MORN1, structure, phospholipids, *Trypanosoma,* Apicomplexa.

ABSTRACT

MORN (membrane occupation and recognition nexus) repeat proteins have a wide taxonomic distribution, being found in both prokaryotes and eukaryotes. Despite this ubiquity, they remain poorly characterised at both a structural and a functional level compared to other common repeat motifs such as leucine-rich repeats, armadillo repeats, WD40 repeats, and ankyrin repeats. In functional terms, they are often assumed to be lipid-binding modules that mediate membrane targeting, but direct evidence for this role is actually lacking. This putative activity was addressed by focusing on a protein composed solely of MORN repeats - *Trypanosoma brucei* MORN1. No evidence for binding to membranes or lipid vesicles by TbMORN1 either in vivo or in vitro could be obtained. TbMORN1 did interact with individual phospholipids but the potential physiological role of this interaction in trypanosomes remains unclear. High- and low-resolution structures of the MORN1 protein from *Trypanosoma brucei* and homologous proteins from the parasites *Toxoplasma gondii* and *Plasmodium falciparum* were obtained using a combination of macromolecular crystallography, small-angle X-ray scattering, and electron microscopy. The structures indicated that MORN repeats can mediate homotypic interactions, and can function as both dimerisation and oligomerisation devices.

INTRODUCTION

MORN (Membrane Occupation and Recognition Nexus) repeats were first discovered in 2000, following a screen for proteins present in the triad junctions of skeletal muscle (Takeshima et al., 2000). The junctophilins, the protein family identified in this screen, were observed to have 8 repeat motifs present in their N-terminal regions. The repeats were given the name MORN based on a proposed role in mediating plasma membrane association of the N-terminal domain of the junctophilins. The MORN repeats were initially classified as being 14 amino acids in length, with an approximate consensus sequence of YEGEWxNGKxHGYG (Takeshima et al., 2000). A bioinformatics analysis at the time indicated that assemblies of 8 consecutive MORN repeats were also present in a putative junctophilin orthologue in a nematode (*Caenorhabditis elegans*), a family of plant (*Arabidopsis thaliana*) lipid kinases, and a bacterial (*Cyanobacterium*) protein (Takeshima et al., 2000). Later genome-era bioinformatics has shown that MORN repeat proteins are in fact found ubiquitously, being present in both eukaryotes and prokaryotes (El-Gebali et al., 2019).

The number of MORN repeat proteins in any given protein can vary greatly, from two to over 20, and they are found in combination with a wide range of other domains and protein repeat motifs. Most published work now favours a 23-amino acid length for a single MORN repeat, with the highly-conserved GxG motif at positions 12-14. A 14-amino acid length is still favoured by some groups, however (Habicht et al., 2015). Notable mammalian MORN repeat proteins besides the junctophilins include ALS2/alsin, at least two radial spoke proteins (RSPH10B, RSPH1/meichroacidin), the histone methyltransferase SETD7, and retinophilin/MORN4 (Tsuchida et al., 1998, Wilson et al., 2002, Otomo et al., 2003, Mecklenburg, 2007).

MORN repeats are generally assumed to be lipid-binding modules, but direct evidence for this function is actually lacking. In junctophilins, there is good evidence that the N-terminal region containing the MORN repeats mediates plasma membrane targeting (Takeshima et al., 2000, Nakada et al., 2018, Rossi et al., 2019). It has not been demonstrated whether the MORN repeats or the other sequences in the N-terminal region are responsible for this however, or if this targeting is due to protein-lipid or protein-protein interactions.

Similarly, although there is good evidence that the N-terminal region (amino acids 1-452) of junctophilin-2 can directly bind lipids, it has not specifically been shown that the MORN repeats are responsible. Binding could potentially be mediated by other nearby sequences, especially the run of over 100 amino acids that occurs between repeats 6 and 7 (Bennett et al., 2013). Work on the family of plant phosphatidylinositol(4)phosphate 5-kinases (PIPKs) that contain MORN repeats has led to suggestions that the repeats might regulate the activity of the kinase domain, bind to phospholipids, or mediate protein-protein interactions (Ma et al., 2006, Im et al., 2007, Camacho et al., 2009). It therefore remains unclear what role(s) this ubiquitous class of repeat motifs actually have (Mikami et al., 2010).

Coupled to this lack of unambiguous functional data is a lack of high-resolution structural information, exemplified by the ongoing lack of consensus as to whether a single repeat is 14 or 23 amino acids. This contrasts sharply with the considerable amount of information available on other classes of protein repeat motifs such as ankyrin repeats, leucine-rich

100 repeats, or WD40 repeats (Andrade et al., 2001, Kajava, 2012). Until very recently, the
101 structure of the SETD7 histone methyltransferase was the sole representative of the MORN
102 repeat protein family in the protein data bank (PDB) (Jacobs et al., 2002, Wilson et al., 2002,
103 Xiao et al., 2003). Even here, the structure of the N-terminal domain containing the repeats is
104 incomplete, and the level of sequence similarity of the repeats to those of junctophilins and
105 other family members makes assignment difficult. Each repeat appears to form a β-hairpin
106 with an acidic surface, but it remains unclear if this is a general property of MORN repeats.
107 The SETD7 structure has not been analysed in this context, with more focus applied to its
108 catalytic methyltransferase domain. In particular, a structure-based definition of the repeat
109 class itself is currently lacking.
110
111 To address this, and additionally to tackle the question of putative lipid binding, it would
112 obviously be advantageous to utilise a protein that is composed solely of MORN repeats. In
113 this way, the contribution of other sequences or domains could be discounted. The MORN1
114 protein from the early-branching eukaryote *Trypanosoma brucei* is an ideal candidate in this
115 regard, and has the advantage of also being well-characterised at a cell biology level
116 (Morriswood et al., 2009, Esson et al., 2012, Morriswood et al., 2013, Morriswood & Schmidt,
117 2015).
118
119 TbMORN1 consists of 15 consecutive 23-amino acid MORN repeats, with barely any
120 intervening sequence whatsoever (Fig. 1A). In *T. brucei*, TbMORN1 is localised to an ~2 μm
121 long cytoskeleton-associated structure (the hook complex) that is found just below the inner
122 leaflet of the plasma membrane. The hook complex encircles the neck of a small invagination
123 of the plasma membrane that contains the root of the cell's single flagellum (Lacomble et al.,
124 2009). This invagination, termed the flagellar pocket, is the sole site of endo- and exocytosis
125 in trypanosome cells and is thought to be analogous to the ciliary pocket that is found at the
126 base of some mammalian primary cilia (Grunfelder et al., 2003, Engstler et al., 2004, Molla-
127 Herman et al., 2010).
128
129 Previous work on TbMORN1 demonstrated by fluorescence recovery after photobleaching
130 (FRAP) that it is a stable component of the hook complex, and a list of its binding partners and
131 near neighbours has been obtained using proximity-dependent biotin identification (BioID)
132 (Esson et al., 2012, Morriswood et al., 2013). In functional terms, depletion of TbMORN1 by
133 RNAi in the mammalian-infective form of the parasite resulted in a lethal phenotype
134 (Morriswood et al., 2009). Functional analysis indicated that the protein might be involved in
135 endocytosis, as well as regulating the flow of macromolecular cargo through the neck of the
136 flagellar pocket (Morriswood & Schmidt, 2015).
137
138 In this study, a detailed biochemical, structural, and functional analysis of the TbMORN1
139 protein was carried out. A truncated form missing the first MORN repeat that was best suited
140 for in vitro work was found not to bind to phospholipid vesicles under any conditions, but was
141 able to associate with individual lipid molecules. In addition, high-resolution crystal structures
142 of a truncated form of the TbMORN1 protein and its homologues from the parasites
143 *Toxoplasma gondii* (TgMORN1) and *Plasmodium falciparum* (PfMORN1) enabled a first
144 structure-based definition of the MORN repeat itself, and provided confirmation that MORN

145 repeats can mediate homotypic interactions - a function that may unify previous observations
146 relating to MORN repeats.
147
148

149 RESULTS

150

151 TbMORN1 forms tail-to-tail dimers via its C-terminus

152

153 TbMORN1 is composed of 15 consecutive 23-amino acid MORN repeats, with a 5-amino acid
154 extension after the 6th repeat (Fig. 1A). An alignment of the repeats in TbMORN1 revealed
155 several highly conserved glycine residues, with a rough consensus of
156 $YxGEWx_2Gx_3GxGx_3Yx_2Gx_2$ (Fig. 1A, sequence logo). Bioinformatic analysis of TbMORN1
157 predicted an all-β secondary structure, with each repeat expected to form a β-hairpin (strand-
158 loop-strand) pattern (Fig. 1A).
159
160 As the full-length TbMORN1 protein displayed low solubility and a propensity for aggregation,
161 limited proteolysis assays were carried out to determine which TbMORN1 constructs were
162 amenable for biochemical and structural studies (Fig. S1A, B). Comparison of the proteolytic
163 fragments obtained at different dilutions suggested progressive digestion occurring from the
164 N-terminus (Fig. S1B, compare K1 and K2, T1/T2/T3). The C-terminus of the molecule
165 (repeats 13-15) seemed to be fairly stable, with no proteolytic digestion observed at this end.
166 In addition, the pattern of fragments generally suggested that the assignment of repeat
167 boundaries based on bioinformatic analysis was accurate.
168
169 Consequently, a panel of different truncations was cloned according to the MORN repeat
170 boundaries predicted by the alignment (Fig. 1A). These truncations were named according to
171 the number of repeats they contained - for example, TbMORN1(1-15) denotes full-length
172 protein. These truncations were expressed in bacteria and purified using a two-step protocol
173 combining affinity purification and size exclusion chromatography (Fig. S1C).
174
175 The oligomeric state and polydispersity of the purified proteins were investigated using size
176 exclusion chromatography coupled to multi-angle light scattering (SEC-MALS). SEC-MALS
177 analysis of TbMORN1(1-15) elution profiles suggested the formation of either aggregates or
178 higher-order assemblies (Fig. 1B). The yields of TbMORN1(1-15) were always very low,
179 making this construct not generally suitable for in vitro assays. By contrast, TbMORN1(2-15)
180 displayed a well-defined monodisperse peak in SEC-MALS, with a molecular weight
181 corresponding to a dimer (Fig. 1B). This strongly suggested that the first MORN repeat
182 mediated oligomerisation. Further successive truncations from the N-terminus (TbMORN1(7-
183 15) and TbMORN1(10-15)) also eluted as monodisperse dimers, suggesting that dimerisation
184 of TbMORN1 is mediated by the C-terminus (Fig. S1D). Consistent with this conclusion,
185 removal of the last MORN repeat in the construct TbMORN1(1-14) resulted in the elution of a
186 mixture of monomers, dimers, and higher-order structures (Fig. 1B). This demonstrated that
187 the C-terminal repeats play an important role in dimer stabilisation.
188

189 Circular dichroism (CD) measurements taken of TbMORN1(1-15), TbMORN1(2-15), and
190 TbMORN1(7-15) indicated β-strand character in all cases, with >30% antiparallel β-strand
191 content for each construct (Fig. S1E), and in good agreement with a priori bioinformatic
192 predictions (Fig. 1A). Thermostability measurements of TbMORN1(1-15), TbMORN1(2-15)
193 and TbMORN1(7-15) using CD returned values in °C of 45.6 +/- 0.1, 43.5+/-0.1, and 42.2+/-
194 0.1 respectively, showing an expected incremental contribution of MORN repeats to the
195 overall stability of the protein.
196
197 To map which residues were likely mediating dimerisation, cross-linking mass spectrometry
198 (XL-MS) was used to analyse TbMORN1(1-15). Two different chemical cross-linkers were
199 used: EDC (1-ethyl-3-(3-dimethylaminopropyl)carbodiimide), which has a zero-length spacer
200 arm and forms bonds between carboxyl groups and primary amines, and BS^3
201 (bis(sulphosuccinimidyl)suberate), which has an 11.4 Å spacer arm and cross-links primary
202 amines. For both chemicals, most cross-links were observed to form between repeats 13, 14,
203 and 15, especially via repeat 14 (Table S1). These data were consistent with those obtained
204 by SEC-MALS (Fig. 1B, Fig. S1D), suggesting that TbMORN1 molecules in solution form tail-
205 to-tail dimers via their C-termini. It remained unclear whether the polypeptide chains in dimers
206 were in a parallel or antiparallel orientation, however.
207

208 TbMORN1 can bind lipid side chains but not phospholipid liposomes

209
210 As a first test of the hypothesis that MORN repeats can directly interact with phospholipids,
211 protein-lipid overlay assays were carried out using PIP strips. Purified TbMORN1(1-15) was
212 found to interact with a number of different phosphoinositide species on the PIP strips,
213 principally PI(3)P, PI(4)P, and PI(5)P, but also PI(3,4)P_2, PI(3,5)P_2, PI(4,5)P_2, and
214 phosphatidic acid (PA) (Fig. 2A). This same trend, with a stronger interaction observed with
215 monophosphate PIPs than diphosphate PIPs, has also been seen in protein-lipid overlay
216 assays using purified junctophilin-2. This might be due to a lower solubility of the
217 monophosphate PIPs, however (Bennett et al., 2013). As a positive control, the PIP strips
218 were incubated with the pleckstrin homology (PH) domain of phospholipase C delta (PLCδ).
219 Strong binding was observed to PI(4,5)P_2 only, as expected (Fig. 2B).
220
221 Of these candidates, the most intriguing was PI(4,5)P_2. It is a known endocytic effector, is
222 enriched in the flagellar pocket membrane of trypanosomes, and depletion of TbMORN1 by
223 RNAi resulted in a phenotype suggestive of an endocytosis defect (Demmel et al., 2014,
224 Morriswood & Schmidt, 2015). Furthermore, a PI(4)P 5-kinase, TbPIPKA, has been shown to
225 have a strongly overlapping distribution with TbMORN1 in vivo (Demmel et al., 2014).
226
227 To confirm that TbMORN1 could interact with PI(4,5)P_2, fluorescence anisotropy was used as
228 a second independent and quantitative approach. In this method, the tumbling of a
229 fluorescently-labelled lipid in solution is reduced upon binding to a larger protein molecule,
230 and the change in the polarisation of the emitted light is measured. TbMORN1(2-15) showed
231 excellent binding to BODIPY TMR-labelled PI(4,5)P_2, with a K_d of approximately 7.5 +/- 4.1
232 μM (Fig. 2C). To narrow down the PI(4,5)P_2 binding site(s) on TbMORN1, truncation
233 constructs were again used. Both TbMORN1(7-15) and TbMORN1(10-15) showed strong

binding to PI(4,5)P_2, with K_d values of 7.7 +/- 2.6 and 1.0 +/- 0.1 μM respectively, indicating that the interaction was occurring in the C-terminal portion of TbMORN1 (Fig. 2C).

Curiously, while the anisotropy signal for the TbMORN1(7-15) was lower than that of TbMORN1(2-15), the highest anisotropy signal of all was obtained for the smallest construct, TbMORN1(10-15) (Fig. 2C). This was surprising, as one would usually expect the largest construct containing the binding site to give the highest anisotropy signal - the larger protein means less tumbling of the fluorophore-conjugated lipid bound to the protein, resulting in greater polarisation of the emitted light and a higher anisotropy signal.

As an additional test, native gel electrophoresis assays were carried out. In these assays, interaction between a protein and a fluorescently-labelled lipid is detected by co-migration of the lipid with the protein. Both TbMORN1(2-15) and TbMORN1(10-15) produced a band shift of BODIPY TMR-labelled PI(4,5)P_2. In contrast to the PIP strip data, no interaction was seen for BODIPY TMR-labelled PI(4)P (Fig. S2A, B). This too was surprising as this lipid had given the strongest signal in the overlay assays (Fig. 2A).

Of note, all of the assays to this point - overlay assays, fluorescence anisotropy, native gel electrophoresis - had looked at the binding of TbMORN1 to isolated lipids below their critical micelle concentration. This situation is somewhat artificial, and so for better physiological relevance the binding of TbMORN1 to phospholipid membranes was investigated using liposome pelleting assays.

The assays were carried out with liposomes of roughly 100 nm diameter, and containing 0-20% PI(4,5)P_2. Varying the amount of PI(4,5)P_2 from 0-20% did not result in any increase in the amount of TbMORN1(2-15) present in the pellet (P) fraction, while strong concentration-dependent co-sedimentation was observed with the positive control Doc2B (Fig. 2D). Quantification of the amount of protein in the pellet relative to the 0% PI(4,5)P_2 condition showed that the amount of TbMORN1(2-15) was within roughly 10% of the control condition at all times (Fig. 2E).

Additional assays were carried out using liposomes of differing diameters (100 and 400 nm) in order to vary curvature, and different cholesterol contents (0 and 40%) in order to concentrate PI(4,5)P_2 into microdomains. Neither approach produced an increase in TbMORN1(2-15) association (Fig. S3A). Therefore, TbMORN1 appeared to bind to isolated molecules of PI(4,5)P_2 but not to liposomes.

The TbMORN1 primary structure was next examined for putative PI(4,5)P_2-binding sites, based on binding sequence motifs derived from known PI(4,5)P_2-binding sites in the PH, PLC-δ1, CALM-N, ENTH, FERM, PTB, and I3P-RBC domains (Franzot et al., 2005). Two candidate sites were identified in the C-terminus of TbMORN1: one in repeat 13, and one in repeat 14. The location of these sites was in agreement with the fluorescence anisotropy assays, which had suggested binding to the C-terminal region of TbMORN1 (Fig. 2C).

278 Site-directed mutagenesis was carried out on these sites in the TbMORN1(2-15)-encoding
279 construct either singly or in combination. These single or double mutants of TbMORN1(2-15)
280 were then expressed, purified, and biophysically characterised. Thermostability of the purified
281 proteins was assessed using differential scanning fluorimetry (DSF), and indicated that
282 mutagenesis of the site in repeat 14 and the double mutant both resulted in slightly decreased
283 stability (i.e. a lower T_m) than TbMORN1(2-15) (Table S2). CD analyses indicated that the
284 constructs retained an all-β secondary structure (Fig. S3C).
285
286 SEC-MALS analysis showed that while mutagenesis of the site in repeat 13 did not alter the
287 dimeric state of TbMORN1(2-15), mutagenesis of the site in repeat 14 resulted in a mixture of
288 monomers and dimers, while mutagenesis of both sites resulted in a monomeric protein (Fig.
289 S3B). This matched the conclusion from the SEC-MALS studies that the dimerisation site also
290 resides in the C-terminal segment (Fig. 1B, Fig. S1D).
291
292 Unexpectedly, all three TbMORN1(2-15) mutant constructs showed unimpaired binding to
293 PI(4,5)P_2 in fluorescence anisotropy assays (Fig. S3D). Furthermore, all three mutants
294 actually had stronger binding affinities for PI(4,5)P_2 than the wild-type TbMORN1(2-15)
295 construct, with K_d values of ~ 1 μM. Although these results might indicate that TbMORN1(2-
296 15) utilises a non-canonical PI(4,5)P_2 binding site, a more parsimonious explanation was that
297 the data reflected a nonspecific interaction. Subsequent experiments addressed this question
298 and favoured this latter interpretation.
299
300 All fluorescence anisotropy assays had been carried out using labelled PI(4,5)P_2 with 16-
301 carbon aliphatic chains. When the assays were repeated using a version of PI(4,5)P_2 with 6-
302 carbon aliphatic chains, no binding was seen (Fig. S4A). A range of lipids (PI, PI(4)P,
303 PI(3,4)P_2, PI(3,5)P_2) with 6-carbon aliphatic chains were then tested for interaction with
304 TbMORN1(2-15) by fluorescence anisotropy, and no binding to any was seen (Fig. S4A).
305
306 Furthermore, it was observed that TbMORN1(2-15) could also bind to PI(3,4,5)P_3 - which had
307 not given a positive result in the overlay assays (Fig. 2A) - if the lipid had 16-carbon aliphatic
308 chains (Fig. S4B). This interaction with 16-carbon PI(4,5)P_2 and PI(3,4,5)P_3 was seen using
309 BODIPY-fluorescein-labelled lipids instead of BODIPY TMR-labelled ones (Fig. S4B). The
310 binding of TbMORN1(2-15) to 16-carbon versions of either PI(4,5)P_2 or PI(3,4,5)P_3 was
311 comparable to that seen for positive controls (Fig. S4C).
312
313 These results strongly suggested that the observed binding of TbMORN1(2-15) to PI(4,5)P_2
314 by both fluorescence anisotropy and native gel electrophoresis was in fact due to interaction
315 with the 16-carbon aliphatic chains and not with the lipid headgroup. An inability to interact
316 with the lipid headgroup was also consistent with the observed lack of interaction of
317 TbMORN1(2-15) with phospholipid membranes in the liposome pelleting assays (Fig. 2D,E,
318 Fig. S3A).
319
320 In conclusion, while protein overlay assays indicated that TbMORN1(1-15) and TbMORN1(2-
321 15) could interact with phospholipid species, subsequent fluorescence anisotropy and native
322 gel electrophoresis assays strongly suggested that this interaction was actually with the

323 aliphatic chains. No evidence for TbMORN1(2-15) binding to phospholipid liposomes in vitro
324 was obtained.
325
326

327 TbMORN1 co-purifies with PE but does not bind to lipid vesicles in vitro

328
329 A caveat to the previous conclusion was that the purified recombinant TbMORN1 was
330 obtained via mechanical lysis of bacterial cells in the absence of detergent (see Materials and
331 Methods). It was therefore possible that TbMORN1 was associating with bacterial lipids that
332 might be occupying the binding sites.
333
334 To test this, purified recombinant TbMORN1(1-15) and TbMORN1(10-15) were treated
335 according to a de-lipidation protocol, and the resulting supernatants were analysed by mass
336 spectrometry. Interestingly, large amounts of phosphatidylethanolamine (PE) were found to
337 have been bound to TbMORN1(1-15) (Fig. 3A). The co-purifying PE displayed a remarkably
338 narrow window of molecular moieties differing in the length of the aliphatic chain (30:0, 33:1,
339 34:1, 36:2). No significant PE presence was detected in supernatants obtained following de-
340 lipidation of TbMORN1(10-15) (Fig 3B). Given that TbMORN1(10-15) showed robust binding
341 to the 16-carbon chain PI(4,5)P_2 (Fig. 2C), this suggested that PE was not occluding the
342 binding site.
343
344 To remove co-purifying lipids, recombinant TbMORN1(1-15) was purified using hydrophobic
345 interaction chromatography - in this regime, almost no lipids were detected in the elutions.
346 Triton X-100 treatment was also found to efficiently remove bound lipids.
347
348 Co-purification of PE with TbMORN1(1-15) is not evidence of physiological interaction, as PE
349 is highly abundant in bacteria and carries a net neutral charge (Cronan, 2003). As such, PE
350 might simply have associated with the recombinant protein following lysis of the bacteria prior
351 to purification. To investigate this, mass spectrometry analysis of whole-cell lipids from
352 bacteria expressing recombinant TbMORN1(1-15) or TbMORN1(10-15) was carried out.
353 Curiously, bacterial cells expressing TbMORN1(1-15) showed elevated levels of PE (Fig. 3C).
354 This effect was not seen in bacterial cells expressing TbMORN1(10-15), which had
355 approximately normal levels of PE (Fig. 3D).
356
357 In summary, TbMORN1(1-15) but not TbMORN1(10-15) was found to have co-purifying PE,
358 and bacterial cells expressing TbMORN1(1-15) appeared to have elevated levels of PE. This
359 suggested that PE might be a plausible candidate for a physiological interaction partner of
360 TbMORN1, and that it requires MORN repeats 1-9 for binding.
361
362 To test the possibility of PE binding, and also to check whether the presence of co-purifying
363 PE was affecting possible PI(4,5)P_2 binding, pelleting assays using sucrose-loaded vesicles
364 (SLVs) were carried out. Sucrose loading increases the vesicle mass and enables much lower
365 centrifugation forces to be used for pelleting, thereby reducing the risk of false positives due
366 to protein aggregates pelleting independently of vesicle association. Three types of SLVs were
367 used: PE-enriched SLVs, PI(4,5)P_2-enriched SLVs, and SLVs reconstituted from purified

368 trypanosome whole-cell lipids. These were incubated with TbMORN1(2-15) purified either in
369 the absence or presence of Triton X-100, i.e. either without or with co-purifying bacterial lipids.
370
371 As expected, in the absence of Triton X-100 treatment to remove bound lipids, purified
372 recombinant TbMORN1(2-15) did not co-sediment with any of the liposome preparations (Fig.
373 4A). Even after purified recombinant TbMORN1(2-15) was treated with Triton X-100 to remove
374 bound lipids, no association with the liposomes was seen (Fig 4B), suggesting that TbMORN1
375 binds only to isolated PEs. As a positive control for pelleting, the PH domain of PLCγ was
376 used. This showed robust and specific pelleting in presence of PI(4,5)P_2-containing
377 liposomes, but in no other conditions (Fig4C, arrow). At this point, the candidate approach to
378 TbMORN1 lipid binding was discontinued.
379
380 As an unbiased and high-throughput approach, TbMORN1 was next tested in a liposome
381 microarray assay (LiMA). LiMA enables sampling of a wide range of liposome compositions
382 and curvatures in a single experiment. Readout is via the detection of two fluorophores - one
383 on a carrier lipid in the liposomes, and one on the protein of interest (Saliba et al., 2014, Saliba
384 et al., 2016). Colocalised signals are regarded as positive hits. For these assays EGFP-
385 TbMORN1(2-15) was expressed and purified. The EGFP-TbMORN1(2-15) protein showed no
386 significant preference or affinity for liposomes across the whole range of conditions tested
387 (Fig. 4D,E). Each lipid was tested at three different concentrations. Of note, no binding was
388 seen to either phosphoinositide lipids or PE. In contrast, the PH domain of PLCδ, which was
389 again used as a positive control, showed a strong and specific binding to PI(4,5)P_2 liposomes
390 and, to a lesser extent, SM-enriched ones (Fig. 4F, note difference in y-axis scale compared
391 to panels D, E).
392
393 In summary, purified recombinant TbMORN1(2-15) showed no binding to liposomes under
394 any conditions assayed (Fig. 2D,E, Fig. S3A, Fig. 4A-F). TbMORN1(2-15) showed robust
395 binding to PI(4,5)P_2 and PI(3,4,5)P_3 molecules in fluorescence anisotropy assays, but only
396 when lipids with 16-carbon aliphatic chains were used (Fig. 2C, Fig. S3D, Fig. S4A, B).
397 TbMORN1(1-15) was found to co-purify with PE. Taken together, these data suggest that
398 TbMORN1 requires large aliphatic hydrophobic chains of the lipid for binding, which would
399 explain the negative results in the liposome-based assays.
400
401
402 ## TbMORN1 does not associate with membranes in vivo
403
404 At this point, the only remaining positive indicators of an interaction of TbMORN1 with lipid
405 came from the PIP strips (Fig. 2A), and the bacterial mass spectrometry data (Fig. 3A, C). The
406 latter data showed that TbMORN1(1-15) but not TbMORN1(10-15) co-purified with PE, and
407 that bacteria expressing TbMORN1(1-15) had elevated PE levels. These elevated cellular PE
408 levels might represent upregulated synthesis to compensate for something binding and
409 sequestering the lipid (Fig. 3A, C).
410
411 Notably, all these positive pieces of evidence related to TbMORN1(1-15), which was
412 polydisperse in vitro and formed large oligomers (Fig. 1B). The membrane-binding activity of

413 these polydisperse oligomers was not possible to test in vitro, as the purification yields of
414 TbMORN1(1-15) were always low. As an alternative, the possible membrane association of
415 full-length TbMORN1 protein was examined in vivo.
416
417 For these experiments, cell lines of bloodstream form *T. brucei* were generated that inducibly
418 expressed full-length TbMORN1(1-15) with an N-terminal Ty1 epitope tag. Induction of Ty1-
419 TbMORN1(1-15) overexpression using tetracycline (Tet) produced a strong growth defect in
420 all three *T. brucei* clones tested (Fig. 5A). A rise in the number of so-called "BigEye" cells with
421 grossly enlarged flagellar pockets was seen in the same 96-hour time window (Fig. 5B). Such
422 a phenotype had previously been seen following depletion of TbMORN1 (Morriswood &
423 Schmidt, 2015). The BigEye phenotype is thought to result from perturbations to membrane
424 traffic, especially endocytosis (Allen et al., 2003).
425
426 Immunoblotting with anti-TbMORN1 antibodies confirmed tight and inducible expression of
427 the ectopic Ty1-TbMORN1 protein (Fig. 5C, left panel). The presence of the Ty1 epitope tag
428 in the ectopic protein was confirmed by blotting with anti-Ty1 antibodies (Fig. 5C, right panel).
429 Quantification of the immunoblots indicated only around 2-fold overexpression of Ty1-
430 TbMORN1 relative to endogenous TbMORN1 protein (Fig. 5D).
431
432 These strong negative effects were unexpected, and could potentially be due either to the
433 overexpression of the MORN1 protein, or to the presence of the Ty1 tag. To check the first
434 point, cells that inducibly overexpressed untagged TbMORN1 from an ectopic locus were
435 generated. Induction of ectopic gene expression by addition of tetracycline resulted in
436 overexpression of TbMORN1 in immunoblots (Fig. S5A). Quantification of overexpression
437 indicated that approximately 7 times more TbMORN1 protein was present in induced cells
438 relative to controls (Fig. S5B). Cells overexpressing untagged TbMORN1 exhibited a very
439 strong growth defect, stronger than that seen for overexpression of Ty1-TbMORN1 (Fig. S5C).
440 Therefore, TbMORN1 protein levels alone were capable of producing a negative effect on
441 growth in the absence of the Ty1 tag.
442
443 It was however not possible to obtain cells that solely expressed Ty1-TbMORN1 by
444 endogenous replacement, despite repeated attempts. This indicated that Ty1-TbMORN1
445 cannot functionally compensate for the loss of the untagged endogenous protein.
446
447 Immunofluorescence microscopy analysis of whole cells labelled with anti-TbMORN1
448 antibodies showed that Ty1-TbMORN1-overexpressing cells displayed a whole-cell labelling
449 pattern, unlike controls (Fig. 5E, left panels). Although no sign of protein aggregation was
450 observed, this suggested that perhaps the Ty1-TbMORN1 protein might not localise correctly.
451 Immunofluorescence microscopy analysis of detergent-extracted cytoskeleton fractions
452 labelled using anti-Ty1 antibodies confirmed that Ty1-TbMORN1 was able to target correctly;
453 as expected, no labelling was seen in controls. (Fig. 5E, right panels).
454
455 To confirm the immunofluorescence microscopy observations, one-step biochemical
456 fractionation using the non-ionic detergent IGEPAL was used. The detergent-soluble
457 cytoplasmic fraction (SN) was separated from the detergent-insoluble cytoskeleton pellet (P)
458 by centrifugation (Fig. 5F). In control cells, endogenous TbMORN1 associated almost entirely

459 with the cytoskeletal (P) fraction (Fig. 5G). Blotting fractions from Ty1-TbMORN1-
460 overexpressing cells with anti-TbMORN1 antibodies showed that the overexpressed Ty1-
461 TbMORN1 was mostly extracted by the detergent (Fig. 5G, arrow 1). However, a small amount
462 did associate with the cytoskeleton (P) fraction. This association was accompanied by a
463 displacement of some of the endogenous protein into the cytoplasmic SN fraction (Fig. 5G,
464 arrows 2).
465
466 Quantification of fractionation data from multiple experiments supported the qualitative
467 analysis (Fig. 5H). Summing the signals of Ty1-TbMORN1 and TbMORN1 present in the
468 cytoskeletal fraction in overexpressing cells indicated that the total amount of cytoskeleton-
469 associated protein was approximately the same as in controls (Fig 5H, grey bar). This
470 suggested that there are a finite number of Ty1-TbMORN1 molecules that can associate with
471 the cytoskeleton. As the total amount of endogenous and ectopic TbMORN1 associated with
472 the cytoskeleton is roughly the same in both overexpressing cells and controls, this suggested
473 also that the dominant negative cellular effects are primarily due to the endogenous and
474 ectopic TbMORN1 in the cytoplasmic fraction.
475
476 To determine if the cytoplasmic fraction of endogenous and ectopic TbMORN1 in the
477 overexpressing cells was membrane-associated or cytosolic, two-step fractionations were
478 carried out. These assays involved a first extraction with digitonin, then a second extraction
479 with IGEPAL. Digitonin has an affinity for cholesterol and other lipids enriched in the plasma
480 membrane, so at the right concentration it should enable the extraction of cytosol while leaving
481 organelles relatively intact (Adam et al., 1990).
482
483 To optimise the conditions for digitonin extraction, a cell line expressing cytosolic GFP as a
484 marker was used (Batram et al., 2014). These cells were extracted with varying concentrations
485 of digitonin, using 1% IGEPAL as a positive control for full extraction, and fractions were
486 separated by centrifugation (Fig. S6A). The supernatant and pellet fractions were
487 immunoblotted with antibodies against GFP and the ER lumenal chaperone BiP (Fig. S6B),
488 and the results quantified (Fig. S6C). At 40 µg/ml, good extraction of GFP was obtained with
489 only minimal extraction of BiP (Fig. S6B, arrow 1). A time course of extraction using 40 µg/ml
490 digitonin was then carried out (Fig. S6D). Increasing the incubation time over a range of 15-
491 30 min did not appear to increase the amount of GFP extraction (Fig. S6E,F). As a result, a
492 25 min incubation time was used in the subsequent experiments.
493
494 A two-step extraction using first digitonin and then IGEPAL was then carried out (Fig. 6A). The
495 digitonin supernatant (SN1) was enriched for cytosol, while the membrane/organelle fraction
496 present in the pellet (P1) was subsequently extracted using IGEPAL and partitioned into SN2.
497 Cells expressing cytosolic GFP were spiked in alongside Ty1-TbMORN1-overexpressing cells
498 in order to use GFP as a cytosolic marker.
499
500 Analysing equal fractions by immunoblotting showed that the Ty1-TbMORN1 and TbMORN1
501 proteins not associated with the cytoskeleton were predominantly cytosolic (Fig. 6B). The GFP
502 cytosolic marker was almost wholly extracted by the digitonin, and accompanied by the
503 majority of the cytoplasmic Ty1-TbMORN1 and TbMORN1 (Fig. 6B, arrows 1).
504

505 The Ty1-TbMORN1 and TbMORN1 that were not extracted by digitonin and therefore present
506 in P1 were not strongly extracted by IGEPAL and barely present in the second supernatant
507 (SN2), while the ER marker BiP was (Fig. 6B, arrows 2). Almost all the Ty1-TbMORN1 and
508 TbMORN1 present in P1 partitioned into the second pellet, P2. Quantification of multiple
509 independent experiments using the three separate clones produced results consistent with
510 the exemplary blot shown (Fig. 6C,D). The presence of the overexpressed Ty1-TbMORN1
511 and displaced endogenous TbMORN1 in the digitonin supernatant (SN1) indicated that they
512 are predominantly cytosolic. This suggested that TbMORN1 does not associate with
513 membranes in vivo.
514
515 In conclusion, the extensive studies conducted on TbMORN1 here provide no evidence that
516 its MORN repeats are able to associate with phospholipid membranes in vivo, or directly
517 interact with phospholipid vesicles in vitro. TbMORN1 was able to bind to individual lipid
518 molecules, notably PE. This interaction does not appear to be mediated by lipid headgroups
519 however, and it is very hard to imagine how it would occur under physiological conditions
520 unless TbMORN1 is a lipid carrier and not a membrane-binding protein.
521
522 If MORN repeats do not bind membranes, then this raises the question of what they really do,
523 and whether this other function might unify the various observations made about MORN
524 repeat proteins to date. ALS2 has been suggested to use its MORN repeats to form an
525 antiparallel dimer (Kunita et al., 2004), and the evidence obtained here showed that
526 TbMORN1 molecules also formed tail-to-tail dimers via their C-termini (Figs. 1, S1).
527 Mammalian PI(4)P 5-kinases are also dimers, implying that the MORN repeats found at the
528 N-termini of the family of plant PIPKs might function to mediate homotypic interactions (Rao
529 et al., 1998). To investigate how the MORN1 dimers were being formed, high-resolution
530 structural studies were used.
531
532
533 ## High-resolution crystal structures of three MORN repeat proteins
534
535 Crystallisation trials were initially performed with TbMORN1(2-15) and TbMORN1(7-15).
536 Diffraction data were obtained for TbMORN1(7-15) in two different crystal forms ($P2_1$ and C2),
537 but attempts to solve the phase problem using experimental phasing approaches (multiple
538 isomorphous replacement, multiple anomalous scattering exploiting selenium and sulphur
539 atom signals) and molecular replacement failed due to low reproducibility of crystals,
540 anisotropy of diffraction data, and absence of sufficient homology of TbMORN1 to other
541 MORN repeat-containing proteins of known structure. At that point, the only MORN repeat-
542 containing protein for which the crystal structure was solved was SETD7, a histone
543 methyltransferase. SETD7 is predicted to contain up to 6 MORN repeats at its N-terminus, but
544 they display low sequence homology to both the MORN repeats of TbMORN1 and the
545 consensus MORN repeat sequence obtained by Pfam. This prevented successful use of
546 molecular replacement as an approach.
547
548 As a new tactic, the MORN1 proteins from the apicomplexan parasites *Plasmodium falciparum*
549 (PfMORN1) and *Toxoplasma gondii* (TgMORN1) were targeted for structure determination.

550 Despite their evolutionary distance, they share high (57% and 54%, respectively) sequence
551 identity with TbMORN1 (Fig. S7A,B). CD measurements of purified recombinant protein
552 indicated that TgMORN1, TgMORN1(7-15), PfMORN1, PfMORN1(2-15) and PfMORN1(7-15)
553 all had an overall β-structure (Fig. S7C,D). This agrees with bioinformatic predictions and is
554 consistent with the data obtained for TbMORN1 (Fig. S1E).
555
556 Diffracting crystals of selenomethionine-labelled PfMORN1(7-15) were obtained and its
557 crystal structure was determined to 2.14 Å resolution using the single-wavelength anomalous
558 dispersion (SAD) method. The structures of TgMORN1(7-15) and both $P2_1$ and C2 crystal
559 forms of TbMORN1(7-15) were subsequently determined to 2.90, 2.35 and 2.53 Å resolution,
560 respectively, with the PfMORN1(7-15) structure used as a search model for the molecular
561 replacement (Fig. 7A-C). The structures of PfMORN1(7-15), TgMORN1(7-15), and both $P2_1$
562 and C2 forms of TbMORN1(7-15) were refined to an R_{work}/R_{free} of 23.0%/26.4%, 28.3%/32.2%,
563 23.2%/25.6% and 22.5%/28.2%, respectively (Table 1). TbMORN1(7-15) $P2_1$ (Fig. 7A), C2
564 (Fig. S8A) and TgMORN1(7-15) (Fig. 7B) crystallised with one dimer in the asymmetric unit,
565 while PfMORN1(7-15) (Fig. 7C) crystallised with one subunit in the asymmetric unit, and the
566 functional dimer was formed via crystallographic symmetry axis.
567
568 All MORN1(7-15) crystal structures show subunit interactions via the C-terminal regions to
569 form antiparallel tail-to-tail dimers, with variable inter-subunit angles and dimerisation
570 interfaces (Fig. 7A-C, Fig. S8A). The two subunits in the TbMORN1(7-15) C2 crystal form and
571 the TgMORN1(7-15) dimer make a rather straight assembly, while in the $P2_1$ form they display
572 a bend of about 30° (Fig. S8A), leading to a rod-shaped particle appearance. This dimer
573 architecture is consistent with the limited proteolysis data, which had indicated that the N-
574 terminal regions of the molecule are more susceptible (Fig. S1A,B). Interestingly, PfMORN1(7-
575 15) displays a V-shaped dimer with an inter-subunit angle of about 45°, and incorporates a
576 structural Zn^{2+} ion at the dimer interface (Fig. 7C). One crystal form of TgMORN1(7-15) also
577 adopts the same V-shape seen for PfMORN1(7-15) (Fig. S9B). Here too, a Zn^{2+} ion is found
578 at the dimer interface.
579
580 Superimposing the TbMORN1(7-15) $P2_1$ subunit with the structures of the TgMORN1(7-15)
581 and PfMORN1(7-15) subunits over 202 C_α atoms yielded rmsd values of 1.0 and 1.1 Å,
582 respectively, revealing high structural similarity between the three proteins. The common
583 structural feature of all three subunits is an elongated and twisted β-sheet. The curved shape
584 of each constituent MORN repeat forms a groove laterally delimited by a rim. An individual
585 MORN1(7-15) subunit is approximately 80 Å in length and displays a longitudinal groove of
586 about 16 Å in depth (Fig. 7A).
587
588 Comparison of a single TbMORN1(7-15) subunit with known three-dimensional structures was
589 carried out using the DALI server (Holm & Rosenstrom, 2010, Holm & Laakso, 2016). This
590 revealed closest similarity with the G-box domain at the C-terminus of the human CPAP
591 protein. CPAP is a centriolar protein essential for microtubule recruitment. The G-box
592 comprises a single elongated β-sheet with all residues being solvent-exposed, and is capable
593 of forming supramolecular assemblies [PDB entry 4LZF, (Hatzopoulos et al., 2013)]. Despite
594 the low sequence identity (10%) between TbMORN1(7-15) and CPAP, the Z-score calculated

595 by DALI suggested a significant similarity between the two structures (rmsd over 155
596 superimposed C_α atoms = 3.9 Å, Z-score = 12).
597

598 A structure-based redefinition of the MORN repeat

599
600 The crystal structures confirmed that each 23-amino acid MORN repeat is composed of a β-
601 hairpin followed by a 6-residue loop that connects to the next MORN repeat. Each β-hairpin
602 is composed of two 6-residue β-strands connected by a 5-residue loop. The MORN repeats
603 from TbMORN1(7-15) could be readily superimposed, showing a high level of structural
604 conservation (Fig. 7D). Based on this high level of conservation, a revised sequence alignment
605 of the TbMORN1 repeats was constructed that better reflects the structural architecture of the
606 protein (Fig. 7E, compare with Fig. 1A). The alignment of repeats 7-15 was obtained directly
607 from structural superpositions and used to bootstrap the alignment of the repeats 1-6.
608
609 The new consensus MORN repeat sequence displays three highly-conserved features: a GxG
610 motif at the start, a conserved glycine (G) at position 10, and a YEGEW motif at positions 13-
611 17 (Fig. 7E). A slightly less conserved LxY motif is at positions 5-7. The GxG motif is at the
612 beginning of the first β-strand, while the YEGEW motif comprises most of the second β-strand.
613
614 The glycine residues at position 10 are in a β-hairpin of type I, where the most commonly-
615 observed residue at this position is a glycine (Hutchinson & Thornton, 1994). The GxG motif
616 is strictly conserved because the first G residue adopts a main chain conformation mapping
617 to the lower right corner of the Ramachandran plot, which is exclusively allowed for glycines.
618 The conformation of this glycine is stabilised via a main-chain hydrogen bond with the
619 tryptophan (W) residue of the YEGEW motif (Fig. 7F). The high conservation of the second
620 glycine residue in the GxG motif is to accommodate the highly conserved neighbouring
621 aromatic residues from the YEGEW and LxY motifs, as any larger side chain would create
622 steric clashes. The tyrosine and tryptophan side chains of the YEGEW and LxY motifs provide
623 a textbook example of aromatic stacking, filling up the groove and stabilising the tertiary
624 structure of the TbMORN1 subunit (Fig. 7F, G). The highly conserved tyrosine of the YEGEW
625 motif is sandwiched in a T-shaped π-stacking interaction between two tryptophan residues,
626 one from its own motif and the second from the following YEGEW motif (Fig. 7F). The tyrosine
627 of the LxY motif is stabilised via hydrophobic and/or aromatic stacking interactions with the
628 leucine residues in its own and the subsequent LxY motif.
629
630 Three MORN repeats of SETD7 display similar general features, but differ in details, and can
631 be aligned with TbMORN1 repeat 7 over 22-23 aligned C_α atoms with an rmsd of 2.3, 1.5 and
632 1.9 Å respectively (Fig. S8B). The first glycine residue in the SETD7 MORN repeats is
633 conserved with that in TbMORN1, while tyrosine, phenylalanine, and valine replace the
634 tryptophan of the YEGEW motif (Fig. S8C).
635
636

637

638 ## TbMORN1 displays an overall negative charge

639

640 The TbMORN1(7-15) antiparallel dimer displays a two-fold symmetry perpendicular to the
641 longitudinal axis of the assembly (Fig. 7A). Analysis of amino acid conservation derived from
642 a sequence alignment of representative MORN repeat-containing proteins showed a well
643 conserved stretch of residues in the groove (Fig. 8A). Due to the twofold symmetric nature of
644 the quaternary structure assembly, structural and surface properties are displayed on opposite
645 sides of the elongated dimeric particle and perpetuated symmetrically along the rims (Fig. 8A-
646 C).

647

648 Each TbMORN1 subunit displays a negative electrostatic potential. A prominent feature of
649 each subunit is the negatively charged patch in the groove, which contributes to the highly
650 negative electrostatic potential of the dimer, together with the generally negatively charged
651 surface of the opposite site. This groove is flanked by a larger non-charged area with a central
652 positively-charged pocket (Fig. 8B, left-hand side, 8C middle). The negatively-charged patch
653 is formed by residues residing on loops of MORN repeats 9–13, and several of them display
654 high sequence conservation throughout the structural alignment (Fig. 8A,B, left-hand side).

655

656 The positive charge of the pocket closer to the dimer interface is contributed by the universally
657 conserved Lys316 residue, which is positioned on a loop connecting MORN repeats 13 and
658 14, and which is juxtaposed with Arg293 from the loop connecting MORN repeats 12 and 13.
659 The Arg293 residue is additionally involved in aromatic stacking interactions with the residues
660 Tyr278, Trp288 and Phe311, the latter forming a large surrounding non-charged area (Fig.
661 8B).

662

663 The rest of the subunit surface towards the N-terminus of each TbMORN1 subunit displays a
664 non-charged and partially hydrophobic character (Fig. 8C), while the opposite side of the
665 subunit displays a fairly uniform distribution of negative charges (Fig. 8B, right-hand side). The
666 overall negative charge of TbMORN1(7-15) and the lack of pronounced positive patches that
667 could serve as binding sites for negatively-charged phospholipid polar heads is consistent with
668 the negative binding data for lipid membranes.

669

670

671 ## TbMORN1 forms an extended antiparallel dimer

672

673 TbMORN1(7-15) in both crystal forms, as well as TgMORN1(7-15) in one crystal form, are
674 made of extended antiparallel dimers. The dimer interface is built from residues in MORN
675 repeats 12-15, which connect the two subunits in an antiparallel, tail-to-tail orientation (Fig.
676 7A-C). In both crystal forms of TbMORN1(7-15), the central core of the dimer interface is the
677 same (Fig. 9A, Fig. S9A). Due to the twofold symmetry, the majority of the stabilising
678 interactions are duplicated and build up an extended dimer interface.

679

680 The tightest overlap between the two subunits occurs at the site of MORN repeats 14 and 15.
681 A series of hydrophobic and aromatic π-stacking interactions between residues from repeats

682 14 and 15, together with hydrogen bonds across the edges, stabilise the dimer (Fig. 9A, Fig.
683 S9A). Furthermore, the very negatively-charged C-terminal region of one TbMORN1 subunit
684 forms an arch above the positively-charged platform contributed by Lys316 and Arg293 (Fig.
685 8B). Two residues from MORN repeat 14 - Lys325 (subunit A) and Asp326 (subunit B) - form
686 a salt bridge, which further stabilises the dimer interface.
687
688 In the $P2_1$ and C2 TbMORN1(7-15) crystal forms, the dimer interfaces occupy surface areas
689 of 747 $Å^2$ and 966 $Å^2$, respectively. Calculations of gain in solvation free energy (Δ^iG) upon
690 dimer formation for TbMORN1(7-15) C2 and $P2_1$ performed with the PDBePISA package
691 (Krissinel & Henrick, 2007) yielded values of -20.1 kcal/mol and -11.3 kcal/mol, respectively,
692 with corresponding p-values of interface specificity 0.01 and 0.08. Δ^iG values lower than -10
693 to -15 kcal/mol and p-values lower than 0.5 are significant for stable protein dimers, indicating
694 highly specific dimerisation interfaces (Krissinel & Henrick, 2007).
695
696 In the C2 crystal form, the dimer is additionally stabilised by two disulphide bridges formed
697 between Cys351 at the C-terminus of repeat 15, and Cys282 from the β-hairpin loop of repeat
698 12 (Fig. S9A). In the $P2_1$ crystal structure, the position of the loop differs from that in the C2
699 dimer, and keeps the C_α atoms of Cys351 and Cys282 at a distance of 11.7 Å, preventing
700 disulphide bond formation. Here, the side chain of Cys351 is engaged in a polar interaction
701 with Asp303 (Fig. 9A, Fig. S9A).
702
703 In comparison to the TbMORN1(7-15) C2 crystal form, the extended TgMORN1(7-15)
704 structure has an approximately 1.5-times smaller dimer interface (601 $Å^2$), which is contributed
705 solely by residues from MORN repeats 13-15 (Fig. 7B, Fig. S9C). This is closer in size to the
706 747 $Å^2$ interface of the $P2_1$ crystal form of TbMORN1(7-15). The final C-terminal part of the
707 protein seems to be flexible and does not engage in the stabilisation of the dimer. In
708 comparison to TbMORN1(7-15), the dimer interface of TgMORN1(7-15) is not built around
709 aromatic stacking, but instead employs hydrophobic interactions between Phe350 and
710 neighbouring small hydrophobic residues, such as Leu335 and Leu327 (Fig. S9C).
711
712 A retroactive validation of the dimer interface came from the earlier $PI(4,5)P_2$-binding work.
713 Mutagenesis of repeat 14 had produced a mixture of monomers and dimers, while the
714 simultaneous mutagenesis of two candidate sites in repeats 13 and 14 had resulted in a pure
715 monomer population (Fig. S3B). Analysis of the interaction and electrostatic maps of
716 TbMORN1(7-15) and its mutagenised variants clearly showed that Arg293 and Lys316,
717 residing in repeats 13 and 14 respectively, are crucial for maintaining TbMORN1 in a stable
718 dimeric state through electrostatic interactions (Fig. 9C). Lys315 (in MORN repeat 14) does
719 not appear to be directly involved in the dimerisation interface, but could peripherally
720 contribute to the stabilisation of the C-terminal region of TbMORN1 through its electrostatic
721 potential. Residues Arg292, Lys296 (both in MORN repeat 13), and Arg321, Lys325 (both in
722 MORN repeat 14) were mapped to the outer surface of the dimer and therefore do not take
723 part in the dimerisation interface (Fig. 9A, Fig. S9A).
724
725 The transition of $TbMORN1(2\text{-}15)^{Mut14}$ from a dimeric to a mixed monomer/dimer population is
726 therefore a direct consequence of the single point mutation K316A, whereas the complete
727 abrogation of dimerisation observed for the TbMORN1(2-15) double mutant can be attributed

728 to a synergistic effect of both R293A and K316A point mutations (Fig. S3B, Fig. 9C), thereby
729 verifying their contribution to dimer formation.
730
731
732 ## The V-shaped and extended dimer forms of apicomplexan MORN1 proteins
733
734 Unlike the extended dimers of TbMORN1(7-15) and TgMORN1(7-15), the V-shaped
735 PfMORN1(7-15) is mainly stabilised by a single Zn^{2+} ion incorporated into the core of its dimer
736 interface, spanning over 665 $Å^2$ (Fig. 7C, Fig 9B). One Cys306 and one Asp309 from each
737 respective subunit tetrahedrally coordinate the Zn^{2+} at expected distances (2.32 Å for Zn^{2+}-S
738 and 1.94 Å for Zn^{2+}-O). In addition, residues from repeats 13-15 are involved in stabilising the
739 dimer via a combination of hydrophobic, polar, and electrostatic interactions across the
740 subunits.
741
742 Although TgMORN1(7-15) was predominantly found as an extended dimer (Fig. 7B), a V-
743 shaped form similar to that of PfMORN1(7-15) was sporadically observed in the crystal lattice
744 (Fig. S9B). The two V-shaped dimers share the same coordination sphere of a Zn^{2+} ion, which
745 in TgMORN1(7-15) is provided by the Cys305 and Asp308 residues (Fig. S9D). The latter
746 residue in turn interacts with the Ser310 residue from the other subunit. While the salt bridge
747 and anion π-interactions are also conserved between the two V-shaped dimers, the aromatic
748 stacking present in the core of the PfMORN1(7-15) dimer interface is functionally replaced in
749 the TgMORN1(7-15) V-shaped dimer by a series of aromatic stacking interactions at its vertex.
750 Although Asp residues 303 (TbMORN1), 308 (TgMORN1) and 309 (PfMORN1) are conserved
751 in all the three proteins, the coordination of a Zn^{2+} ion clearly demands the presence of both
752 cysteine and aspartate residues. Such pairs are present in PfMORN1 and TgMORN1, but not
753 in TbMORN1, where the cysteine residue at the corresponding position is replaced by Leu301.
754 The coordination residues map to the β-hairpin of MORN repeat 13, which in TgMORN1 and
755 PfMORN1, but not TbMORN1, contains an insertion of a glutamate residue - Glu307 and
756 Glu308, respectively. Taking part in an anion π-interaction with a phenylalanine residue
757 (Phe303 and Phe304, respectively), the resulting Glu-Phe pairs effectively stabilise the
758 TgMORN1 and PfMORN1 dimers in their V-shaped form. Moreover, these very same
759 glutamate residues further stabilise the two V-shaped dimers by being involved in a salt bridge
760 with lysine residues (Lys321 in TgMORN1 and Lys322 in PfMORN1). At the equivalent
761 position in TbMORN1, Lys316 does not participate in a salt bridge, but rather points towards
762 the negative patch at the C-terminal part of the other subunit and stabilises the extended dimer
763 via electrostatic interactions.
764
765 To see whether it was possible to predict if a MORN repeat protein formed either extended or
766 V-shaped dimers, or both, a comparative sequence analysis was carried out. The sequences
767 of 15 selected MORN repeat proteins from various protist lineages were aligned with the C-
768 terminal parts of TbMORN1, TgMORN1 and PfMORN1 encompassing repeats 12-15 (Fig.
769 S10). The residues in the crystal structures of TgMORN1(7-15) and PfMORN1(7-15) forming
770 the Zn^{2+}-coordination sphere and anion π-interaction were taken as a fingerprint for a V-
771 shaped dimer. All sequences of MORN repeat proteins from kinetoplastids contain a leucine
772 residue (Leu301 in the case of *T. brucei*) at the position of the coordinating Cys residue, and
773 lack the Phe-Glu either side of it forming the anion π-interaction pair - as these residues are

774 essential for V-shape dimerisation, the kinetoplastid proteins are all thus predicted to form
775 extended dimers only. Conversely, all protein sequences in the dataset from apicomplexans
776 (*Toxoplasma gondii, Plasmodium falciparum, Gregarina niphandrode*s, *Babesia microti*,
777 *Cryptosporidium parvum, Eimeria acervuline, Theileria equi*) contained these cysteine,
778 phenylalanine, and glutamate residues. This suggests that all these apicomplexan proteins -
779 probably MORN1 homologues - can adopt both extended and V-shaped forms. In addition,
780 the sequences from the alveolates *Symbiodinium microadriaticum* and *Perkinsus marinus*,
781 and the stramenopile *Aureococcus anophagefferens* also contain these three residues,
782 implying that they too might adopt both extended and V-shaped conformations.
783 Apicomplexans belong to the Alveolata clade, and both alveolates and stramenopiles are in
784 the SAR supergroup (Adl et al., 2019). This suggests that the ability to adopt two
785 conformations might have arisen within this specific clade, and possibly explains its absence
786 from the kinetoplastid sequences, as kinetoplastids are excavates. The functional implications
787 of this built-in structural plasticity seemingly modulated by the presence of zinc ions remain
788 intriguing.
789

790 ## MORN1 proteins adopt extended conformations in solution

791
792 The crystal structures were all consistent with the earlier results of the cross-linking mass
793 spectrometry experiments carried out on TbMORN1 in solution, which had indicated close
794 proximity between repeats 13-15 (Table S1). To confirm the presence of V-shaped and
795 extended dimers in solution, all three MORN1 proteins were structurally analysed using small-
796 angle X-ray scattering (SAXS). SAXS analysis of TbMORN1(7-15) and TgMORN1(7-15)
797 indicated an extended dimer in solution, and the crystal structures could be docked into the
798 calculated molecular envelopes without difficulty (Fig. 10A, B, Fig. S9E). The SAXS analysis
799 of PfMORN1(7-15) indicated an extended structure, similar to that seen for TbMORN1(7-15)
800 and TgMORN1(7-15) (Fig. 10C). This supports the prediction that TgMORN1 and PfMORN1
801 are capable of adopting two different conformations. Subsequent SAXS produced a molecular
802 envelope for TbMORN1(2-15) into which an extrapolated version of the model of TbMORN1(7-
803 15) could be docked as an extended dimer (Fig. 10D, Fig. S9E).
804
805 Rotary shadowing EM on TbMORN1(2-15) produced results consistent with the SAXS
806 analysis, showing small kinked rods approximately 25 nm in length (Fig. 10E). The population
807 was homogeneous, consistent with the monodispersity of this sample observed by SLS (Fig.
808 1B). Comparison of the maximal dimer dimension (D_{max}) for TbMORN1(2-15) obtained from
809 SAXS and EM showed a very good agreement between the two values of 250-260 Å. Rotary
810 shadowing EM was also carried out on the small amount of TbMORN1(1-15) that eluted from
811 the SEC column. Full-length TbMORN1 was far more heterogeneous than TbMORN1(2-15),
812 consistent with the polydispersity observed by SLS (Fig. 1B). In addition to single kinked rods,
813 longer filamentous assemblies of varying length were occasionally observed (Fig. 10F).
814 Rarely, much larger meshlike assemblies of full-length TbMORN1 could be observed (Fig.
815 10G), offering a tantalising clue into the higher-order assembly properties of the protein. These
816 properties will be investigated in future work.
817

DISCUSSION

MORN repeat proteins are found ubiquitously in the tree of life, but the function of MORN repeats themselves has remained unclear and supported by very limited structural information to date. MORN repeats were first named almost 20 years ago, in a paper identifying the junctophilin protein family (Takeshima et al., 2000).

While there is abundant evidence that junctophilins associate with the plasma membrane, and that the MORN repeat-containing region is likely to mediate this, there is to the authors' knowledge no report demonstrating that the junctophilin MORN repeats directly interact with lipids (Takeshima et al., 2000, Munro et al., 2016, Woo et al., 2016, Perni et al., 2017, Jayasinghe et al., 2018, Nakada et al., 2018, Rossi et al., 2019). Despite this, the evidence that the MORN repeat-containing region mediates plasma membrane targeting has been repeatedly cited as evidence that MORN repeats directly bind lipids. MORN repeats are thus widely assumed to be lipid-binding modules, despite there actually being no evidence for direct membrane binding. Warnings that the function of MORN repeats has not really been elucidated, and that extant data are frequently contradictory, have been largely overlooked (Mikami et al., 2010).

This study set out to test the lipid-binding hypothesis by using a protein composed exclusively of MORN repeats, TbMORN1. The data provide something of a cautionary tale.

At first, the evidence obtained using overlay assays and fluorescence anisotropy indicated an ability to bind specific phospholipids (Fig. 2A, C). This binding appears to be mediated primarily by the aliphatic chains of the phospholipids however, as no binding was ever seen in the fluorescence anisotropy assays when small (6-carbon) lipids or polar headgroups were used.

Purified recombinant TbMORN1(1-15) was unexpectedly found to co-purify with PE. Bacteria expressing TbMORN1(1-15) showed elevated levels of PE, which might suggest that TbMORN1 was binding and sequestering the lipid, requiring them to upregulate synthesis (Fig. 3A, C). Almost no PE was found to co-purify with TbMORN1(10-15), and none was detected with the apicomplexan MORN1 proteins. This suggests that the N-terminal part of TbMORN1 might be a major interaction area for PE.

It is worth noting that neither PE nor any other lipids were observed in the crystal structure of TbMORN1(7-15). This might again be due to the fact that TbMORN1(7-15) does not contain the N-terminal part of the molecule, or possibly because the lysine methylation step used to enhance crystallisation altered its surface-exposed lysine residues, making them unavailable for electrostatic interactions with lipid molecules due to the loss of positive charge. Despite this evidence for binding to PE, no sign of direct binding by TbMORN1 to lipid vesicles containing variable amounts of (PI(4,5)P_2 in vitro (Fig. 2D,E, Fig. 4) or to membranes in vivo (Fig. 6) could be obtained.

862 A remaining question then is whether this ability to bind fatty acid chains greater than 6-carbon
863 length is physiological, or an artefact. Given that TbMORN1 is a cytoskeleton-associated
864 protein, it is hard to imagine how it would be able to get access to the hydrophobic chains of
865 membrane-embedded phospholipids in vivo, although it is localised directly under the
866 cytoplasmic leaflet of the plasma membrane. The electrostatic profile of TbMORN1(7-15) is
867 also not suggestive of membrane binding, with a strong overall negative charge profile (Fig
868 8B). Consequently, a physiological interaction with phospholipid membranes seems very
869 unlikely.
870
871 It is important to note that phospholipid binding and membrane binding are two separate
872 things. Not interacting with membranes might not preclude the TbMORN1 proteins extracting
873 PE or other phospholipids out of membranes without stably interacting with the membranes
874 themselves. A similar hypothesis would be that TbMORN1 functions as a carrier/transporter
875 of lipids with aliphatic chains within a certain length, as for example found for non-vesicular
876 phosphatidylserine transport by oxysterol-binding proteins from the site of synthesis to the site
877 of biological activity (Maeda et al., 2013). What would be the corresponding physiological role
878 in the context of the flagellar pocket in trypanosomes is difficult to envisage at present, For
879 now, the simplest interpretation remains that there is no interaction of TbMORN1 with lipid
880 membranes, and consequently no physiological interaction with membrane-embedded
881 phospholipids either.
882
883 Due to the twofold symmetry of both extended and V-shaped MORN1 dimers, the dimeric
884 particle displays the conserved groove on opposite sides, therefore excluding this region for
885 interaction with the membranes and leaving as an option the rims lining the groove (Fig. 8A-
886 B). In the extended dimers, the two rims display a concave and a convex curvature, suggestive
887 of membrane sculpting BAR domain proteins which interact with membranes mainly via non-
888 specific electrostatic interactions (Salzer et al., 2017, Carman & Dominguez, 2018). These
889 curved surfaces in MORN1 dimers nevertheless do not display a pronounced positive charge,
890 nor the typical membrane insertion motifs characteristic for BAR domain proteins, thus refuting
891 the hypothesis for membrane binding via non-specific electrostatic interactions. In conclusion,
892 the quaternary structure architecture together with surface properties of the MORN1 dimers
893 do not support membrane binding.
894
895 There are however a small number of caveats that might still allow a lipid-binding activity to
896 be present. In vitro, the best indications for lipid binding came from the full-length protein,
897 TbMORN1(1-15). TbMORN1(1-15) gave a positive result on lipid blots (Fig. 2A), co-purified
898 with PE (Fig. 3A), and its expression correlated with increased PE levels in bacteria (Fig. 3C).
899 No co-purification of PE was seen with the apicomplexan MORN1 proteins despite >50%
900 identity at an amino acid level. This lipid-binding activity therefore seems specific to
901 TbMORN1. The elevation of PE levels seen in bacteria expressing TbMORN1(1-15) is highly
902 unusual, and the authors do not currently have a good explanation apart from invoking lipid
903 sequestration and transport to specific sites (Chung et al., 2015, Moser von Filseck et al.,
904 2015). If the PE co-purifying with recombinant TbMORN1(1-15) was just carry-over, then the
905 lipid profile should resemble that of total bacterial cellular lipids, which is not the case.
906 Furthermore, the bound PEs display a narrow range of aliphatic chains, suggesting specificity
907 of binding/recognition.

908
909 Lipids in trypanosomes have, in general, much longer aliphatic chains than those in bacteria.
910 In *T. brucei*, PE accounts for around 10-20% of total lipid, with aliphatic chains of 36:0 being
911 the dominant isoform (Richmond et al., 2010). In *E. coli*, PE is the predominant zwitterionic
912 lipid and accounts for around 80% of total lipid (Epand & Epand, 2009). As the length of the
913 side chains in bacterial lipids is predominantly 14 and 16 carbon atoms (Pramanik & Keasling,
914 1997), PE molecules with 16 carbon atoms chains are the most common. Notably,
915 TbMORN1(1-15) overexpressed in *E. coli* co-purified with PE species of much greater length
916 (30:0 – 36:2) (Fig. 3A), which was also reflected in increased production of these PE species
917 in overexpressing bacteria (Fig. 3C). Taken together, these data strongly suggest the
918 specificity of TbMORN1(1-15) towards PE species with aliphatic chains of a length
919 characteristic for *T. brucei*.
920
921 Similarly, in vivo, it remains a possibility that the cytoskeleton-associated fraction is associated
922 with the plasma membrane, potentially indirectly by binding to membrane-embedded partners.
923 The data presented here show only that TbMORN1 and Ty1-TbMORN1, when not associated
924 with cytoskeleton, are cytosolic rather than associated with the membrane/organelle fraction.
925 The cause of the negative phenotypic effects resulting from overexpression of either untagged
926 or Ty1-tagged TbMORN1 remains unclear.
927
928 As a final possibility, it might also be the case that a post-translational modification of
929 TbMORN1 is essential for lipid binding, and is either not added in bacteria or lost during
930 purification. Testing the activity of TbMORN1 expressed in a eukaryotic expression system or
931 translated in vitro would be a means of exploring this.
932
933 These data have clear implications for other MORN repeat proteins. Junctophilins do appear
934 to bind lipids, but it is not clear if the MORN repeats are mediating this or are merely within
935 the region/domain involved (Bennett et al., 2013). There is evidence for the role of the N-
936 terminal part of junctophilins mediating plasma membrane localisation, but this does not rule
937 out an indirect association via protein-protein interactions being the primary driver (Takeshima
938 et al., 2000). It now also appears that palmitoylation may play a significant role in junctophilin
939 association with the plasma membrane (Jiang et al., 2019), Another recent report on
940 junctophilin-2 showed that upon cleavage by an endogenous protease, the N-terminal region
941 translocates to the nucleus via a nuclear localisation signal and functions there as a
942 transcription factor (Guo et al., 2018). The original paper on the junctophilin family noted the
943 nuclear localisation of some truncations of junctophilin-1, but the significance of this was not
944 appreciated at the time (Takeshima et al., 2000).
945
946 It is difficult to say whether this translocation and nuclear function is easier or harder to explain
947 if the MORN repeats in the N-terminus are dedicated lipid-binding modules. Lipid-binding is
948 known to cause conformational changes in junctophilin-2, and such conformational changes
949 in reverse may well drive the protease-mediated dissociation, but again it is not clear if these
950 changes are in any way due to the MORN repeats themselves. Additionally, it has been
951 observed that the MORN repeats of ALS2 are not required for targeting to endosomes,
952 although the exact domain mediating targeting is not agreed upon (Yamanaka et al., 2003,
953 Kunita et al., 2004).

954
955 In summary, the presence of MORN repeats in a protein should not be taken as indicative of
956 lipid binding or lipid membrane binding without experimental evidence. Equally, evidence of
957 binding from PIP strips alone should be interpreted with caution, given that the entire
958 phospholipid moieties are being presented to the protein in a non-physiological setting.
959
960 If MORN repeats are not lipid membrane modules by default, this raises the question of what
961 they might actually be doing. The structural studies presented here make a case that one
962 conserved function of MORN repeats is in homotypic interactions, and possibly also in higher-
963 order assembly.
964
965 The three high-resolution structures described in this work are amongst the first canonical
966 MORN repeat proteins to be detailed. Given that the structures are from representatives of
967 two of the five eukaryotic supergroups - the excavates, and the SAR (stramenopiles,
968 alveolates, Rhizaria) clade - this demonstrates how the fundamental structure of the MORN
969 repeat has been conserved over evolutionary time.
970
971 All three MORN1 proteins analysed here formed tail-to-tail dimers via their C-termini with the
972 polypeptide chains aligned in an antiparallel arrangement. The all-β structure of the proteins
973 produces a twisting elongated structure, with a groove lined with aromatic side chains running
974 longitudinally through it. While this manuscript was in preparation, Li et al. published a high-
975 resolution structure of the MORN4/retinophilin protein in complex with the myosin 3a tail.
976 Binding was mediated by this central groove, showing that it can be used for very high-affinity
977 protein-protein interactions (Li et al., 2019).
978
979 The three high-resolution MORN1 crystal structures were consistent with the lower-resolution
980 SAXS data obtained on the same proteins in solution (Fig. 10, Table S1). The apicomplexan
981 MORN1 proteins appear capable of forming both extended and V-shaped conformations. The
982 key residues mediating the dimer interface in the V-shaped form were defined, and shown to
983 be conserved throughout the Apicomplexa. It thus seems likely that all apicomplexan MORN1
984 proteins can adopt these two conformations.
985
986 MORN1 proteins in Apicomplexa have been shown to be a key component of the basal
987 complex, which undergoes a constriction event at the end of the cell division cycle (Gubbels
988 et al., 2006, Hu, 2008). It is therefore tempting to speculate that these extended (Zn-free) and
989 V-shaped (Zn-bound) conformations represent the pre- and post-constriction states of the
990 MORN1 proteins in the basal complex. If so, this would constitute a remarkable rearrangement
991 of the molecules in the dimer, which would move through about 145° (Supplementary Video
992 1). It is interesting in this context to note that high levels of Zn ions are required to support the
993 growth of the blood-stage *P. falciparum* parasite (Marvin et al., 2012).
994
995 The high-resolution structures also enabled a new structure-based consensus sequence for
996 a MORN repeat to be defined (Fig. 7E). A single MORN repeat forms a β-hairpin, one of the
997 conserved building blocks of structural biology, with a long loop attached. The structural basis
998 for the conservation of individual residues within the MORN repeat has been defined (Fig. 7E,

F). These structures strongly argue that an individual MORN repeat is longer than the 14 amino acids sometimes suggested. Despite the lower level of sequence conservation in the loop following the hairpin, a 23-amino acid length seems the most parsimonious definition from a structural perspective.

One interesting consequence of this redefinition of the repeat is that it suggests that full-length TbMORN1 begins with an incomplete repeat, a feature also noted in the MORN4/retinophilin structure (Li et al., 2019). The (M)IYSEGE residues at the very N-terminus are predicted to form only a single β-strand rather than a complete hairpin (Fig. 7E). Li et al. suggested that this incomplete repeat could function as a capping element, but given that the first repeat in MORN1 is critical for oligomerisation leading to formation of filamentous structures, an alternative explanation is possible: the N-terminus of a second TbMORN1 molecule (itself encoding a single β-strand) could complete this hairpin through intermolecular interactions. Oligomerisation would thus be driven by a "split-MORN repeat" mechanism where a complete hairpin is formed by the interaction of the N-termini of two proteins. Further work will be needed to test this hypothesis. The concluding data presented here suggest that TbMORN1 utilises this oligomerisation capacity to build mesh-like assemblies, which can reach considerable size in vitro (Fig. 10G). The biophysical properties of these meshworks, in particular their tensile strength, are likely to be another fruitful avenue of investigation.

MATERIALS AND METHODS:

Antibodies and other reagents

All custom antibodies have been described previously. The rabbit anti-TbMORN1 were made for a previous project (Morriswood et al., 2013). The mouse monoclonal anti-Ty1 (BB2) antibodies were a gift from Cynthia He (University of Singapore) (Bastin et al., 1996). The mouse monoclonal anti-PFR1,2 antibodies (L13D6) were a gift from Keith Gull (University of Oxford) (Kohl et al., 1999). The anti-BiP antibodies were a gift from Jay Bangs (University at Buffalo) (Bangs et al., 1993). The rabbit anti-GFP antibodies were a gift from Graham Warren (MRC Laboratory for Molecular Cell Biology) (Pelletier et al., 2002). The following antibodies were obtained from commercial sources: anti-strep tag StrepMAB-Classic (IBA Biosciences), HRP-conjugated anti-mouse (ThermoFisher Scientific), anti-GST (Santa Cruz Biotechnology). Defatted BSA was purchased from Sigma-Aldrich.

Cloning and mutagenesis of expression constructs

The 1077 bp TbMORN1 open reading frame (ORF) (UniProt accession no. Q587D3; TriTrypDB database accession no. Tb927.6.4670) was amplified by PCR from genomic DNA obtained from *Trypanosoma brucei brucei* strain Lister 427 and ligated into vector pETM-13 encoding a Strep-tag at the 3' end of the insert. TbMORN1 truncations were generated using this construct as a template by ligase-independent cloning (Doyle, 2005). The sequences for TbMORN1(2-15) and TbMORN1(1-14) were additionally ligated into the pCoofy12 vector

1043 encoding a 3C protease-cleavable N-terminal Twin-Strep-tag (Scholz et al., 2013) by
1044 sequence and ligation-independent cloning (Li & Elledge, 2012). Mutagenesis constructs were
1045 generated by standard methods using the pre-existing pCoofy12_TbMORN1(2-15) construct
1046 as the template (Hemsley et al., 1989). All primer sequences are available upon request. For
1047 LiMA experiments, the construct encoding the EGFP-TbMORN1(2-15) was cloned in a two-
1048 step procedure by sequence and ligation-independent cloning followed by Gibson assembly
1049 using pCoofy12_TbMORN1(2-15) and the pEGFP-C1 vector (Gibson et al., 2009). The 1092
1050 bp TgMORN1 (UniProt accession no. Q3S2E8) and 1095 bp PfMORN1 (UniProt accession
1051 no. Q8IJ93) ORFs were amplified by PCR from genomic DNA. Truncations of the TgMORN1
1052 and PfMORN1 constructs were generated using ligase-independent cloning. The TgMORN1
1053 constructs were additionally ligated into the pET14 vector encoding a 3C protease-cleavable
1054 N-terminal His10-tag. The PfMORN1 constructs were additionally ligated into the pCoofy32
1055 encoding a 3C protease-cleavable N-terminal His10-tag and C-terminal OneStrep-tag.
1056
1057
1058 **Recombinant protein expression and purification**
1059 Rosetta 2 (DE3)pLysS bacterial cells transformed with the required expression plasmids were
1060 grown at 37 °C with shaking in the presence of the appropriate antibiotics. Large scale
1061 expression was carried out either in Luria-Broth or in auto-induction (ZY) medium (Studier,
1062 2005), with 500 ml media being inoculated with 3-5 ml of pre-cultured cells. Cells in Luria-
1063 Broth were grown to an OD_{600} ~ 0.8 – 1.0, after which 50 μM IPTG was added to induce
1064 recombinant protein expression. The cells were then incubated at lower temperature
1065 (overnight, 20 °C). The cells were then harvested by centrifugation (5000 x g, 30 min), and
1066 either lysed immediately or stored at -80 °C. For purification, the cells were resuspended in
1067 lysis buffer (50 mM Tris-HCl pH 8.5, 200 mM NaCl, 5% (w/v) glycerol, 1 mM DTT, protease
1068 inhibitor cocktail, benzonase). The pellet emulsions were first homogenised by mixing on ice
1069 using a T 10 basic Ultra-Turrax dispersing instrument (IKA), and lysis was accomplished using
1070 a single cycle in a cell disruptor (Constant systems Ltd), with the pressure set to 1.35 kPa.
1071 Lysates were clarified by centrifugation (18,000 x g, 45 min, 4 °C), and a two-step fast protein
1072 liquid chromatography (FPLC) purification protocol using an ÄKTA Protein Purification System
1073 (GE Healthcare Life Sciences) at 8 °C was then followed to obtain the recombinant protein.
1074 The supernatants were applied to two connected Strep-Trap HP 5 ml columns packed with
1075 Strep-Tactin ligand immobilized in an agarose matrix (GE Healthcare Life Sciences) (GE
1076 Healthcare Life Sciences) previously equilibrated with equilibration buffer (50 mM Tris-HCl pH
1077 8.5, 200 mM NaCl, 2% (w/v) glycerol, 1 mM DTT). Flow speed was adjusted to 2.5 ml/min.
1078 When 100% step gradient of elution buffer (equilibration buffer plus 2.5 mM D-desthiobiotin)
1079 was applied, the bound proteins were eluted in a single chromatographic peak. Selected peak
1080 fractions were examined by SDS-PAGE for protein content and purity, pooled accordingly,
1081 and concentrated in Amicon Ultra centrifugal filter units (MerckMillipore, various pore sizes)
1082 according to the manufacturer's instructions. These affinity-purified protein concentrates were
1083 then applied to a previously equilibrated HiLoad 16/600 Superdex 200 pg column (GE
1084 Healthcare Life Sciences) packed with dextran covalently bound to highly cross-linked
1085 agarose, enabling separation of proteins with MW in the range of 10 – 600 kDa. Flow speed
1086 was adjusted to 1 ml/min and fractions of 1.5 ml were collected. Fractions corresponding to
1087 the targeted chromatographic peak were examined for protein content by SDS-PAGE, pooled
1088 accordingly to their purity, concentrated, and stored at -80 °C until use.

1089
1090 **Limited proteolysis**
1091 Purified recombinant His-TbMORN1(1-15) at 1 mg/ml was separately incubated with three
1092 proteases with different cleavage specificities (α-chymotrypsin, trypsin, and proteinase K) in
1093 20 mM Tris-HCl pH 8.5, 200 mM NaCl, 2% glycerol, 0.2 mM $CaCl_2$ (15 min, RT). The proteases
1094 were used at dilutions of 1:100 - 1:2000. The reactions were stopped by the addition of SDS-
1095 Coomassie sample loading buffer for analysis by gel electrophoresis. The indicated protein
1096 bands were extracted from the gel and subjected to mass spectrometry analysis.
1097
1098
1099 **Size-exclusion chromatography coupled to multi-angle light scattering (SEC MALS)**
1100 The MW and oligomeric state of purified proteins were verified by size exclusion
1101 chromatography (SEC) coupled to multi-angle light scattering (MALS), using a Superdex 200
1102 Increase 10/300 GL column (GE Healthcare Life Sciences). Up to five protein samples of 100
1103 μl were dialysed against 2x 1 L of freshly-prepared, degassed gel filtration buffer (20 mM Tris-
1104 HCl pH 8.5, 200 mM NaCl, 2% (w/v) glycerol, 0.5 mM DTT) (overnight, 4 °C). Gel filtration
1105 buffer was also used for overnight equilibration of the column and in the subsequent
1106 measurements. Protein samples were clarified by centrifugation using a TLA-55 rotor in an
1107 Optima MAX-XP table top ultracentrifuge (Beckman Coulter) (90,720 x g, 30 min, 4 °C). 100
1108 μl of 2 – 4 mg/ml protein samples were applied to a column using the 1260 Infinity HPLC
1109 system (Agilent Technologies) coupled to a MiniDawn Treos detector (Wyatt Technologies)
1110 with a laser emitting at 690 nm. An RI-101 detector (Shodex) was used for refractive index
1111 determination and the Astra 7 software package (Wyatt Technologies) for data analysis. No
1112 correction of refractive index was necessary due to the 2% (w/v) glycerol content in the buffer.
1113
1114
1115 **Circular dichroism (CD)**
1116 Far-UV CD was used both for measurement of secondary structure and for validation of the
1117 thermostability of TbMORN1 constructs. To avoid the absorption of Tris and NaCl below 180
1118 nm (Kelly et al., 2005), three protein samples of 100 μl were first dialysed against 2x 1 L of
1119 dialysis buffer (20 mM NaH_2PO_4, 20 mM Na_2HPO_4, 200 mM NaF) (overnight, 4 °C). The pH
1120 8.0 was adjusted by mixing the mono- and dibasic sodium phosphate solutions. The dialysed
1121 proteins were clarified by centrifugation in an Optima MAX-XP tabletop ultracentrifuge
1122 (Beckman Coulter Life Sciences) (90,720 x g, 30 min, 4 °C). The concentration of protein
1123 samples was adjusted to 0.25 mg/ml. CD measurements were carried out in a quartz cuvette
1124 with an optical path length of 0.5 mm (Stana Scientific Ltd) using a Chirascan Plus
1125 spectrophotometer (Applied Photophysics) equipped with the Chirascan-plus DMS software
1126 package. The CD profiles for secondary structure calculations were obtained at RT in the
1127 range of 190 – 260 nm. Further analysis was carried out using the BeStSel server, which is
1128 specialised in the analysis of CD data from proteins rich in β-strands (Micsonai et al., 2015,
1129 Micsonai et al., 2018). Data were converted to Δε ($M^{-1}cm^{-1}$) and uploaded to the BeStSel
1130 online server. Melting experiments were performed in the range of 190 – 260 nm, 20 – 80 °C,
1131 with a temperature ramp of 0.8 °C/min. Data were analysed with Global 3 software package.
1132
1133
1134

1135 **Chemical cross-linking coupled to mass spectrometry (XL-MS)**
1136 For chemical cross-linking with EDC (1-ethyl-3-(3-dimethylaminopropyl)carbodiimide
1137 hydrochloride) or BS^3 (bis(sulfosuccinimidyl)suberate), 200-300 μl of approximately 30 μM
1138 TbMORN1 sample was dialysed twice against 1 L of EDC buffer (20 mM MES-NaOH pH 6.8,
1139 200 mM NaCl) or BS^3 buffer (20 mM HEPES-NaOH pH 8.0, 200 mM NaCl) (overnight, 4 °C).
1140 Following dialysis, the protein was clarified by centrifugation (90,720 x g, 30 min, 4 °C) using
1141 a TLA-55 rotor in an Optima MAX-XP tabletop ultracentrifuge (Beckman Coulter Life
1142 Sciences). EDC (ThermoFischer Scientific) was first equilibrated to RT and then a stock
1143 solution in EDC buffer was prepared. 1.3 μM TbMORN1 previously dialysed in EDC buffer
1144 was mixed with 0, 200, and 400 μM EDC (all final concentrations) in a total volume of 40 μl.
1145 After a 30 min incubation at RT, 10 μl of SDS loading buffer was added and the mixtures were
1146 further denatured by heating (95 °C, 10 min). The experiments with BS^3 were carried out
1147 identically except that BS^3 buffer and 3.4 μM TbMORN1 were used, and the incubation time
1148 was 120 min. Samples were separated by SDS-PAGE, stained with Coomassie dye, and
1149 selected bands corresponding to monomers and dimers cross-linked with 400 μM cross-linker
1150 were excised and subjected to enzymatic digestion and subsequent mass spectrometry
1151 analysis. Coomassie Brilliant Blue-stained excised bands were destained with a mixture of
1152 acetonitrile and 50 mM ammonium bicarbonate (ambic), in two consecutive steps (each 10
1153 min, RT). The proteins were reduced using 10 mM DTT in 50 mM ambic for (30 min, 56 °C),
1154 alkylated with 50 mM iodoacetamide in 30 mM ambic in the dark (30 min, RT), and digested
1155 with trypsin (Promega, mass spectroscopy grade) (overnight, 37 °C). The reaction was
1156 stopped using 10% (v/v) formic acid and extracted peptides were desalted using C18
1157 Stagetips (Rappsilber et al., 2007). Peptides were analysed on an UltiMate 3000 HPLC
1158 RSLCnano system coupled to a Q Exactive HF mass spectrometer, equipped with a
1159 Nanospray Flex ion source (all Thermo Fisher Scientific). Peptides were loaded onto a trap
1160 PepMap 300 C18 column of dimensions 5 mm x 300 µm i.d., packed with 5 µm particles with
1161 a pore size of 100 Å (Thermo Fisher Scientific, cat. no. 164718) and separated on an analytical
1162 C18 100 column of dimensions 500 mm x 75 µm i.d., packed with 2 µm particles with a pore
1163 size of 100 Å (Thermo Fisher Scientific, cat. no. 164942), applying a linear gradient from 2%
1164 to 40% solvent B (80% acetonitrile, 0.1% formic acid) at a flow rate of 230 nl/min over 120
1165 min. The mass spectrometer was operated in a data-dependent mode at high resolution of
1166 both MS1 and MS2 level. Peptides with a charge of +1, +2 or of a higher than +7, were
1167 excluded from fragmentation. To identify cross-linked peptides, the spectra were searched
1168 using pLink software v1.23 (Yang et al., 2012). Q Exactive HF raw-files were pre-processed
1169 and converted to mgf-files using pParse (Yuan et al., 2012). The MaxQuant database
1170 (Tyanova et al., 2016) was used to search the spectra for the most abundant protein hits.
1171 Carbamidomethylation of cysteine and oxidation of methionine residues were set as variable
1172 modifications. Trypsin was set as an enzyme specificity, and EDC or BS^3 was set as a cross-
1173 linking chemistry. In case of EDC, aspartic and glutamic acid residues, as well as C-termini of
1174 proteins, were allowed to be linked with lysine residues. In the case of BS^3, lysine residues
1175 and N-termini of proteins were allowed to be linked with lysine residues, N-termini of proteins,
1176 as well as to serine, threonine and tyrosine residues. Search results were filtered for 1% FDR
1177 (false discovery rate) on the PSM (number of peptide-spectrum matches) level and a
1178 maximum allowed precursor mass deviation of 5 ppm. To remove low quality PSMs, an
1179 additional e-Value cutoff of < 0.001 was applied. In order to distinguish intra- from inter-
1180 molecular chemical cross-links, results from monomers and dimers were compared. A

potential inter-molecular cross-link must have shown the following criteria: (1) minimally 3 peptide PSMs in dimer and (2) minimally 3-times more PSMs in dimer than in monomer.

Protein-lipid overlay assays (PIP strips)

PIP strips were purchased from Echelon Biosciences (cat. no. P-6001). PBS-T (PBS, 0.1% TWEEN-20) was used as a general buffer. Purified recombinant TbMORN1(1-15) was clarified by centrifugation (20,817 x g, 20 min, 4 °C) prior to use. The PIP strips were blocked using blocking buffer (3% (w/v) defatted BSA, PBS-T) (60 min, RT) and then incubated with 5 μg/ml of TbMORN1 in 10 ml of blocking solution (60 min, RT). After three washes with PBS-T, the membranes were overlaid with anti-strep antibodies diluted in blocking solution (60 min, RT). After a further three PBS-T washes, the membranes were overlaid with HRP-conjugated secondary antibodies (60 min, RT). The membranes were then washed three times with PBS-T and visualised by ECL (Western Blotting substrate, Thermo Fisher) using a Fusion FX imager (Vilber Lourmat). All binding and wash steps were carried out with gentle agitation of the membranes. For the positive control, the PIP strip was overlaid with GST-tagged PLC-δ1 PH domain (Echelon Biosciences) and mouse monoclonal anti-GST antibodies (Santa Cruz Biotechnology) were used.

Fluorescence anisotropy

Stocks of BODIPY TMR-labelled PI C6, PI(4)P C6, PI(3,4)P_2 C6, PI(3,5)P_2 C6, PI(4,5)P_2 C6 and PI(4,5)P_2 C16 were sonicated (5 min, RT) in a sonication bath, and in parallel with purified recombinant TbMORN1(2-15), TbMORN1(7-15), TbMORN1(10-15), were clarified by centrifugation (20,817 x g, 20 min, 4 °C). The concentrations of lipid stocks were determined with a Hitachi U-3501 UV-VIS spectrophotometer, using quartz absorbance cuvettes and an optical path length of 10 mm (Hellma Analytics). For this purpose, the maximum absorbance of BODIPY TMR dye at λ = 544 nm was measured; its extinction coefficient ε = 60,000 $cm^{-1}M^{-1}$. The total volume of each respective sample was 110 μl. The concentration of selected TbMORN1 constructs was varied from 0 to 35 μM (or more), while the concentration of added lipid was kept constant at 0.1 μM. Measurements were performed on a Perkin Elmer LS50B fluorimeter in quartz cuvettes with an optical path length of 10 x 2 mm (Hellma Analytics). To ensure a constant temperature of 20 °C in the measured sample, the measurement cell was connected to a water bath. The parameters for fluorescence anisotropy (r) measurements were: λ_{ex} = 544 nm and aperture of excitation slit = 15 nm; λ_{em} = 574 nm and aperture of emission wavelength = 20 nm; time of integration = 1 s and T = 20 °C. The grating factor (G factor), which provides grating correction for the optical system, was determined on samples with exclusively 0.1 μM lipid and kept constant during measurement of each concentration series. Triplicates of each protein concentration point were measured and afterwards averaged using Excel software. Graphs were drawn and fitted in SigmaPlot ver. 13.0. The equation used for fitting was a four parameters logistic curve where:

$$y = \min + \frac{(\max - \min)}{1+(\frac{x}{EC50})^{-Hillslope}},$$

1225 Options were set to default; initial parameters values, as well as parameters min, max, EC50,
1226 Hillslope, were selected automatically, parameter constraints were max > min and EC50 > 0,
1227 number of iterations was 200, and tolerance was kept at $1e^{-10}$. The reduced chi-square method
1228 was used to compute parameters' standard errors. Experimental r values of respective 0.1 μM
1229 BODIPY TMR-lipid and protein-TMR BODIPY-lipid mixtures were compared with theoretical
1230 values obtained by Perrin equation.
1231
1232
1233 **Mass spectrometry analysis of extracted lipids**
1234 Lipid extractions from purified recombinant full length and truncated TbMORN1 were achieved
1235 by three successive vigorous extractions with ethanol (90% v/v) according to a published
1236 protocol (Fyffe et al., 2006). The pooled extracts were dried using N_2 gas in a glass vial and
1237 re-extracted using a modified Bligh and Dyer method (Richmond et al., 2010). For whole *E.*
1238 *coli* lipid extracts, cells were washed with PBS and extracted following the modified Bligh and
1239 Dyer method. All extracts were dried under N_2 gas in glass vials and stored at 4 ^{o}C. Extracts
1240 were dissolved in 15 μl of choloroform:methanol (1:2) and 15 μl of acetonitrile:propan-2-
1241 ol:water (6:7:2) and analysed with an Absceix 4000 QTrap, a triple quadrupole mass
1242 spectrometer equipped with a nano-electrospray source. Samples were delivered using a
1243 Nanomate interface in direct infusion mode (~125 nl/min). Lipid extracts were analysed in
1244 both positive and negative ion modes using a capillary voltage of 1.25 kV. MS/MS scanning
1245 (daughter, precursor and neutral loss scans) were performed using nitrogen as the collision
1246 gas with collision energies between 35-90 V, allowing lipid structure assignments.
1247
1248
1249 **Preparation of sucrose-loaded vesicles (SLVs) and pelleting assay**
1250 To generate synthetic SLVs, lipids reconstituted in $CHCl_3$ were mixed in the following ratio:
1251 30% DOPC; 35% DOPE; 15% DOPS; 20% cholesterol. 5 mol % PI(4,5)P_2 was added in place
1252 of 5 mol% DOPE in the PI(4,5)P_2-containing liposomes. Lipids were extracted from
1253 bloodstream form *T. brucei* according to an established protocol (Bligh & Dyer, 1959). Briefly,
1254 mid-log phase cells were harvested by centrifugation (750 x g, 10 min, RT), washed once with
1255 PBS, then resuspended in 100 µl PBS and transferred to a glass tube. 375 µl of 1:2 (v/v)
1256 $CHCl_3$:MeOH was added and the mixture was vortexed (20 s) and then incubated with
1257 continuous agitation (15 min, RT). A further 125 µl $CHCl_3$ was then added to make the mixture
1258 biphasic, and following brief vortexing 125 µl ddH_2O was added. The mixture was vortexed
1259 again and then separated by centrifugation (1000 x g, 5 min, RT). The lower organic layer was
1260 then transferred to a new glass vial, dried under a nitrogen stream, and kept at 4 °C until use.
1261 For the preparation of SLVs from trypanosomal lipids the lyophilized lipids (extract from $8x10^7$
1262 cell equivalents) were reconstituted in 50 µl $CHCl_3$. 6 µM Rhodamine B dihexadecanoyl
1263 phosphoethanolamine (Rh-DHPE) was added to all lipid mixtures to facilitate the visualisation
1264 of the SLVs. The lipid mixtures were dried under a nitrogen stream, and the lipid films hydrated
1265 in 20 mM HEPES pH 7.4, 0.3 M sucrose. The lipid mixtures were subjected to 4 cycles of
1266 freezing in liquid nitrogen followed by thawing in a sonicating water bath at RT. The vesicles
1267 were pelleted by centrifugation (250,000 x g, 30 min, RT) and resuspended in 20 mM HEPES
1268 pH 7.4, 100 mM KCl to a total lipid concentration of 1 mM. SLVs were incubated with 1.5 µM
1269 purified TbMORN1(2-15) at a 1:1 ratio (30 min, RT). To separate soluble and SLV-bound
1270 TbMORN1(2-15), the vesicles were pelleted by centrifugation (8,700 x g, 30 min, RT), and

1271 equal volumes of supernatant and resuspended pellet were separated by SDS-PAGE and
1272 analysed by Coomassie staining.
1273
1274
1275 **Liposome microarray assay (LiMA)**
1276 LiMA (Saliba et al., 2014) was performed according to the standard protocol (Saliba et al.,
1277 2016). TbMORN1(2-15) tagged N-terminally with EGFP and two positive controls, PLCδ1-PH
1278 and Lactadherin-C2, both fused to superfolder GFP (sfGFP), were applied to microarrays
1279 printed with different signalling lipids. In brief, lipids of interest were combined with the carrier
1280 lipid DOPC, PEGylated PE, and PE labelled with Atto 647 dye (PE-Atto 647, 0.1 mol%). Lipid
1281 mixtures containing 2, 5, and 10 mol% of the signalling lipid were spotted onto a thin agarose
1282 layer (TAL). The agarose layers were hydrated using buffer A (20 mM Tris-HCl pH 8.5, 200
1283 mM NaCl) and vesicles formed spontaneously. Efficiency of liposome formation was verified
1284 by fluorescence microscopy. The protein was diluted to 7 µM in buffer A and 40 µl was applied
1285 to each array. Microarrays were incubated (20 min, RT) and subsequently washed three times
1286 with 40 µl of buffer A. Chips were analysed by automated fluorescence microscopy. Positions
1287 of liposomes were determined by tracking the fluorescence of PE-Atto 647 and images were
1288 taken for 3 ms and 5 ms exposure times. In parallel, the fluorescence of EGFP was determined
1289 for 1, 5, 10, 30, 75, 100, 200 and 300 ms exposures. Images were processed using CellProfiler
1290 and CPAnalyst. Only EGFP signals that overlapped with Atto 647 signals were taken into
1291 account. Normalised binding intensity (NBI) was calculated as the ratio between EGFP and
1292 Atto 647 fluorescence, normalised by exposure time. Three microarrays were examined,
1293 carrying liposomes with the following signalling lipids; PIP-chip: DOPA, DOPE, DOPI, DOPS,
1294 DODAG, cardiolipin, BMP, DOPI(4,5)P_2, DOPG; GLP-chip: ceramide C16, ceramide(1)P C16,
1295 ceramide(1)P C18, S(1)P, S, SM, DOPI(4,5)P_2, DOPS; SL-chip: DOPI(3)P, brain PI(4)P,
1296 DOPI(5)P, DOPI(3,4)P_2, DOPI(3,5)P_2, brain PI(4,5)P_2, DOPI(3,4,5)P_3, DOPS and cholesterol.
1297 Each microarray was performed in triplicate.
1298
1299
1300 **Cell culture and cell line generation**
1301 Bloodstream form *T. brucei* cells were maintained in HMI-9 media supplemented with 10%
1302 foetal bovine serum (Sigma-Aldrich, St. Louis, USA) at 37 °C and 5% CO_2 in cell culture flasks
1303 with filter lids (Greiner). For overexpression studies, 427 strain "single marker" cells - which
1304 express T7 RNA polymerase and the Tetracycline repressor protein, both maintained under
1305 2.5 µg/ml G418 selection - were used (Wirtz et al., 1999). For optimisation of digitonin
1306 extraction conditions, the GFP^{ESPro}-221^{ES}.121^{tet} cell line, which constitutively expresses GFP
1307 from the VSG expression site, was used (Batram et al., 2014). Constructs for overexpression
1308 of Ty1-tagged TbMORN1 and untagged TbMORN1 were obtained by cloning the required
1309 ORFs into the pLEW100v5-HYG plasmid; the identity of the inserts was verified by DNA
1310 sequencing followed by BLAST analysis against the TbMORN1 ORF (Tb927.6.4670). The
1311 plasmids were linearised by NotI digestion, and plasmid DNA was purified by ethanol
1312 precipitation. Linearisation was verified using agarose gel electrophoresis. Stable cell lines
1313 were generated by using 20 µg of the linearised plasmids to transfect ~$3x10^7$ "single marker"
1314 cells in transfection buffer (90 mM Na_2PO_4, 5 mM KCl, 0.15 mM $CaCl_2$, 50 mM HEPES pH
1315 7.3) using the X-001 program of an Amaxa Nucleofector II (Lonza, Switzerland) ((Burkard et
1316 al., 2007, Schumann Burkard et al., 2011). Clones were obtained from the transfected cells

1317 by limiting dilution under 5 μg/ml hygromycin selection. The presence of the transgene in the
1318 genomic DNA of isolated clones was verified by PCR.
1319
1320
1321 **Growth curves and BigEye cell counts**
1322 22 ml cells at a defined starting concentration were divided into two flasks of 10 ml each, and
1323 overexpression of the ectopic transgene was initiated in one flask by the addition of
1324 tetracycline to a final concentration of 1 μg/ml. For overexpression of Ty1-TbMORN1, a
1325 starting concentration of $1x10^4$ cells/ml was used, and the cells were split and reseeded at this
1326 concentration after 48 h. For overexpression of untagged TbMORN1, a starting concentration
1327 of $1x10^3$ cells/ml was used with no reseeding. Tetracycline was refreshed every 24 h in both
1328 cases. Population density was measured using a Z2 Coulter Counter (Beckman Coulter,
1329 Krefeld, Germany) at the indicated timepoints. For quantification of BigEye cell incidence at
1330 the indicated timepoints, the cultures were briefly agitated to mix the cells, which were then
1331 allowed to settle for 30 min. The culture flasks were then examined directly using an inverted
1332 phase contrast microscope (Leitz Labovert) and a 10x objective lens. Three fields of view were
1333 chosen at random for each flask and the number of normal and BigEye cells manually
1334 quantified, using higher magnification where necessary. Given the low magnification used, the
1335 numbers presented are likely to be underestimates of the true incidence.
1336
1337
1338 **Immunoblotting**
1339 To obtain whole cell lysates, cell concentration was measured using a Z2 Coulter Counter,
1340 and a defined volume was then transferred to 15 ml Falcon tubes. The cells were pelleted by
1341 centrifugation (750 x g, 10 min, RT), resuspended in 1 ml PBS, and transferred to microfuge
1342 tubes. The cells were again pelleted (1800 x g, 2 min, RT), and the cell pellet then directly
1343 resuspended in SDS loading buffer to a final concentration of 2×10^5 cells/μl. The lysates were
1344 heated (95 °C, 10 min) before use. Lysates were separated by SDS-PAGE ($1.4x10^6$ cells/lane
1345 in a 15-well gel of 1.0 mm thickness), and the proteins then transferred to nitrocellulose
1346 membranes. The membranes were blocked in blocking buffer (10% milk, PBS, 0.3% TWEEN-
1347 20) (30 min, RT), and then incubated with the indicated primary antibodies in blocking buffer
1348 (1 h, RT). The membranes were washed three times in PBS-T (PBS, 0.3% TWEEN-20), and
1349 were then incubated with IRDye-conjugated secondary antibodies in PBS-T (1 h, RT). After a
1350 further three washes in PBS-T the membranes were briefly dried between sheets of filter paper
1351 and then imaged using an Odyssey CLx (LI-COR Biosciences, Bad Homberg, Germany).
1352 Processing and quantification was carried out using ImageStudioLite software (LI-COR
1353 Biosciences).
1354
1355
1356 **Immunofluorescence microscopy**
1357 Cell concentration was measured using a Z2 Coulter Counter, and 10^6 cells per coverslip were
1358 taken. The cells were transferred to 15 ml Falcon tubes, and fixed directly in media by the
1359 addition of paraformaldehyde solution to a final concentration of 4% (37 °C, 20 min). 10 ml
1360 trypanosome dilution buffer (TDB; 20 mM Na_2HPO_4, 2 mM NaH_2PO_4, 5 mM KCl, 80 mM NaCl,
1361 1 mM $MgSO_4$, 20 mM glucose) was then added, and the cells were pelleted by centrifugation

1362 (750 x g, 10 min, RT). The supernatant was removed, the cell pellet was resuspended in 500
1363 μl TDB, and the cells were transferred to poly-L-lysine-coated coverslips in a 24-well plate.
1364 The cells were attached to the coverslips by centrifugation (750 x g, 4 min, RT), and the cells
1365 were permeabilised using a solution of 0.25% TritonX-100 in PBS (5 min, RT). The cells were
1366 washed with PBS, blocked using a solution of 3% BSA in PBS (30 min, RT), and sequentially
1367 incubated with primary and secondary antibodies diluted in PBS (1 h, RT for each) with three
1368 PBS wash steps after each incubation. After the final wash, the coverslips were rinsed in
1369 ddH_2O, excess fluid removed by wicking, and mounted on glass slides using Fluoromount-
1370 DAPI (Southern Biotech). For analysis of detergent-extracted cytoskeletons, cells were
1371 washed using TDB and attached to poly-L-lysine coverslips as described above. The cells
1372 were incubated in extraction buffer (0.5% IGEPAL, 0.1 M PIPES-NaOH pH 6.9, 2 mM EGTA,
1373 1 mM $MgSO_4$, 0.1 mM EDTA, cOmplete protease inhibitors [Roche]) (5 min, RT), washed
1374 three times with extraction buffer, and then fixed with ice-cold MeOH (-20 °C, 30 min).
1375 Blocking, antibody incubation steps, and mounting were as described above. All liquid
1376 handling was carried out using a P1000 micropipette, and pipetting was done as gently as
1377 possible to minimise shear forces. The coverslips were imaged using a Leica DMI6000B
1378 inverted microscope equipped with a Leica DFC365 camera and a 100x oil objective lens
1379 (NA1.4) and running Leica Application Suite X software. The same exposure times were used
1380 for acquisition of +/-Tet samples, and 40 z-slices of 0.21 μm thickness were taken per field of
1381 view. Image processing was carried out using ImageJ. Maximum intensity z-projections are
1382 shown.
1383
1384
1385 **Fractionation**
1386 Cell concentration was measured using a Z2 Coulter Counter, and an equal number of cells
1387 (~2.5×10^7 per experiment) was taken from the control (-Tet) and overexpression (+Tet)
1388 samples and transferred to 50 ml Falcon tubes. The cells were pelleted by centrifugation (750
1389 x g, 10 min, 4 °C), and the cell pellets then resuspended in 1 ml TDB and transferred to
1390 microfuge tubes. The cells were pelleted by centrifugation (1800 x g, 2 min, 4 °C), and then
1391 resuspended in 200 μl extraction buffer (see Immunofluorescence microscopy section for
1392 composition). After a short incubation (15 min, RT, orbital mixer), a 5% (10 μl) input sample
1393 was taken, and the mixtures separated by centrifugation (3400 x g, 2 min, 4 °C) into detergent-
1394 soluble (cytoplasmic) supernatant and detergent-insoluble (cytoskeleton) pellet fractions. The
1395 supernatant was transferred to a fresh microfuge tube, its exact volume noted, and a 5%
1396 sample taken. The tube containing the pellet was centrifuged a second time (3400 x g, 2 min,
1397 4 °C) in order to bring down material sticking to the tube wall; this second supernatant was
1398 discarded. The pellet was resuspended in 200 μl extraction buffer and a 5% sample (10 μl)
1399 taken. SDS loading buffer was added to the input, supernatant, and pellet samples to a final
1400 volume of 20 μl, and denaturation assisted by heating (95 °C, 10 min). Equal fractions were
1401 loaded onto polyacrylamide gels, separated by SDS-PAGE, and analysed by immunoblotting.
1402 In the exemplary blot shown (Fig. 5G), each sample is a 4.5% fraction, equivalent to ~10^6 cells
1403 in the Input fraction. For optimisation of extraction conditions using digitonin, essentially the
1404 same protocol was followed except that ultra-pure digitonin (Calbiochem) in TDB buffer was
1405 used and incubations were carried out at 24 °C in a heating block. For the two-step
1406 digitonin/IGEPAL fractionations (Fig. 8), cells were pelleted by centrifugation (750 x g, 10 min,

1407 RT), resuspended in 1 ml TDB, transferred to microfuge tubes, and pelleted again (750 x g, 3
1408 min, RT). The cell pellet was resuspended in 400 μl of 40 μg/ml digitonin in TDB and extracted
1409 (25 min, 24 °C), after which a 5% input sample was taken. The mixture was then separated
1410 by centrifugation (750 x g, 5 min, RT) and 320 μl of the cytosolic fraction (SN1) transferred to
1411 a fresh tube and a 5% sample was taken. The cell pellet was then resuspended with 1 ml TDB
1412 and the extracted cells again pelleted by centrifugation (750 x g, 5 min, RT). The extracted
1413 cells were then resuspended in 400 μl extraction buffer (see Immunofluorescence section
1414 above for composition) and incubated (24 °C, 15 min, heating block with shaker). After the
1415 incubation, a 5% sample (P1) was taken, and the extracted cells pelleted by centrifugation
1416 (3400 x g, 2 min, RT). 320 μl of the supernatant (SN2) was transferred to a fresh microfuge
1417 tube and a 5% sample was taken. The pellet was resuspended in 1 ml TDB and centrifuged
1418 again (750 x g, 5 min, RT). The pellet (P2) was then resuspended in 400 μl extraction buffer.
1419 SDS loading buffer was added to the 5% samples (I, SN1, SN2, P1, P2) to a final volume of
1420 40 μl. Samples were analysed by immunoblotting as detailed above.
1421
1422
1423 **Crystallisation**
1424 Crystallisation of TbMORN1(7-15), TgMORN1(7-15) and PfMORN1(7-15) was performed at
1425 22 °C using a sitting-drop vapour diffusion technique and micro-dispensing liquid handling
1426 robots (Phoenix RE (Art Robbins Instruments) and Mosquito (TTP labtech)). In the case of
1427 TbMORN1(7-15), crystals only appeared from reductively methylated protein, using a
1428 standard protocol (Walter et al., 2006). The best diffracting crystals of TbMORN1(7-15) were
1429 grown at a protein concentration of 3.5 mg/ml in the following conditions: 0.166 M Tris-HCl pH
1430 8.8, 0.15 M $MgCl_2$, 0.45 M KI, 24% PEG 2000 MME, and 4% glycerol. The tetragonal crystals
1431 of TgMORN1(7-15) were obtained at a protein concentration of 10 mg/ml in the following
1432 conditions: 0.1 M Tris-HCl pH 8.2, 15% PEG 3350, 0.2 M NaCl. The diffracting crystals of both
1433 selenomethionine-containing crystals and native crystals of PfMORN1(7-15) were obtained at
1434 a protein concentration of 8 mg/ml in the conditions "B11" from the Morpheus II crystallisation
1435 screen (Molecular Dimensions): 2 mM divalents mix (0.5 mM $MnCl_3$, 0.5 mM $CoCl_2$, 0.5 mM
1436 $NiCl_2$, 0.5 mM $Zn(OAc)_2$, 0.1 M Buffer System 6, pH 8.5 (Gly-Gly, AMPD), and 50%
1437 precipitation Mix 7 (20 % PEG 8000, 40% 1,5-Pentanediol). The crystals were flash cooled in
1438 liquid nitrogen prior to data collection.
1439
1440
1441 **X-ray diffraction data collection and crystal structure determination**
1442 Initially, the structure of PfMORN1(7-15) was determined using the single-wavelength
1443 anomalous diffraction (SAD) method. The selenomethionine dataset was collected at the
1444 beamline ID29 (ESRF, Grenoble) at 100K at the peak of selenium using a wavelength of 0.979
1445 Å. The data frames were processed using the XDS package (Kabsch, 2010), and converted
1446 to mtz format with the program AIMLESS (Winn et al., 2011). The apo-PfMORN1(7-15)
1447 structure was solved using single anomalous diffraction with AUTOSOL software from the
1448 PHENIX package. The structures of TgMORN1(7-15) and TbMORN1(7-15) were then solved
1449 using the molecular replacement program PHASER (McCoy et al., 2007) with the atomic
1450 coordinates of PfMORN1(7-15) as a search model. The structures were then refined with
1451 REFMAC and Phenix Refine and rebuilt using Coot (Murshudov et al., 1997, Emsley &

Cowtan, 2004, Adams et al., 2010). The structures were validated and corrected using the PDB_REDO server (Joosten et al., 2014). The figures were produced using Pymol and Chimera software. Coordinates have been deposited in the protein data bank (accession codes 6T4D, 6T4R, 6T68, 6T69, 6T6Q). Data collection and refinement statistics are reported in Table 1.

Small angle X-ray scattering (SAXS)

Synchrotron radiation X-ray scattering from various MORN constructs in solution were collected at different synchrotron facilities (Table S3). TgMORN1(7-15), TbMORN1(7-15) as well as PfMORN1(7-15) were collected at the EMBL P12 beamline of the storage ring PETRA III (DESY, Hamburg, Germany) (Blanchet et al., 2015). Images were recorded using a photon counting Pilatus-2M detector at a sample to detector distance of 3.1 m and a wavelength (λ) of 1.2 Å covering the range of momentum transfer $0.01 < s < 0.5$ Å^{-1}; with $s = 4\pi\sin\theta/\lambda$, where 2θ is the scattering angle. To obtain data from a monodisperse sample from TgMORN1(7-15) and TbMORN1(7-15), a size exclusion chromatography column directly coupled to the scattering experiment (SEC-SAXS) was employed. The parallel collection of UV and light scattering data allowed the protein to be monitored while it eluted from the column (Graewert et al., 2015). Throughout the complete chromatography process, 1 s sample exposures were recorded. As mobile phase, the various buffers were used: TbMORN1(7-15): 20mM Tris-HCl pH 8.5, 200 mM NaCl, 2% (v/v) glycerol, 1 mM DTT. TgMORN1(7-15): 20 mM Tris-HCl pH 7.5, 100 mM NaCl. 100 μl of purified sample (3.8 mg/mL TbMORN1(7-15) and 2.6 mg/ml TgMORN1(7-15)) were injected onto a Superdex 200 10/300 (GE Healthcare) column and the flow rate was set to 0.5 ml/min. SAXS data were recorded from macromolecular free fractions corresponding to the matched solvent blank. PfMORN1(7-15) was measured in batch mode from a concentration series spanning 1-8 mg/ml. 20 mM Tris-HCl pH 7.5, 100 mM NaCl buffer was measured for background subtraction. As a concentration dependent increase in size was detectable further analysis were based solely on the data collected at 1 mg/ml. In a similar manner as described above, TbMORN1(2-15) data were collected at ESRF BM29 beamline (Pernot et al., 2013) in SEC-SAXS mode with the setup described in by Brennich et al. (Brennich et al., 2017). SAXS data from the run were collected at a wavelength of 0.99 Å using a sample-to-detector (PILATUS 1 M, DECTRIS) distance of 2.867 m. Here too, a Superdex 200 10/300 (GE Healthcare) column was used as well as 20 mM Tris-HCl pH 7.5, 100 mM NaCl as mobile phase. 100 µl of 5.8 mg/ml TbMORN1(2-15) were injected. Data reduction to produce final scattering profiles of dimeric MORN1 constructs were performed using standard methods. Briefly, 2D-to-1D radial averaging was performed using the SASFLOW pipeline (Franke et al., 2017). For data collected at ESRF EDNA pipeline (Brennich et al., 2016) was used. CHROMIXS was used for the visualisation and reduction of the SEC-SAXS datasets (Panjkovich & Svergun, 2018). Aided by the integrated prediction algorithms in CHROMIXS the optimal frames within the elution peak and the buffer regions were selected. Single buffer frames were then subtracted from sample frames one by one, scaled and averaged to produce the final subtracted curve. The indirect inverse Fourier transform of the SAXS data and the corresponding probable real space-scattering pair distance distribution (p(r) versus r profile) of the various MORN1 constructs were calculated using GNOM (Svergun, 1992), from which the R_g and D_{max} were determined. The p(r) versus r profile were also used for *ab initio* bead modelling of selected MORN1 constructs. For this, 20 independent runs of DAMMIF (Franke

& Svergun, 2009) in the case of TbMORN1(2-15) and DAMMIN (Svergun, 1999) in case of the shorter MORN1(7-15) constructs were performed. From these the most probable models were selected by DAMAVER (Volkov & Svergun, 2003). The ab initio modelling was performed with and without symmetry constraints (p2 symmetry to reflect the dimeric state of the protein). Comparison with theoretical curves calculated from the X-tal structures described here was performed with Crysol (Svergun et al., 1995). Due to the elongated nature of the molecules, fits were improved by increasing LM (maximum order of harmonics) to 50. The molecular mass (MM) was evaluated based on concentration independent methods according to Porod (Porod, 1951) and as implemented in the ATSAS package. Dimensionless Kratky plots were constructed according to (Receveur-Brechot & Durand, 2012)_and the reference point for globular proteins at √3, 1.1 indicated. Graphical representation was produced using Pymol Molecular Graphics System (Schrödinger, LLC.). The SAXS data (Table S3) and ab initio bead models as well as fits to the crystal structures described within this work have been deposited into the Small-Angle Scattering Biological Data Bank (SASBDB) (Valentini et al., 2015) under the accession codes SASDG97, SASDGA7, SASDGB7, SASDGC7.

Transmission electron microscopy (EM) with rotary shadowing

TbMORN1 and TbMORN1(2-15) were purified according to the two-step procedure detailed above. They were then diluted in spraying buffer (100 mM $NH_4CH_3CO_2$-NaOH pH 8.5, 30% (v/v) glycerol) to a final concentration of 50 – 100 μg/ml. Diluted samples were sprayed onto freshly cleaved mica chips (Christine Gröpl) and immediately transferred into a MED020 high vacuum evaporator (BAL-TEC) equipped with electron guns. While rotating, samples were coated with 0.6 nm of Platinum (BALTIC) at an angle of 4°, followed by 6 nm of Carbon (Oerlicon) at 90°. The obtained replicas were floated off the mica chips, transferred to 400 mesh Cu/Pd grids (Agar Scientific), and examined using a Morgagni 268D transmission electron microscope (FEI) operated at 80 kV. Images were acquired using an 11 megapixel Morada CCD camera (Olympus-SIS).

ACKNOWLEDGEMENTS

Financial support was from Austrian Science Fund (FWF) grants P22265-B12 FWF (to Graham Warren) P27016-B21 (to Brooke Morriswood and Kristina Djinovic-Carugo), P28135 and P30584 (both to Tom Leonard). Kristina Djinovic-Carugo's research was additionally supported by Austrian Science Fund (FWF) Projects I525 and I1593, P22276, P19060 and W1221, Federal Ministry of Economy, Family and Youth through the initiative “Laura Bassi Centres of Expertise”, funding the Centre of Optimized Structural Studies, N°253275, by the Wellcome Trust Collaborative Award (201543/Z/16), COST action BM1405 - Non-globular proteins - from sequence to structure, function and application in molecular physiopathology (NGP-NET), WWTF (Vienna Science and Technology Fund) Chemical Biology project LS17-008, and by the University of Vienna. Funding also came from Medical Research Council grant MR/Mo20118/1 (to Terry Smith). We are indebted to Graham Warren (MRC Laboratory for Molecular Cell Biology, University College London), for comments and support. We are grateful to Sonja Lorenz (University of Würzburg) for critical reading of the manuscript. Valeria

1542 Stefania carried out the SAXS measurements. The Martens group at the Max Perutz Labs
1543 Vienna provided the Doc2B protein; Iva Lucic in the Leonard group supplied the Akt protein.
1544 Euripedes Almeida Ribeiro advised on fluorescence anisotropy measurements. Markus
1545 Engstler (University of Würzburg) provided the bloodstream form GFP cells as well as lab
1546 space and support. Susanne Fenz (University of Würzburg) assisted with the purification of
1547 trypanosome lipids. The authors thank the staff of MX and SAXS beamlines at ESRF in
1548 Grenoble and EMBL-Hamburg for their excellent support. EM data were recorded at the EM
1549 Facility of the Vienna BioCenter Core Facilities GmbH (VBCF), a member of the Vienna
1550 BioCenter (VBC), Austria. Proteomics analyses were performed by the Mass Spectrometry
1551 Facility at Max Perutz Labs Vienna using the VBCF instrument pool.
1552
1553
1554
1555

1556 # References

1557 Adam SA, Marr RS, Gerace L (1990) Nuclear protein import in permeabilized mammalian
1558 cells requires soluble cytoplasmic factors. *J Cell Biol* 111: 807-16

1559 Adams PD, Afonine PV, Bunkoczi G, Chen VB, Davis IW, Echols N, Headd JJ, Hung LW,
1560 Kapral GJ, Grosse-Kunstleve RW, McCoy AJ, Moriarty NW, Oeffner R, Read RJ,
1561 Richardson DC, Richardson JS, Terwilliger TC, Zwart PH (2010) PHENIX: a comprehensive
1562 Python-based system for macromolecular structure solution. *Acta Crystallogr D Biol*
1563 *Crystallogr* 66: 213-21

1564 Adl SM, Bass D, Lane CE, Lukes J, Schoch CL, Smirnov A, Agatha S, Berney C, Brown
1565 MW, Burki F, Cardenas P, Cepicka I, Chistyakova L, Del Campo J, Dunthorn M, Edvardsen
1566 B, Eglit Y, Guillou L, Hampl V, Heiss AA et al. (2019) Revisions to the Classification,
1567 Nomenclature, and Diversity of Eukaryotes. *J Eukaryot Microbiol* 66: 4-119

1568 Allen CL, Goulding D, Field MC (2003) Clathrin-mediated endocytosis is essential in
1569 Trypanosoma brucei. *Embo J* 22: 4991-5002

1570 Andrade MA, Perez-Iratxeta C, Ponting CP (2001) Protein repeats: structures, functions, and
1571 evolution. *J Struct Biol* 134: 117-31

1572 Bangs JD, Uyetake L, Brickman MJ, Balber AE, Boothroyd JC (1993) Molecular cloning and
1573 cellular localization of a BiP homologue in Trypanosoma brucei. Divergent ER retention
1574 signals in a lower eukaryote. *J Cell Sci* 105 (Pt 4): 1101-13

1575 Bastin P, Bagherzadeh Z, Matthews KR, Gull K (1996) A novel epitope tag system to study
1576 protein targeting and organelle biogenesis in Trypanosoma brucei. *Mol Biochem Parasitol*
1577 77: 235-9

1578 Batram C, Jones NG, Janzen CJ, Markert SM, Engstler M (2014) Expression site
1579 attenuation mechanistically links antigenic variation and development in Trypanosoma
1580 brucei. *Elife* 3: e02324

1581 Bennett HJ, Davenport JB, Collins RF, Trafford AW, Pinali C, Kitmitto A (2013) Human
1582 junctophilin-2 undergoes a structural rearrangement upon binding PtdIns(3,4,5)P3 and the

1583 S101R mutation identified in hypertrophic cardiomyopathy obviates this response. *Biochem*
1584 *J* 456: 205-17

1585 Blanchet CE, Spilotros A, Schwemmer F, Graewert MA, Kikhney A, Jeffries CM, Franke D,
1586 Mark D, Zengerle R, Cipriani F, Fiedler S, Roessle M, Svergun DI (2015) Versatile sample
1587 environments and automation for biological solution X-ray scattering experiments at the P12
1588 beamline (PETRA III, DESY). *J Appl Crystallogr* 48: 431-443

1589 Bligh EG, Dyer WJ (1959) A rapid method of total lipid extraction and purification. *Can J*
1590 *Biochem Physiol* 37: 911-7

1591 Brennich ME, Kieffer J, Bonamis G, Antolinos AD, Hutin S, Pernot P, Round A (2016) Online
1592 data analysis at the ESRF bioSAXS beamline, BM29. *Journal of Applied Crystallography* 49:
1593 203-212

1594 Brennich ME, Round AR, Hutin S (2017) Online Size-exclusion and Ion-exchange
1595 Chromatography on a SAXS Beamline. *J Vis Exp*

1596 Burkard G, Fragoso CM, Roditi I (2007) Highly efficient stable transformation of bloodstream
1597 forms of Trypanosoma brucei. *Mol Biochem Parasitol* 153: 220-3

1598 Camacho L, Smertenko AP, Perez-Gomez J, Hussey PJ, Moore I (2009) Arabidopsis Rab-E
1599 GTPases exhibit a novel interaction with a plasma-membrane phosphatidylinositol-4-
1600 phosphate 5-kinase. *J Cell Sci* 122: 4383-92

1601 Carman PJ, Dominguez R (2018) BAR domain proteins-a linkage between cellular
1602 membranes, signaling pathways, and the actin cytoskeleton. *Biophys Rev* 10: 1587-1604

1603 Chung J, Torta F, Masai K, Lucast L, Czapla H, Tanner LB, Narayanaswamy P, Wenk MR,
1604 Nakatsu F, De Camilli P (2015) INTRACELLULAR TRANSPORT. PI4P/phosphatidylserine
1605 countertransport at ORP5- and ORP8-mediated ER-plasma membrane contacts. *Science*
1606 349: 428-32

1607 Cronan JE (2003) Bacterial membrane lipids: where do we stand? *Annu Rev Microbiol* 57:
1608 203-24

1609 Demmel L, Schmidt K, Lucast L, Havlicek K, Zankel A, Koestler T, Reithofer V, de Camilli P,
1610 Warren G (2014) The endocytic activity of the flagellar pocket in Trypanosoma brucei is
1611 regulated by an adjacent phosphatidylinositol phosphate kinase. *Journal of cell science* 127:
1612 2351-64

1613 Doyle SA (2005) High-throughput cloning for proteomics research. *Methods Mol Biol* 310:
1614 107-13

1615 El-Gebali S, Mistry J, Bateman A, Eddy SR, Luciani A, Potter SC, Qureshi M, Richardson
1616 LJ, Salazar GA, Smart A, Sonnhammer ELL, Hirsh L, Paladin L, Piovesan D, Tosatto SCE,
1617 Finn RD (2019) The Pfam protein families database in 2019. *Nucleic Acids Res* 47: D427-
1618 D432

1619 Emsley P, Cowtan K (2004) Coot: model-building tools for molecular graphics. *Acta*
1620 *Crystallogr D Biol Crystallogr* 60: 2126-32

1621 Engstler M, Thilo L, Weise F, Grunfelder CG, Schwarz H, Boshart M, Overath P (2004)
1622 Kinetics of endocytosis and recycling of the GPI-anchored variant surface glycoprotein in
1623 Trypanosoma brucei. *Journal of cell science* 117: 1105-15

1624 Epand RM, Epand RF (2009) Lipid domains in bacterial membranes and the action of
1625 antimicrobial agents. *Biochim Biophys Acta* 1788: 289-94

1626 Esson HJ, Morriswood B, Yavuz S, Vidilaseris K, Dong G, Warren G (2012) Morphology of
1627 the trypanosome bilobe, a novel cytoskeletal structure. *Eukaryot Cell* 11: 761-72

1628 Franke D, Petoukhov MV, Konarev PV, Panjkovich A, Tuukkanen A, Mertens HDT, Kikhney
1629 AG, Hajizadeh NR, Franklin JM, Jeffries CM, Svergun DI (2017) ATSAS 2.8: a
1630 comprehensive data analysis suite for small-angle scattering from macromolecular solutions.
1631 *J Appl Crystallogr* 50: 1212-1225

1632 Franke D, Svergun DI (2009) DAMMIF, a program for rapid ab-initio shape determination in
1633 small-angle scattering. *J Appl Crystallogr* 42: 342-346

1634 Franzot G, Sjoblom B, Gautel M, Djinovic Carugo K (2005) The crystal structure of the actin
1635 binding domain from alpha-actinin in its closed conformation: structural insight into
1636 phospholipid regulation of alpha-actinin. *J Mol Biol* 348: 151-65

1637 Fyffe SA, Alphey MS, Buetow L, Smith TK, Ferguson MA, Sorensen MD, Bjorkling F, Hunter
1638 WN (2006) Reevaluation of the PPAR-beta/delta ligand binding domain model reveals why it
1639 exhibits the activated form. *Mol Cell* 21: 1-2

1640 Gibson DG, Young L, Chuang RY, Venter JC, Hutchison CA, 3rd, Smith HO (2009)
1641 Enzymatic assembly of DNA molecules up to several hundred kilobases. *Nat Methods* 6:
1642 343-5

1643 Graewert MA, Franke D, Jeffries CM, Blanchet CE, Ruskule D, Kuhle K, Flieger A, Schafer
1644 B, Tartsch B, Meijers R, Svergun DI (2015) Automated pipeline for purification, biophysical
1645 and x-ray analysis of biomacromolecular solutions. *Sci Rep* 5: 10734

1646 Grunfelder CG, Engstler M, Weise F, Schwarz H, Stierhof YD, Morgan GW, Field MC,
1647 Overath P (2003) Endocytosis of a glycosylphosphatidylinositol-anchored protein via
1648 clathrin-coated vesicles, sorting by default in endosomes, and exocytosis via RAB11-positive
1649 carriers. *Mol Biol Cell* 14: 2029-40

1650 Gubbels MJ, Vaishnava S, Boot N, Dubremetz JF, Striepen B (2006) A MORN-repeat
1651 protein is a dynamic component of the Toxoplasma gondii cell division apparatus. *J Cell Sci*
1652 119: 2236-45

1653 Guo A, Wang Y, Chen B, Wang Y, Yuan J, Zhang L, Hall D, Wu J, Shi Y, Zhu Q, Chen C,
1654 Thiel WH, Zhan X, Weiss RM, Zhan F, Musselman CA, Pufall M, Zhu W, Au KF, Hong J et
1655 al. (2018) E-C coupling structural protein junctophilin-2 encodes a stress-adaptive
1656 transcription regulator. *Science* 362

1657 Habicht J, Woehle C, Gould SB (2015) Tetrahymena Expresses More than a Hundred
1658 Proteins with Lipid-binding MORN Motifs that can Differ in their Subcellular Localisations. *J*
1659 *Eukaryot Microbiol* 62: 694-700

1660 Hatzopoulos GN, Erat MC, Cutts E, Rogala KB, Slater LM, Stansfeld PJ, Vakonakis I (2013)
1661 Structural analysis of the G-box domain of the microcephaly protein CPAP suggests a role in
1662 centriole architecture. *Structure* 21: 2069-77

1663 Hemsley A, Arnheim N, Toney MD, Cortopassi G, Galas DJ (1989) A simple method for site-
1664 directed mutagenesis using the polymerase chain reaction. *Nucleic Acids Res* 17: 6545-51

1665 Holm L, Laakso LM (2016) Dali server update. *Nucleic Acids Res* 44: W351-5

1666 Holm L, Rosenstrom P (2010) Dali server: conservation mapping in 3D. *Nucleic Acids Res*
1667 38: W545-9

1668 Hu K (2008) Organizational changes of the daughter basal complex during the parasite
1669 replication of Toxoplasma gondii. *PLoS Pathog* 4: e10

1670 Hutchinson EG, Thornton JM (1994) A revised set of potentials for beta-turn formation in
1671 proteins. *Protein Sci* 3: 2207-16

1672 Im YJ, Davis AJ, Perera IY, Johannes E, Allen NS, Boss WF (2007) The N-terminal
1673 membrane occupation and recognition nexus domain of Arabidopsis phosphatidylinositol
1674 phosphate kinase 1 regulates enzyme activity. *J Biol Chem* 282: 5443-52

1675 Jacobs SA, Harp JM, Devarakonda S, Kim Y, Rastinejad F, Khorasanizadeh S (2002) The
1676 active site of the SET domain is constructed on a knot. *Nat Struct Biol* 9: 833-8

1677 Jayasinghe I, Clowsley AH, Lin R, Lutz T, Harrison C, Green E, Baddeley D, Di Michele L,
1678 Soeller C (2018) True Molecular Scale Visualization of Variable Clustering Properties of
1679 Ryanodine Receptors. *Cell Rep* 22: 557-567

1680 Jiang M, Hu J, White FKH, Williamson J, Klymchenko AS, Murthy A, Workman SW, Tseng
1681 GN (2019) S-Palmitoylation of junctophilin-2 is critical for its role in tethering the
1682 sarcoplasmic reticulum to the plasma membrane. *J Biol Chem* 294: 13487-13501

1683 Joosten RP, Long F, Murshudov GN, Perrakis A (2014) The PDB_REDO server for
1684 macromolecular structure model optimization. *IUCrJ* 1: 213-20

1685 Kabsch W (2010) Xds. *Acta Crystallogr D Biol Crystallogr* 66: 125-32

1686 Kajava AV (2012) Tandem repeats in proteins: from sequence to structure. *J Struct Biol* 179:
1687 279-88

1688 Kelly SM, Jess TJ, Price NC (2005) How to study proteins by circular dichroism. *Biochim*
1689 *Biophys Acta* 1751: 119-39

1690 Kohl L, Sherwin T, Gull K (1999) Assembly of the paraflagellar rod and the flagellum
1691 attachment zone complex during the Trypanosoma brucei cell cycle. *J Eukaryot Microbiol*
1692 46: 105-9

1693 Krissinel E, Henrick K (2007) Inference of macromolecular assemblies from crystalline state.
1694 *J Mol Biol* 372: 774-97

1695 Kunita R, Otomo A, Mizumura H, Suzuki K, Showguchi-Miyata J, Yanagisawa Y, Hadano S,
1696 Ikeda JE (2004) Homo-oligomerization of ALS2 through its unique carboxyl-terminal regions

1697 is essential for the ALS2-associated Rab5 guanine nucleotide exchange activity and its
1698 regulatory function on endosome trafficking. *J Biol Chem* 279: 38626-35

1699 Lacomble S, Vaughan S, Gadelha C, Morphew MK, Shaw MK, McIntosh JR, Gull K (2009)
1700 Three-dimensional cellular architecture of the flagellar pocket and associated cytoskeleton in
1701 trypanosomes revealed by electron microscope tomography. *Journal of cell science* 122:
1702 1081-90

1703 Li J, Liu H, Raval MH, Wan J, Yengo CM, Liu W, Zhang M (2019) Structure of the
1704 MORN4/Myo3a Tail Complex Reveals MORN Repeats as Protein Binding Modules.
1705 *Structure*

1706 Li MZ, Elledge SJ (2012) SLIC: a method for sequence- and ligation-independent cloning.
1707 *Methods Mol Biol* 852: 51-9

1708 Ma H, Lou Y, Lin WH, Xue HW (2006) MORN motifs in plant PIPKs are involved in the
1709 regulation of subcellular localization and phospholipid binding. *Cell Res* 16: 466-78

1710 Maeda K, Anand K, Chiapparino A, Kumar A, Poletto M, Kaksonen M, Gavin AC (2013)
1711 Interactome map uncovers phosphatidylserine transport by oxysterol-binding proteins.
1712 *Nature* 501: 257-61

1713 Marvin RG, Wolford JL, Kidd MJ, Murphy S, Ward J, Que EL, Mayer ML, Penner-Hahn JE,
1714 Haldar K, O'Halloran TV (2012) Fluxes in "free" and total zinc are essential for progression
1715 of intraerythrocytic stages of Plasmodium falciparum. *Chem Biol* 19: 731-41

1716 McCoy AJ, Grosse-Kunstleve RW, Adams PD, Winn MD, Storoni LC, Read RJ (2007)
1717 Phaser crystallographic software. *J Appl Crystallogr* 40: 658-674

1718 Mecklenburg KL (2007) Drosophila retinophilin contains MORN repeats and is conserved in
1719 humans. *Mol Genet Genomics* 277: 481-9

1720 Micsonai A, Wien F, Bulyaki E, Kun J, Moussong E, Lee YH, Goto Y, Refregiers M, Kardos J
1721 (2018) BeStSel: a web server for accurate protein secondary structure prediction and fold
1722 recognition from the circular dichroism spectra. *Nucleic Acids Res* 46: W315-W322

1723 Micsonai A, Wien F, Kernya L, Lee YH, Goto Y, Refregiers M, Kardos J (2015) Accurate
1724 secondary structure prediction and fold recognition for circular dichroism spectroscopy. *Proc*
1725 *Natl Acad Sci U S A* 112: E3095-103

1726 Mikami K, Saavedra L, Sommarin M (2010) Is membrane occupation and recognition nexus
1727 domain functional in plant phosphatidylinositol phosphate kinases? *Plant Signal Behav* 5:
1728 1241-4

1729 Molla-Herman A, Ghossoub R, Blisnick T, Meunier A, Serres C, Silbermann F, Emmerson C,
1730 Romeo K, Bourdoncle P, Schmitt A, Saunier S, Spassky N, Bastin P, Benmerah A (2010)
1731 The ciliary pocket: an endocytic membrane domain at the base of primary and motile cilia. *J*
1732 *Cell Sci* 123: 1785-95

1733 Morriswood B, Havlicek K, Demmel L, Yavuz S, Sealey-Cardona M, Vidilaseris K, Anrather
1734 D, Kostan J, Djinovic-Carugo K, Roux KJ, Warren G (2013) Novel Bilobe Components in
1735 Trypanosoma brucei Identified Using Proximity-Dependent Biotinylation. *Eukaryot Cell* 12:
1736 356-67

1737 Morriswood B, He CY, Sealey-Cardona M, Yelinek J, Pypaert M, Warren G (2009) The
1738 bilobe structure of Trypanosoma brucei contains a MORN-repeat protein. *Mol Biochem*
1739 *Parasitol* 167: 95-103

1740 Morriswood B, Schmidt K (2015) A MORN-repeat protein facilitates protein entry into the
1741 flagellar pocket of Trypanosoma brucei. *Eukaryot Cell*

1742 Moser von Filseck J, Copic A, Delfosse V, Vanni S, Jackson CL, Bourguet W, Drin G (2015)
1743 INTRACELLULAR TRANSPORT. Phosphatidylserine transport by ORP/Osh proteins is
1744 driven by phosphatidylinositol 4-phosphate. *Science* 349: 432-6

1745 Munro ML, Jayasinghe ID, Wang Q, Quick A, Wang W, Baddeley D, Wehrens XH, Soeller C
1746 (2016) Junctophilin-2 in the nanoscale organisation and functional signalling of ryanodine
1747 receptor clusters in cardiomyocytes. *J Cell Sci* 129: 4388-4398

1748 Murshudov GN, Vagin AA, Dodson EJ (1997) Refinement of macromolecular structures by
1749 the maximum-likelihood method. *Acta Crystallogr D Biol Crystallogr* 53: 240-55

1750 Nakada T, Kashihara T, Komatsu M, Kojima K, Takeshita T, Yamada M (2018) Physical
1751 interaction of junctophilin and the CaV1.1 C terminus is crucial for skeletal muscle
1752 contraction. *Proc Natl Acad Sci U S A* 115: 4507-4512

1753 Otomo A, Hadano S, Okada T, Mizumura H, Kunita R, Nishijima H, Showguchi-Miyata J,
1754 Yanagisawa Y, Kohiki E, Suga E, Yasuda M, Osuga H, Nishimoto T, Narumiya S, Ikeda JE
1755 (2003) ALS2, a novel guanine nucleotide exchange factor for the small GTPase Rab5, is
1756 implicated in endosomal dynamics. *Hum Mol Genet* 12: 1671-87

1757 Panjkovich A, Svergun DI (2018) CHROMIXS: automatic and interactive analysis of
1758 chromatography-coupled small-angle X-ray scattering data. *Bioinformatics* 34: 1944-1946

1759 Pelletier L, Stern CA, Pypaert M, Sheff D, Ngo HM, Roper N, He CY, Hu K, Toomre D,
1760 Coppens I, Roos DS, Joiner KA, Warren G (2002) Golgi biogenesis in Toxoplasma gondii.
1761 *Nature* 418: 548-52

1762 Perni S, Lavorato M, Beam KG (2017) De novo reconstitution reveals the proteins required
1763 for skeletal muscle voltage-induced Ca(2+) release. *Proc Natl Acad Sci U S A* 114: 13822-
1764 13827

1765 Pernot P, Round A, Barrett R, De Maria Antolinos A, Gobbo A, Gordon E, Huet J, Kieffer J,
1766 Lentini M, Mattenet M, Morawe C, Mueller-Dieckmann C, Ohlsson S, Schmid W, Surr J,
1767 Theveneau P, Zerrad L, McSweeney S (2013) Upgraded ESRF BM29 beamline for SAXS
1768 on macromolecules in solution. *J Synchrotron Radiat* 20: 660-4

1769 Porod G (1951) Die Rontgenkleinwinkelstreuung Von Dichtgepackten Kolloiden Systemen
1770 .1. *Kolloid Z Z Polym* 124: 83-114

1771 Rao VD, Misra S, Boronenkov IV, Anderson RA, Hurley JH (1998) Structure of type IIbeta
1772 phosphatidylinositol phosphate kinase: a protein kinase fold flattened for interfacial
1773 phosphorylation. *Cell* 94: 829-39

1774 Rappsilber J, Mann M, Ishihama Y (2007) Protocol for micro-purification, enrichment, pre-
1775 fractionation and storage of peptides for proteomics using StageTips. *Nat Protoc* 2: 1896-
1776 906

1777 Receveur-Brechot V, Durand D (2012) How random are intrinsically disordered proteins? A
1778 small angle scattering perspective. *Curr Protein Pept Sci* 13: 55-75

1779 Richmond GS, Gibellini F, Young SA, Major L, Denton H, Lilley A, Smith TK (2010)
1780 Lipidomic analysis of bloodstream and procyclic form Trypanosoma brucei. *Parasitology*
1781 137: 1357-92

1782 Rossi D, Scarcella AM, Liguori E, Lorenzini S, Pierantozzi E, Kutchukian C, Jacquemond V,
1783 Messa M, De Camilli P, Sorrentino V (2019) Molecular determinants of homo- and
1784 heteromeric interactions of Junctophilin-1 at triads in adult skeletal muscle fibers. *Proc Natl*
1785 *Acad Sci U S A* 116: 15716-15724

1786 Saliba AE, Vonkova I, Ceschia S, Findlay GM, Maeda K, Tischer C, Deghou S, van Noort V,
1787 Bork P, Pawson T, Ellenberg J, Gavin AC (2014) A quantitative liposome microarray to
1788 systematically characterize protein-lipid interactions. *Nat Methods* 11: 47-50

1789 Saliba AE, Vonkova I, Deghou S, Ceschia S, Tischer C, Kugler KG, Bork P, Ellenberg J,
1790 Gavin AC (2016) A protocol for the systematic and quantitative measurement of protein-lipid
1791 interactions using the liposome-microarray-based assay. *Nat Protoc* 11: 1021-38

1792 Salzer U, Kostan J, Djinovic-Carugo K (2017) Deciphering the BAR code of membrane
1793 modulators. *Cell Mol Life Sci* 74: 2413-2438

1794 Scholz J, Besir H, Strasser C, Suppmann S (2013) A new method to customize protein
1795 expression vectors for fast, efficient and background free parallel cloning. *BMC Biotechnol*
1796 13: 12

1797 Schumann Burkard G, Jutzi P, Roditi I (2011) Genome-wide RNAi screens in bloodstream
1798 form trypanosomes identify drug transporters. *Mol Biochem Parasitol* 175: 91-4

1799 Studier FW (2005) Protein production by auto-induction in high density shaking cultures.
1800 *Protein Expr Purif* 41: 207-34

1801 Svergun D, Barberato C, Koch MHJ (1995) CRYSOL - A program to evaluate x-ray solution
1802 scattering of biological macromolecules from atomic coordinates. *Journal of Applied*
1803 *Crystallography* 28: 768-773

1804 Svergun DI (1992) Determination of the Regularization Parameter in Indirect-Transform
1805 Methods Using Perceptual Criteria. *Journal of Applied Crystallography* 25: 495-503

1806 Svergun DI (1999) Restoring low resolution structure of biological macromolecules from
1807 solution scattering using simulated annealing. *Biophys J* 76: 2879-86

1808 Takeshima H, Komazaki S, Nishi M, Iino M, Kangawa K (2000) Junctophilins: a novel family
1809 of junctional membrane complex proteins. *Mol Cell* 6: 11-22

1810 Tsuchida J, Nishina Y, Wakabayashi N, Nozaki M, Sakai Y, Nishimune Y (1998) Molecular
1811 cloning and characterization of meichroacidin (male meiotic metaphase chromosome-
1812 associated acidic protein). *Dev Biol* 197: 67-76

1813 Tyanova S, Temu T, Cox J (2016) The MaxQuant computational platform for mass
1814 spectrometry-based shotgun proteomics. *Nat Protoc* 11: 2301-2319

1815 Valentini E, Kikhney AG, Previtali G, Jeffries CM, Svergun DI (2015) SASBDB, a repository
1816 for biological small-angle scattering data. *Nucleic Acids Res* 43: D357-63

1817 Volkov VV, Svergun DI (2003) Uniqueness of ab initio shape determination in small-angle
1818 scattering. *Journal of Applied Crystallography* 36: 860-864

1819 Walter TS, Meier C, Assenberg R, Au KF, Ren J, Verma A, Nettleship JE, Owens RJ, Stuart
1820 DI, Grimes JM (2006) Lysine methylation as a routine rescue strategy for protein
1821 crystallization. *Structure* 14: 1617-22

1822 Wilson JR, Jing C, Walker PA, Martin SR, Howell SA, Blackburn GM, Gamblin SJ, Xiao B
1823 (2002) Crystal structure and functional analysis of the histone methyltransferase SET7/9.
1824 *Cell* 111: 105-15

1825 Winn MD, Ballard CC, Cowtan KD, Dodson EJ, Emsley P, Evans PR, Keegan RM, Krissinel
1826 EB, Leslie AG, McCoy A, McNicholas SJ, Murshudov GN, Pannu NS, Potterton EA, Powell
1827 HR, Read RJ, Vagin A, Wilson KS (2011) Overview of the CCP4 suite and current
1828 developments. *Acta Crystallogr D Biol Crystallogr* 67: 235-42

1829 Wirtz E, Leal S, Ochatt C, Cross GA (1999) A tightly regulated inducible expression system
1830 for conditional gene knock-outs and dominant-negative genetics in Trypanosoma brucei. *Mol*
1831 *Biochem Parasitol* 99: 89-101

1832 Woo JS, Srikanth S, Nishi M, Ping P, Takeshima H, Gwack Y (2016) Junctophilin-4, a
1833 component of the endoplasmic reticulum-plasma membrane junctions, regulates Ca2+
1834 dynamics in T cells. *Proc Natl Acad Sci U S A* 113: 2762-7

1835 Xiao B, Jing C, Wilson JR, Walker PA, Vasisht N, Kelly G, Howell S, Taylor IA, Blackburn
1836 GM, Gamblin SJ (2003) Structure and catalytic mechanism of the human histone
1837 methyltransferase SET7/9. *Nature* 421: 652-6

1838 Yamanaka K, Vande Velde C, Eymard-Pierre E, Bertini E, Boespflug-Tanguy O, Cleveland
1839 DW (2003) Unstable mutants in the peripheral endosomal membrane component ALS2
1840 cause early-onset motor neuron disease. *Proc Natl Acad Sci U S A* 100: 16041-6

1841 Yang B, Wu YJ, Zhu M, Fan SB, Lin J, Zhang K, Li S, Chi H, Li YX, Chen HF, Luo SK, Ding
1842 YH, Wang LH, Hao Z, Xiu LY, Chen S, Ye K, He SM, Dong MQ (2012) Identification of
1843 cross-linked peptides from complex samples. *Nat Methods* 9: 904-6

1844 Yuan ZF, Liu C, Wang HP, Sun RX, Fu Y, Zhang JF, Wang LH, Chi H, Li Y, Xiu LY, Wang
1845 WP, He SM (2012) pParse: a method for accurate determination of monoisotopic peaks in
1846 high-resolution mass spectra. *Proteomics* 12: 226-35
1847

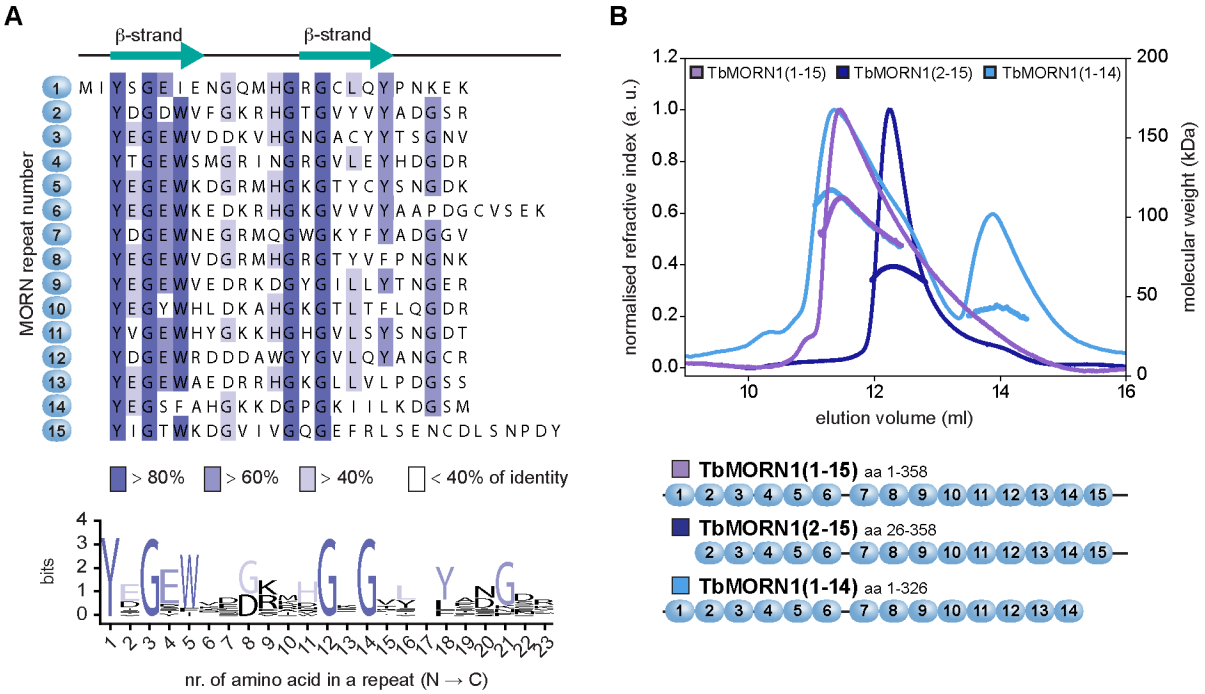

Figure 1. TbMORN1 primary structure and dimerisation. (A) Primary structure of TbMORN1, with individual MORN repeats shown in alignment, and coloured according to amino acid conservation. A schematic of the predicted secondary structure of each repeat is shown above the alignment. A consensus amino acid sequence of the individual MORN repeats from TbMORN1 based on the alignment is shown in the sequence logo. (B) TbMORN1 dimerises via its C-terminus. SEC-MALS profiles of TbMORN1(1-15), TbMORN1 (2-15), and TbMORN1 (1-14). Schematics are shown underneath. TbMORN1(1-15) tended to form high-order assemblies, whereas removal of the first MORN repeat resulted in a monodisperse dimer. Removal of the last MORN repeat in TbMORN1 (1-14) resulted in a polydisperse mixture of higher-order assemblies, dimers, and monomers.

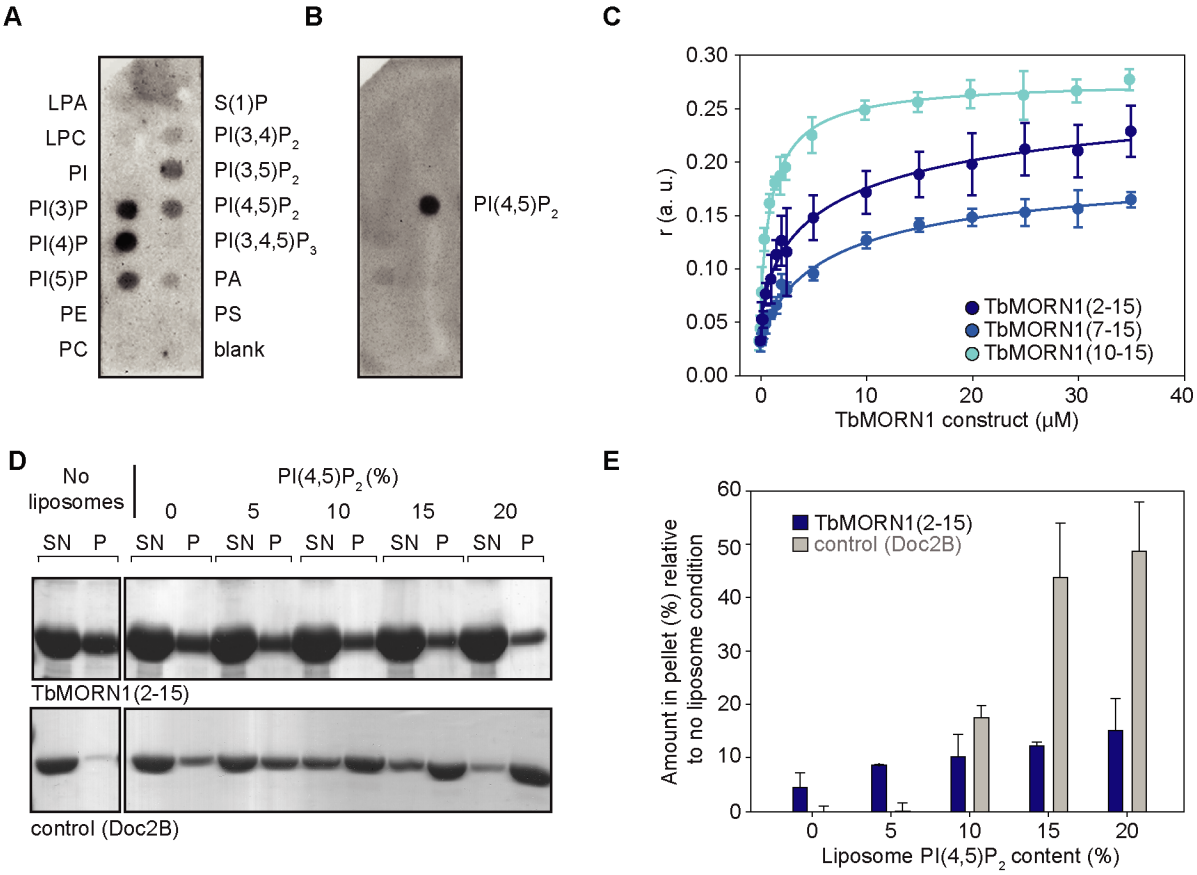

Figure 2. TbMORN1 interacts with phospholipids but not liposomes. (A) Purified recombinant TbMORN1 binds to multiple phospholipid species in protein-lipid overlay assays. PIP strips were incubated with purified recombinant TbMORN1(1-15) protein, and bound proteins were detected by immunoblotting with an anti-His tag antibody. Abbreviations: PI(n)P, phosphatidylinositol (n) phosphate; PA, phosphatidic acid; LPA, lysophosphatidic acid; LPC, lysophosphatidylcholine; PI, phosphatidylinositol; PE, phosphatidylethanolamine; PC, phosphatidylcholine; S(1)P, sphingosine-1-phosphate; PS, phosphatidylserine. Data were obtained from 3 independent experiments using 2 biological replicates; an exemplary blot is shown. (B) PIP strip overlaid with the PH domain of PLCδ, a positive control for PI(4,5)P_2 binding. Data were obtained from 3 independent experiments using 2 biological replicates; an exemplary blot is shown. The PIP strips presented here were exposed to the light source for the same time. (C) Fluorescence anisotropy measurements of 0.1 μM BODIPY TMR-PI(4,5)P_2 in the presence of TbMORN1(2-15), (7-15) and (10-15). All three truncations of TbMORN1 interacted with PI(4,5)P_2 with binding affinities in the low micromolar range. Data obtained from 3 independent experiments using 3 biological replicates, with 10 technical replicates for each experiment. Traces show mean values, bars are s.e.m. (D) Liposome co-sedimentation assay. POPC liposomes containing 0, 5, 10, 15 and 20% of porcine brain PI(4,5)P_2 were incubated with 10 μM TbMORN1(2-15). TbMORN1(2-15) was found in both pellet (P) and supernatant (SN) fractions but did not increase proportionally to PI(4,5)P_2 concentration. The positive control, Doc2B, bound PI(4,5)P_2 in a concentration-dependent manner, with a shift from SN to P fractions proportional to the increase in % of PI(4,5)P_2 present in the liposomes. Data were obtained from 2 independent experiments using 2 biological replicates; an exemplary blot is shown. (E) Quantification of the liposome pelleting assays. The amount of protein in the pellet fraction is presented relative to the amount present in the pellet fraction of the no liposome condition.

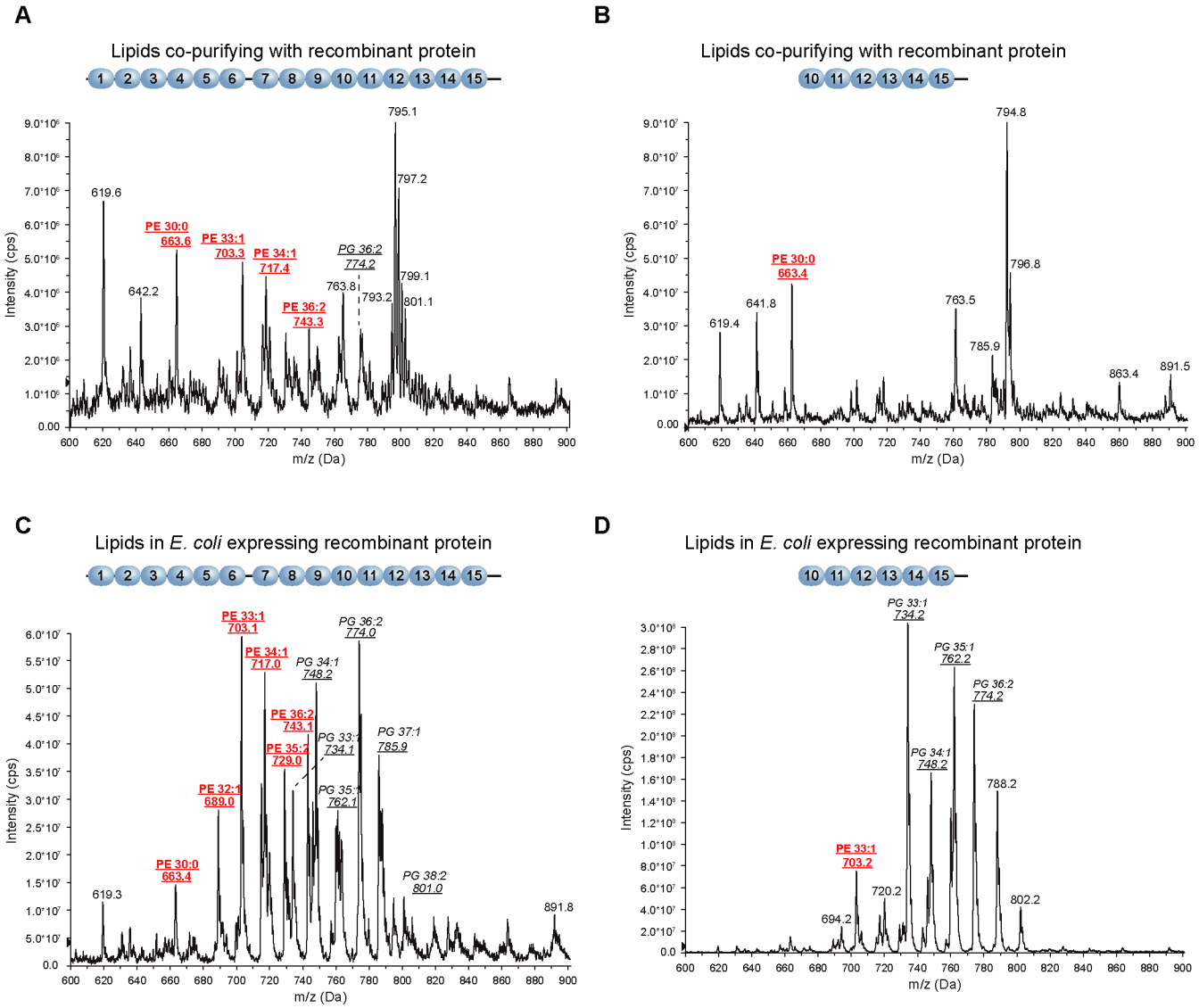

Figure 3. Recombinant TbMORN1 co-purifies with PE and increases *E. coli* PE levels. Negative ion mode survey scan (600-900 m/z) of lipid extracts from the indicated conditions. (A,B) Lipid extracts from purified recombinant TbMORN1(1-15) (A) and TbMORN1(10-15) (B). A large amount of PE co-purified with TbMORN1(1-15) but very little was associated with TbMORN1(10-15). (C,D) Lipid extracts from *E. coli* cells expressing the indicated constructs. (C) Cells expressing TbMORN1(1-15) had elevated PE levels. (D) Cells expressing TbMORN1(10-15) showed no changes to cellular lipid ratios compared to wild-type (empty vector control). In all cases, phospholipid identity was confirmed by daughter fragmentation and reported here. Schematics of the recombinant TbMORN1 constructs are shown above the traces.

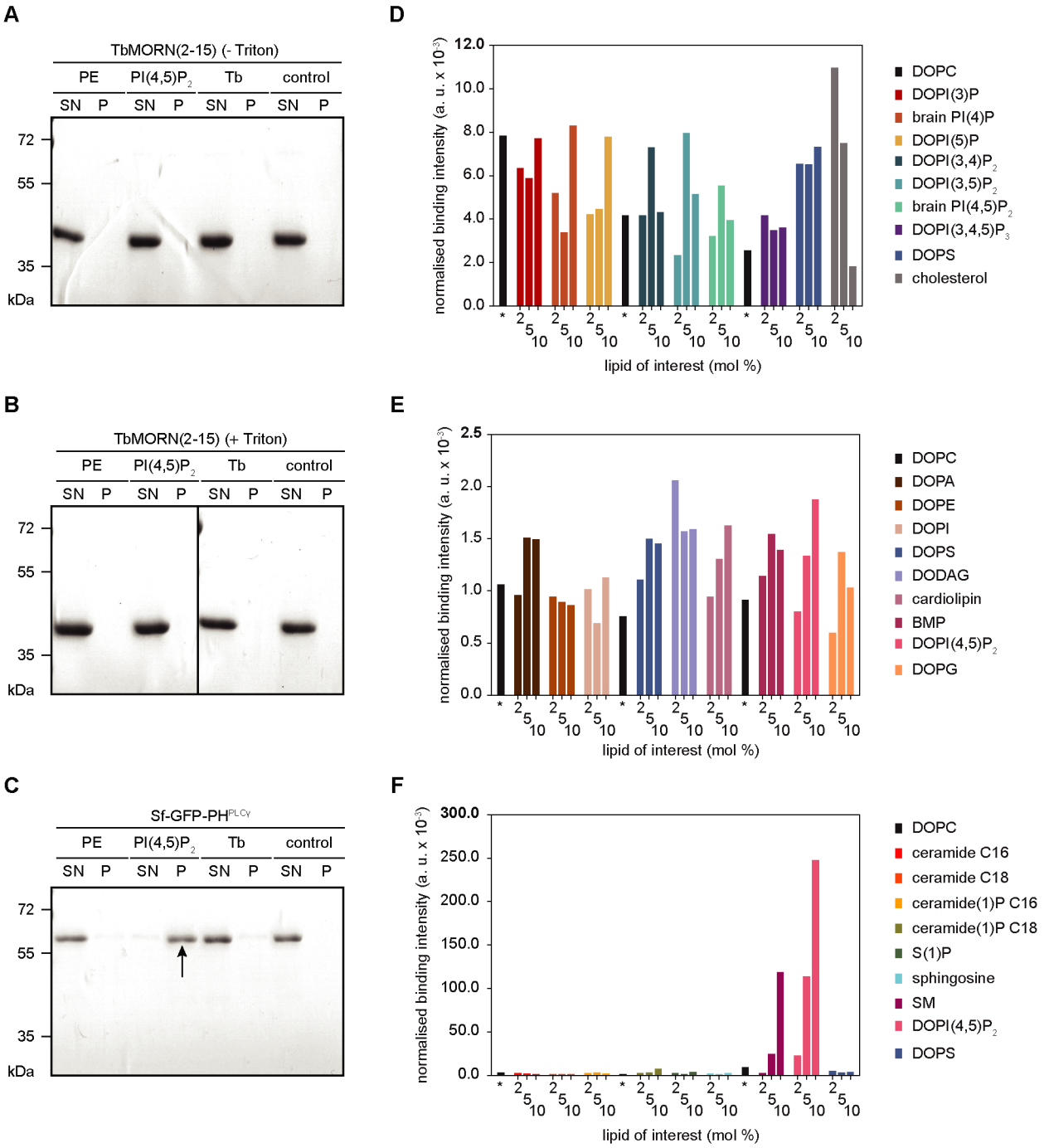

Figure 4. TbMORN1(2-15) does not bind to liposomes in vitro. (A-C) Liposome pelleting assays using sucrose-loaded vesicles (SLVs). His-TbMORN1(2-15) was purified in the absence (A) or presence (B) of Triton X-100 in the lysis buffer. The purified proteins were incubated with SLVs, which were then pelleted by centrifugation. Supernatant (SN) and pellet (P) fractions were analysed by SDS-PAGE using Coomassie staining. The SLVs were made from commercial lipids with an excess of either PE or PI(4,5)P_2, and also reconstituted from purified whole-cell trypanosome lipids (Tb). A no-SLV condition was included as an additional negative control. (C) The PH domains of PLCγ was used as a positive control for PI(4,5)P_2 binding. As expected, the PLCγ PH domain co-sedimented with PI(4,5)P_2-containing SLVs and was entirely present in the P fraction in this condition (arrow). The recombinant TbMORN1 proteins remained in the SN fraction in all conditions. (D-F) Liposome microarray analysis. Microchips carrying giant unilamellar vesicles (GUVs) with lipids of interest at three different concentrations (2, 5 and 10 mol %) were incubated with purified recombinant EGFP-TbMORN1(2-15). No significant binding was observed. (D) n (independent replicates) = 7; (E) n (independent replicates) = 3. (F) Microchip incubated with PLC-δ1 PH domain. A specific and concentration-dependent binding between the PLC-δ1 PH domain and DOPI(4,5)P_2 and SM was observed. DOPC, a carrier lipid, was used as an internal negative control of binding, as well as a marker for tracking positions of liposomes on a given microarray. n (independent replicates) = 1. Note the different scales on the y-axes of the three charts.

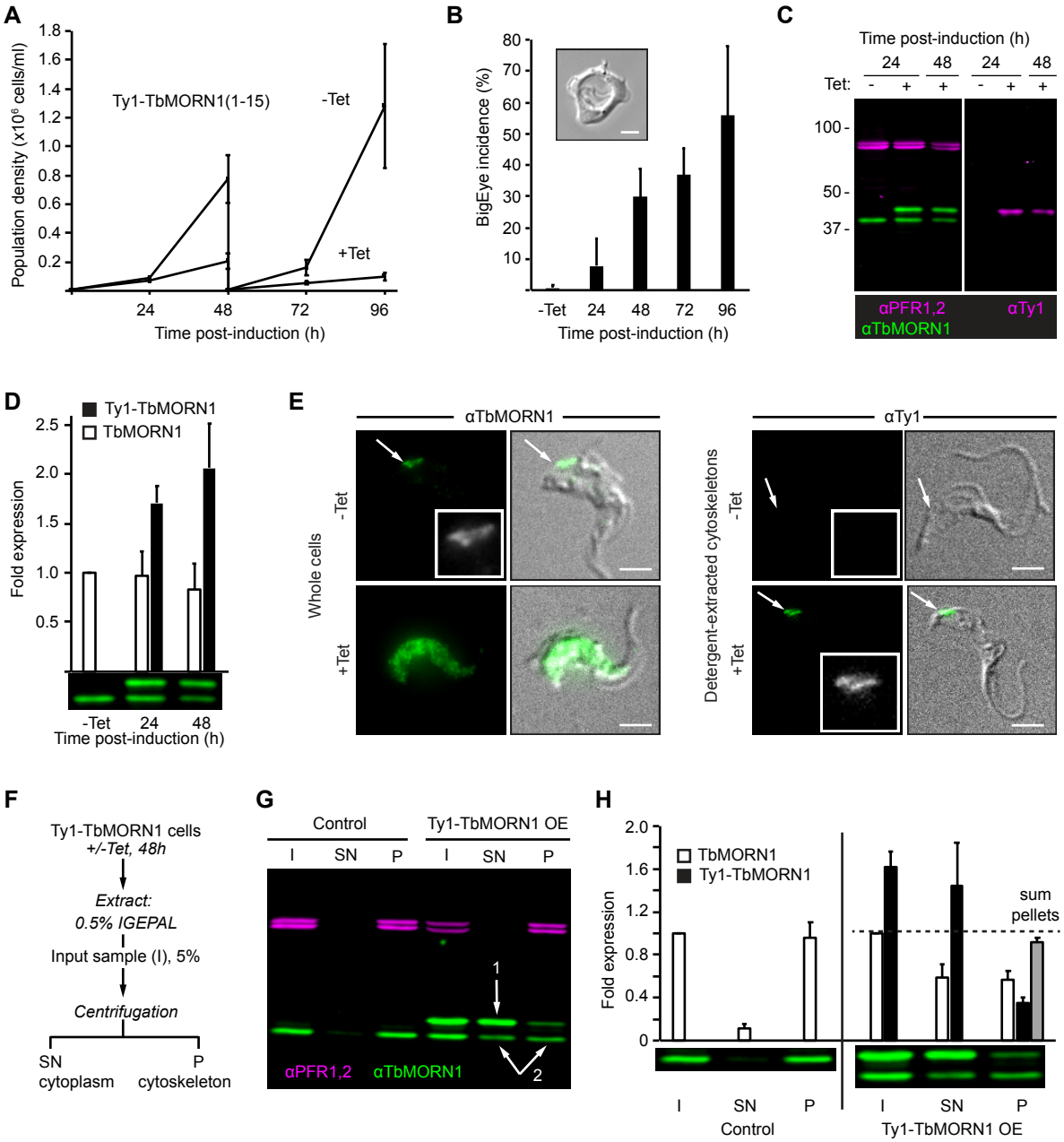

Figure 5. Overexpression of Ty1-tagged TbMORN1 causes a dominant negative phenotype. (A) Overexpression of Ty1-TbMORN1 is deleterious. Growth curves of control (-Tet) cells, and cells inducibly expressing Ty1-TbMORN1(1-15) (+Tet). Population density was measured every 24h, and the cultures split and reseeded at 48h. Data were compiled from 3 separate clones, each induced in 3 independent experiments; bars show mean +/- SD. (B) Overexpression of Ty1-TbMORN1 produces a BigEye phenotype. The incidence of BigEye cells was counted in control (-Tet) and Ty1-TbMORN1-expressing cells at the indicated timepoints. Data were compiled from 3 separate clones, each induced in 3 independent experiments; bars show mean + SD. The inset shows an example BigEye cell. Scale bar, 2 µm. (C) Tight induction of Ty1-TbMORN1 expression. Whole-cell lysates were harvested from control (-Tet) and Ty1-TbMORN1-expressing cells (+Tet) at the indicated timepoints and probed with anti-TbMORN1 and anti-Ty1 antibodies. PFR1,2 were used as a loading control. At least three independent inductions were carried out for each clone; an exemplary blot is shown. (D) Quantification of overexpression. The levels of endogenous TbMORN1 and ectopic Ty1-TbMORN1 in immunoblots were normalised relative to the PFR1,2 signal. Data were compiled using 3 separate clones, each induced in at least two independent experiments; bars show mean + SD. (E) Ty1-TbMORN1 can localise correctly to the cytoskeleton. Whole cells or detergent-extracted cytoskeletons were fixed and labelled with anti-TbMORN1 or anti-Ty1 antibodies. The fluorescence signal is shown with the transmitted light image of the cell overlaid; inset shows the fluorescence signal from the antibody in greyscale. Results confirmed for 3 separate clones, exemplary images are shown. Scale bars, 2 µm. (F) Schematic of the fractionation protocol. (G) Overexpression of Ty1-TbMORN1 displaces the endogenous protein from the cytoskeleton. Control and Ty1-TbMORN1-expressing cells were fractionated as shown in panel F and the I, SN, and P fractions were blotted. PFR1,2 was used as a marker for the cytoskeleton. Expression of Ty1-TbMORN1 was accompanied by a displacement of endogenous TbMORN1 from the insoluble (P) fraction into the soluble (SN) fraction (arrows 1,2). Equal fractions (5%) were loaded in each lane. 3 independent experiments using 3 separate clones were carried out; an exemplary blot is shown. (H) Quantification of the fractionation data. Bars show mean + SD.

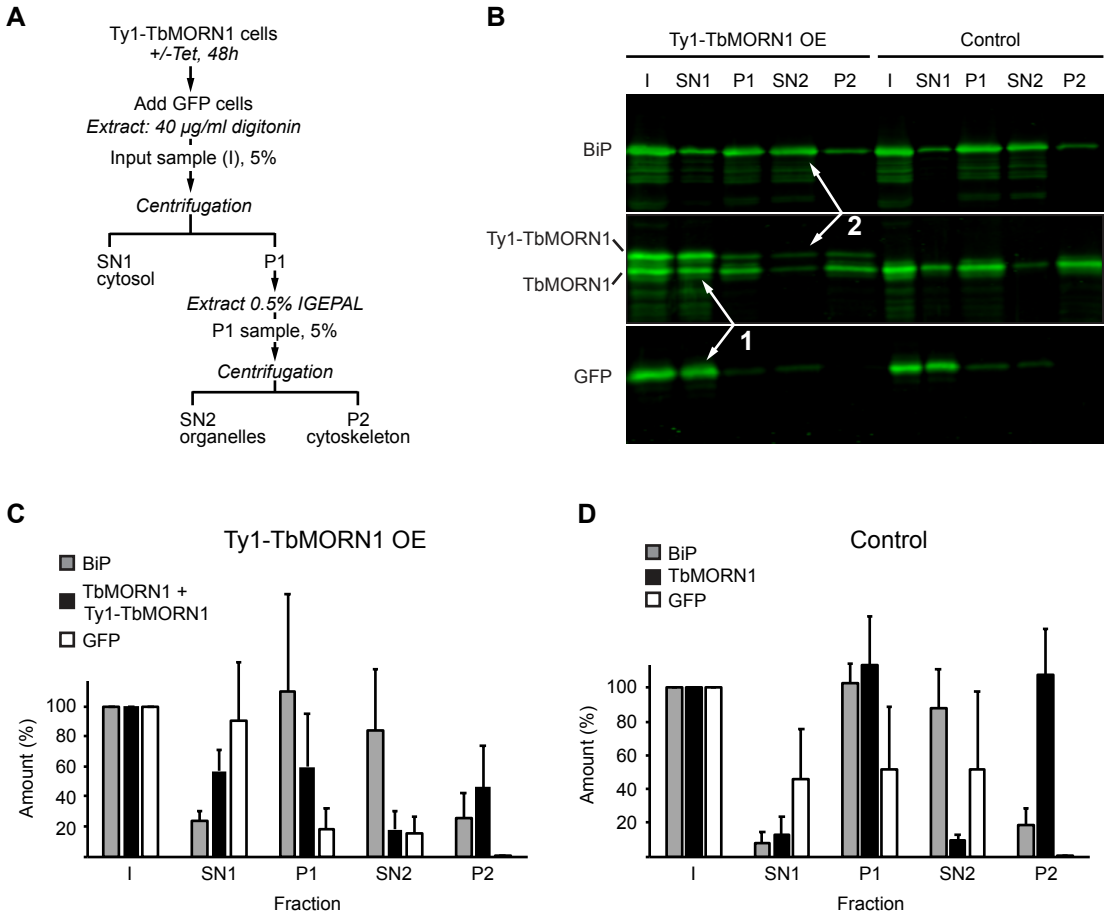

Figure 6. Overexpressed Ty1-TbMORN1 is predominantly cytosolic. (A) Schematic of the two-step fractionation scheme. (B) Immunoblots of fractions taken from control and Ty1-TbMORN1 overexpressing cells, using anti-BiP, anti-TbMORN1 and anti-GFP antibodies. Note that the membrane was cut into three strips for the immunoblot. Equal fractions (5%) were loaded in each lane. The overexpressed Ty1-TbMORN1 was predominantly extracted by digitonin and partitioned with the cytosolic GFP into the SN1 fraction (arrows 1). Very little of the remainder was subsequently extracted with non-ionic detergent into the SN2 fraction (arrows 2), with most partitioning into the cytoskeleton-associated P2 fraction. Three independent experiments were carried out using cells from three clones pooled together; an exemplary blot is shown. (C,D) Quantification of the immunoblots of the two-step fractionation. Data were compiled from three independent experiments, each using cells pooled from three separate clones. Bars show mean values + SD.

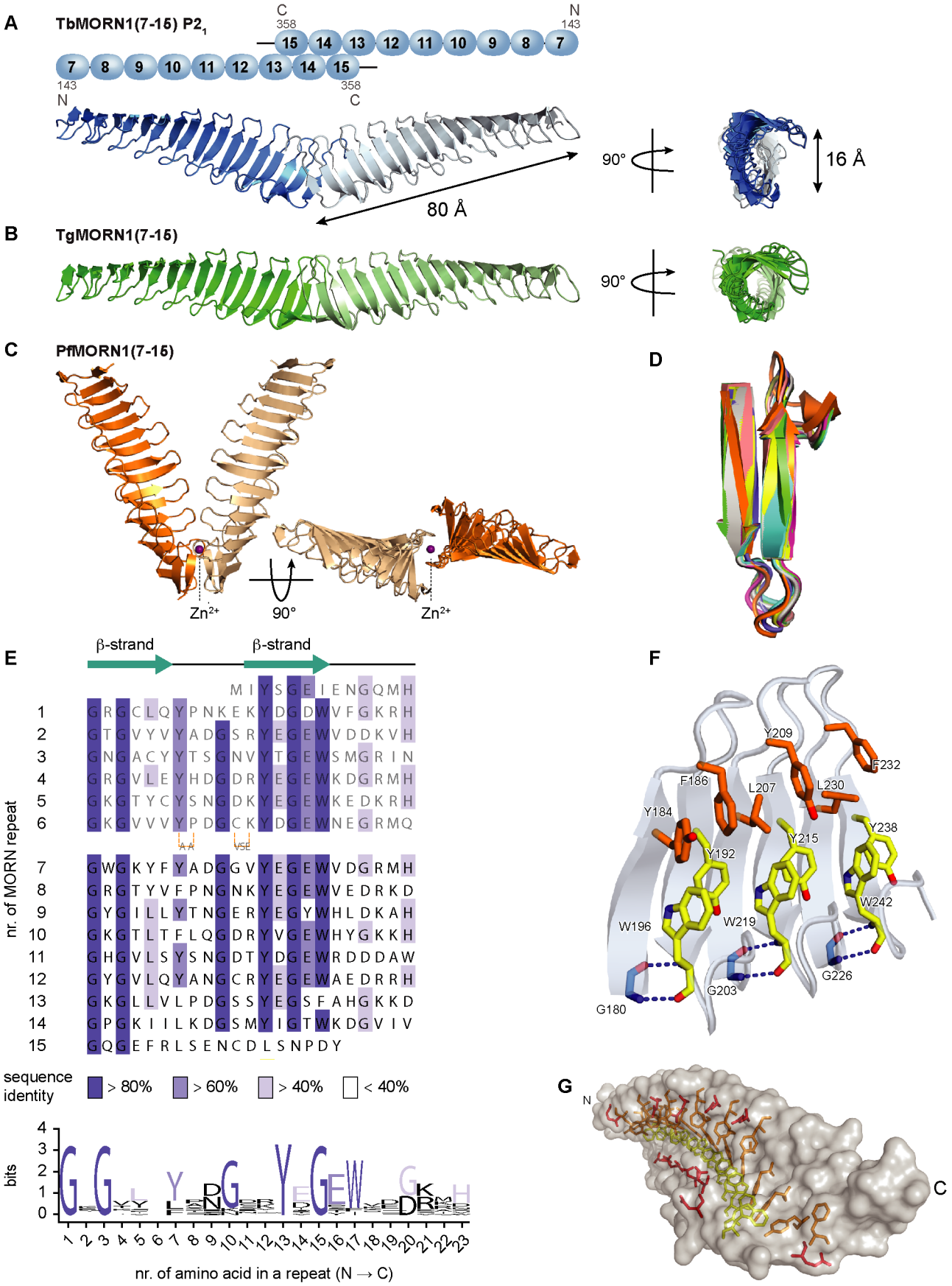
A
TbMORN1(7-15) P2₁
C
358
N
143
15 14 13 12 11 10 9 8 7
7 8 9 10 11 12 13 14 15
143
N
358
C
90°
16 Å
80 Å
B
TgMORN1(7-15)
90°
C
PfMORN1(7-15)
Zn2+
90°
Zn2+
D
E
β-strand
β-strand
nr. of MORN repeat
sequence identity
> 80%
> 60%
> 40%
< 40%
bits
nr. of amino acid in a repeat (N → C)
F
Y209
F232
F186
L207
L230
Y184
Y238
Y215
Y192
W242
W196
W219
G226
G203
G180
G
N
C

Figure 7. High-resolution structures of MORN repeat proteins and a structural redefinition of the MORN repeat. (A) Schematic depiction and crystal structure of the TbMORN1(7-15) dimer in its P21 crystal form. Amino acid numbers and N- and C-termini are indicated in the schematic. The crystal structure is shown in two orientations, with main dimensions indicated in Å. The structure contains 2 x 9 MORN repeats, and is an antiparallel homodimer with the subunits arranged in a splayed tail-to-tail configuration. The secondary structure consists of exclusively antiparallel beta-strands and peripherally positioned loops, which together form a longitudinal gutter through the middle of the protein. (B) Crystal structure of TgMORN1(7-15) shown in two orientations. The number of MORN repeats and the configuration is the same as for TbMORN1(7-15) in panel A. (C) Crystal structure of PfMORN1(7-15) shown in two orientations. The bound zinc ion is labelled. The structure contains 2x 9 MORN repeats, again in tail-to-tail configuration but with an overall V-shaped arrangement. (D) Alignment of all 9 TbMORN1(7-15) MORN repeats in the crystal structure reveals a high level of structural conservation. (E) A revised consensus MORN repeat sequence, based on the crystal structures. A new alignment of the MORN repeats in TbMORN1 is shown. Repeats 7-15 are present in the crystal structure; repeats 1-6 are inferred. Conservation of sequence identity is indicated by colour intensity. Each MORN repeat consists of a β-hairpin, built up of two 6-residue β-strands connected by a 5-residue loop. The β-hairpin is followed by a 6-residue loop that connects to the next MORN repeat. The new 23-residues long consensus MORN repeat starts with the GxG motif. (F) The tertiary structure of individual MORN repeats is stabilised by hydrogen bonds between the first G of the GxG motif and the W from the YEGEW motif. MORN repeat arrays are further stabilised by aromatic stacking between the highly conserved aromatic residues in the YEGEW and LxY motifs, and by T-shaped π-stacking interactions of the highly conserved Y of the YEGEW motif, which is sandwiched between the W residue of its own motif, and the W residue in the next YEGEW motif. (G) A single TbMORN1(7-15) subunit viewed at an oblique angle. The residues of the YEGEW and LxY motifs involved in aromatic stacking line the surface of the longitudinal gutter running through the middle of the protein.

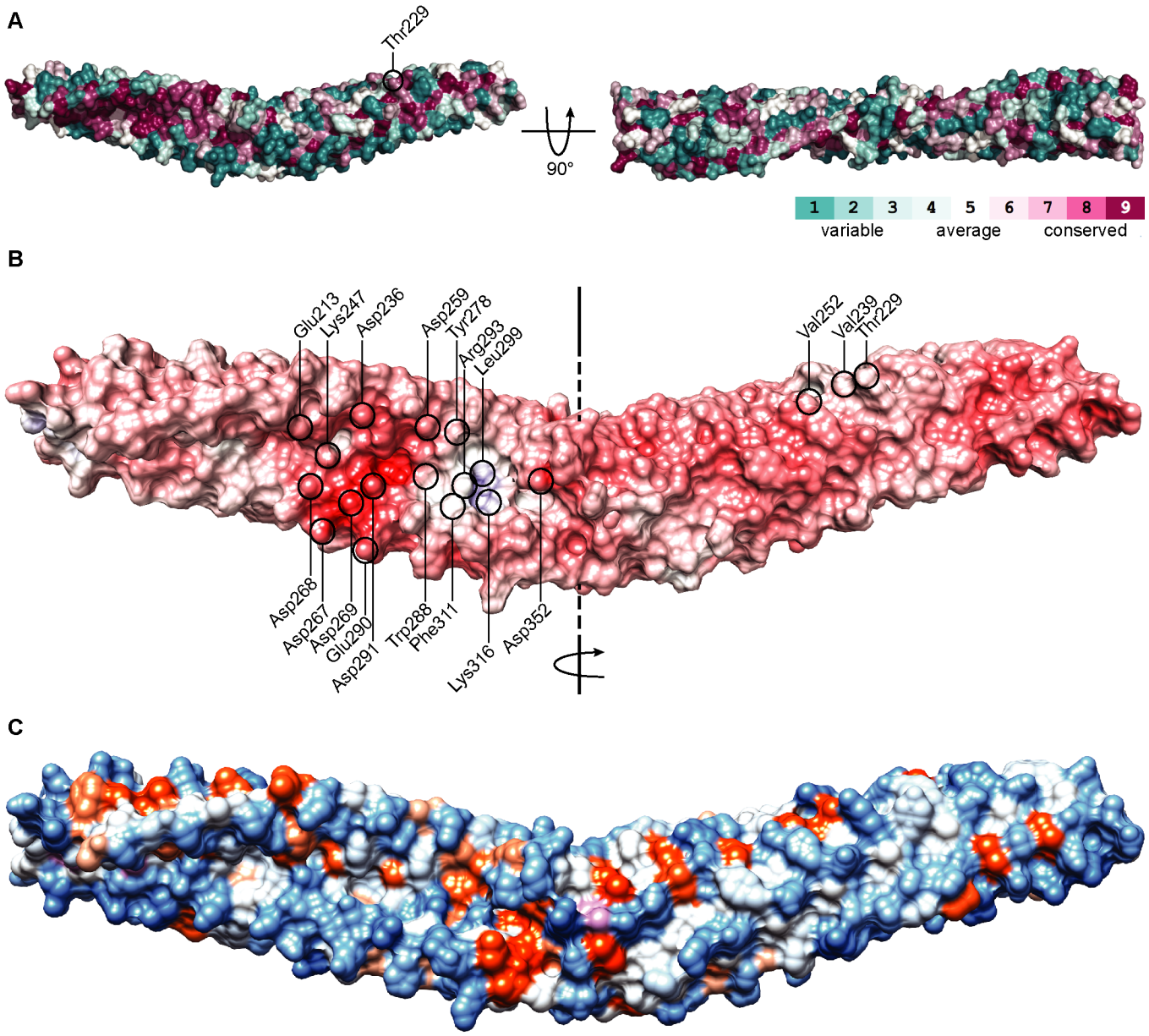

Figure 8. Conservation and properties of residues in TbMORN1(7-15). (A) Conservation map of the TbMORN1(7-15) $P2_1$ crystal structure reveals a highly conserved stretch of residues along the gutter. The structure is shown in two orientations, with residues colour-coded according to the level of conservation. (B) An electrostatic map of TbMORN1(7-15) $P2_1$. Colour scale: red = -13 kT; blue = +13 kT. Individual residues contributing to its surface electrostatics are labelled, namely those of the two negatively-charged loops building up a negative patch inside the gutter, and the residues contributing to a small positively-charged region close to the dimer interface. (C) Hydrophobic map of TbMORN1(7-15) $P2_1$. Colour scale: blue = hydrophilic; orange = hydrophobic, pink = methionine residues.

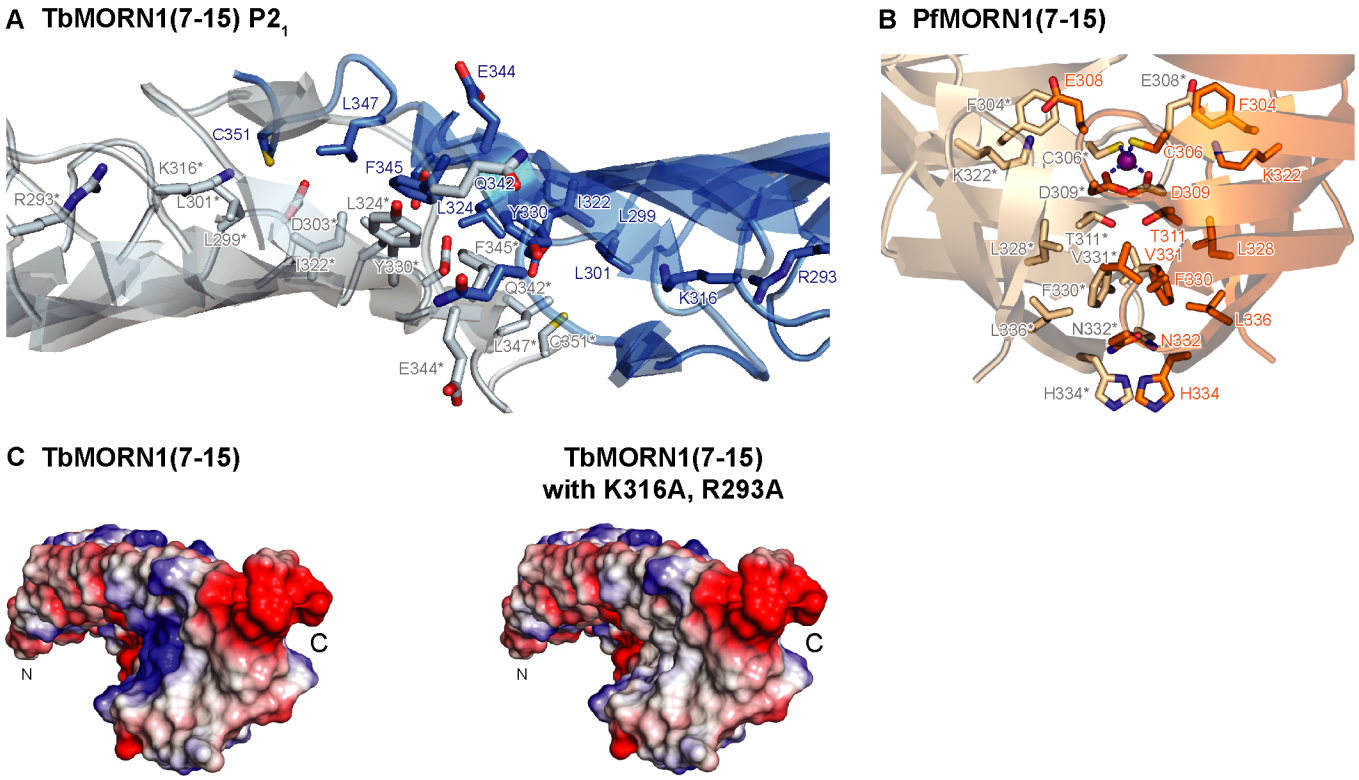

Figure 9. Dimerisation interfaces of TbMORN1(7-15) and PfMORN1(7-15). (A) The dimerisation interface of TbMORN1(7-15) P2$_1$ involves residues from MORN repeats 12-15, which stabilised the interface via aromatic π-stacking (Tyr330 and Phe345 from the respective subunits), hydrophobic interactions (Leu301, Leu347, Ile339, Ile322, Leu324), and additionally via hydrogen bonding interactions at the edges of the dimer interface. In comparison to the TbMORN1(7-15) C2 crystal structure, there are no disulphide bridges stabilising the dimerisation interface of TbMORN1(7-15) P2$_1$. (B) The dimerisation interface of the V-shaped PfMORN1(7-15) dimer is smaller and is additionally stabilised by the incorporation of a structural Zn^{2+} ion, which is tetrahedrally coordinated by Cys306 and Asp309 residues from each respective subunit. Thr311 holds the side chain of Asp309 in the appropriate orientation. The dimer interface is additionally stabilised by symmetric hydrogen bonding between the Thr311 pair, aromatic stacking between the Phe330 pair, a hydrophobic cluster formed by Leu328, Val331 and Leu336, two salt bridges between Lys322 and Glu308 from the respective subunits, anion-π interaction of a side chain of Glu308 with Phe304, and a combination of aromatic stacking (His334 pair) and polar interactions (His334, Asn332) at the vertex of the dimer. (C) An electrostatic map calculated for a single subunit of TbMORN1(7-15). The structure on the right shows the predicted effect of two point mutations, R293A from MORN repeat 13, and K316A from MORN repeat 14. The mutations are expected to result in the loss of a postively-charged patch close to the dimer interface, and consequently disrupt the dimerisation of the TbMORN1(2-15) constructs.

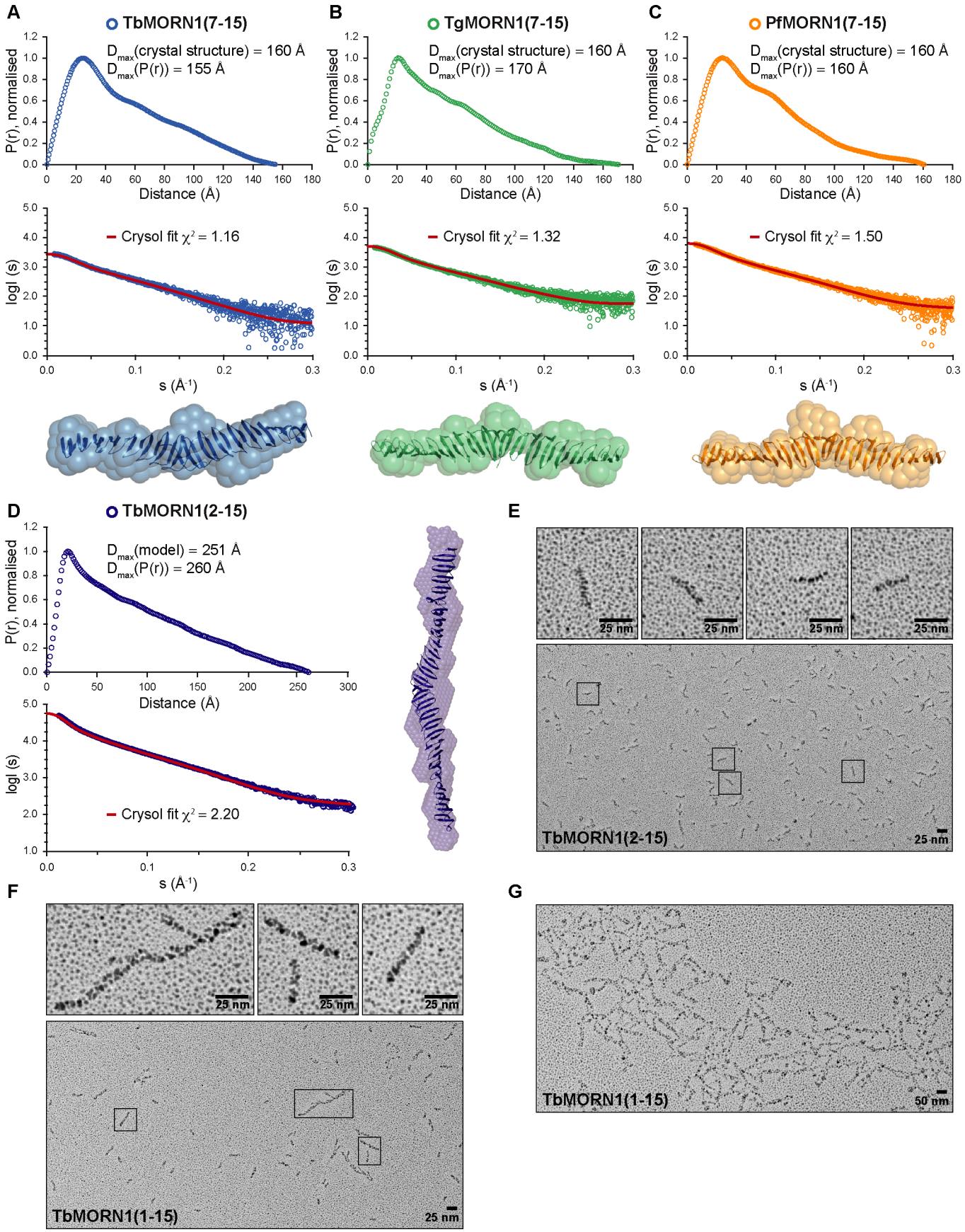
A
TbMORN1(7-15)
Dmax(crystal structure) = 160 Å
Dmax(P(r)) = 155 Å
P(r), normalised
Distance (Å)
Crysol fit χ2 = 1.16
logI (s)
s (Å-1)
B
TgMORN1(7-15)
Dmax(crystal structure) = 160 Å
Dmax(P(r)) = 170 Å
Crysol fit χ2 = 1.32
C
PfMORN1(7-15)
Dmax(crystal structure) = 160 Å
Dmax(P(r)) = 160 Å
Crysol fit χ2 = 1.50
D
TbMORN1(2-15)
Dmax(model) = 251 Å
Dmax(P(r)) = 260 Å
Crysol fit χ2 = 2.20
E
25 nm
TbMORN1(2-15)
F
TbMORN1(1-15)
G
50 nm
TbMORN1(1-15)

Figure 10. MORN1 proteins form extended dimers in solution. (A-D) SAXS experiments on TbMORN1(7-15) (A), TgMORN1(7-15) (B), PfMORN1(7-15) (C), and TbMORN1(2-15) (D). For each respective protein, the results include a P(r) plot with derived experimental D_{max} value compared with a D_{max} value derived from the structure, an experimental SAXS scattering data with a fit calculated by the Crysol programme, and a SAXS-based ab initio molecular envelope. In the case of TbMORN1(2-15), the theoretical D_{max} value was derived from a structural model, which was generated by spiking the TbMORN1(7-15) structure with additional structures of individual TbMORN1(7-15) subunits. (E-G) EM with rotary shadowing of TbMORN1(2-15) and full-length TbMORN1. (E) TbMORN1(2-15) forms a homogenous population of extended dimers of approximately 25 nm in length (see insets for individual examples). (F) Full-length TbMORN1 is heterogeneous and includes rare filaments of 175-200 nm in length (first inset) and individual dimers (second and third inset). (G) Large oligomers of full-length TbMORN1 assembled in a mesh-like structure. Magnification, 71,000x; scale bars, 25 nm, 50 nm as indicated. n (independent replicates) = 2, n (biological replicates) = 2.

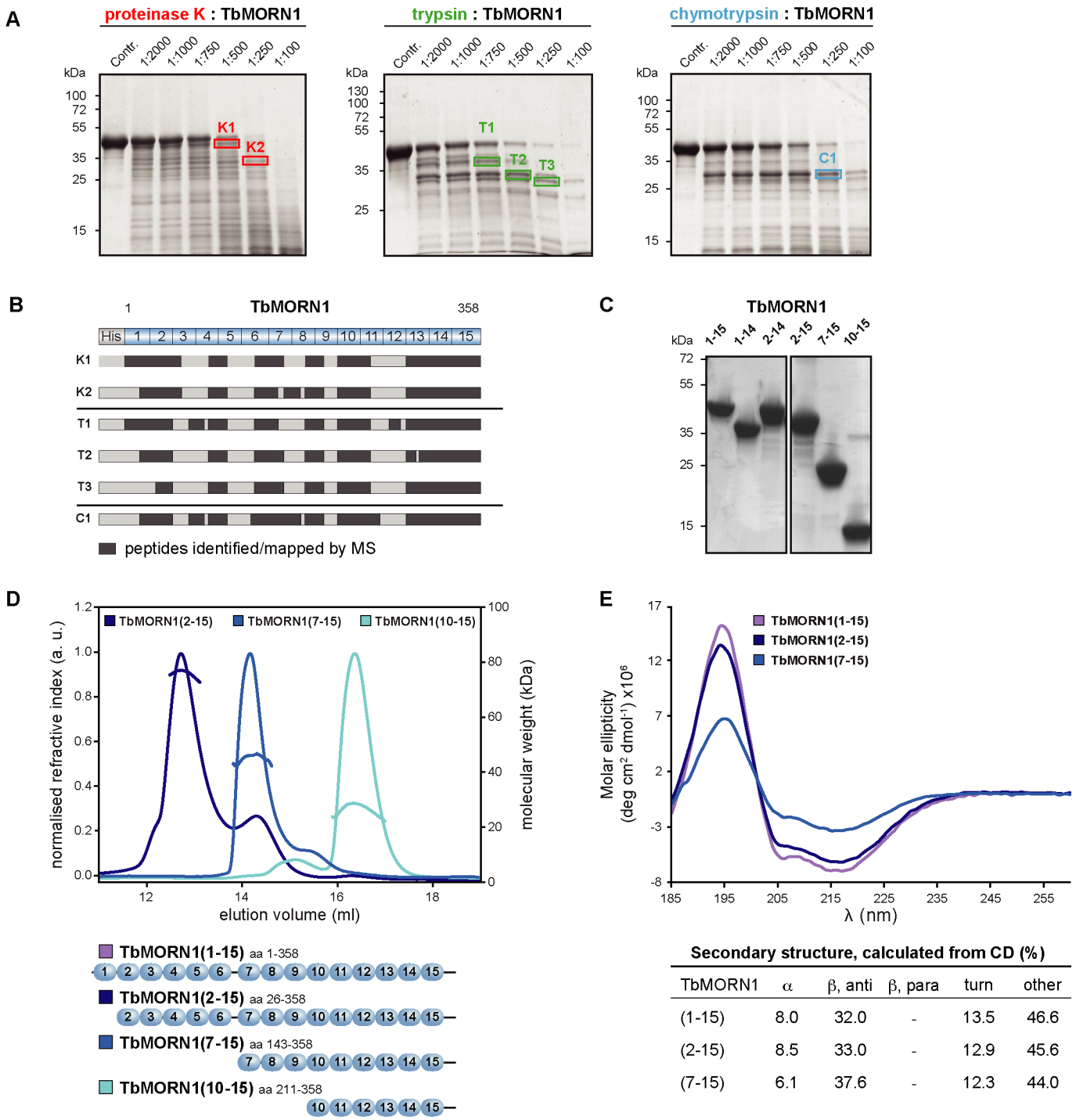

Secondary structure, calculated from CD (%)

TbMORN1	α	β, anti	β, para	turn	other
(1-15)	8.0	32.0	-	13.5	46.6
(2-15)	8.5	33.0	-	12.9	45.6
(7-15)	6.1	37.6	-	12.3	44.0

Figure S1. Low-resolution structural analysis of TbMORN1. (A) Full-length TbMORN1 with an N-terminal HisTag was subjected to limited proteolysis using proteinase K (red), trypsin (green), and chymotrypsin (cyan) at protease:protein ratios (w/w) as indicated on each panel. Samples were resolved by SDS-PAGE and selected bands (labelled boxes) corresponding to proteolytic products were excised and analysed by mass spectrometry. Control (Contr.) corresponds to protein without protease treatment. (B) Mass spectrometry analysis of the excised proteolytic products indicated in panel A. Peptides identified and mapped by mass spectrometry are shown as dark grey boxes; a schematic of the full-length construct is shown above, with individual MORN repeats labelled. Note that the proteolytic products show progressive degradation from their N-termini, while the C-terminal part is stable. (C) Coomassie-stained SDS-PAGE gel showing purified recombinant TbMORN1 truncations. (D) SEC-MALS traces of TbMORN1 (2-15), (7-15), and (10-15). Chromatographic separation was done using a Superdex 200 Increase 10/300 GL column. The three proteins all eluted as dimers. Schematics are shown underneath. (E) Far-UV CD profiles of TbMORN1, TbMORN1(2-15) and (10-15). A positive peak at 195 nm and a negative one at 218 nm demonstrated that the constructs are all β-proteins. The secondary structure content predictions for each construct were calculated in BeStSel and are shown below the CD graph.

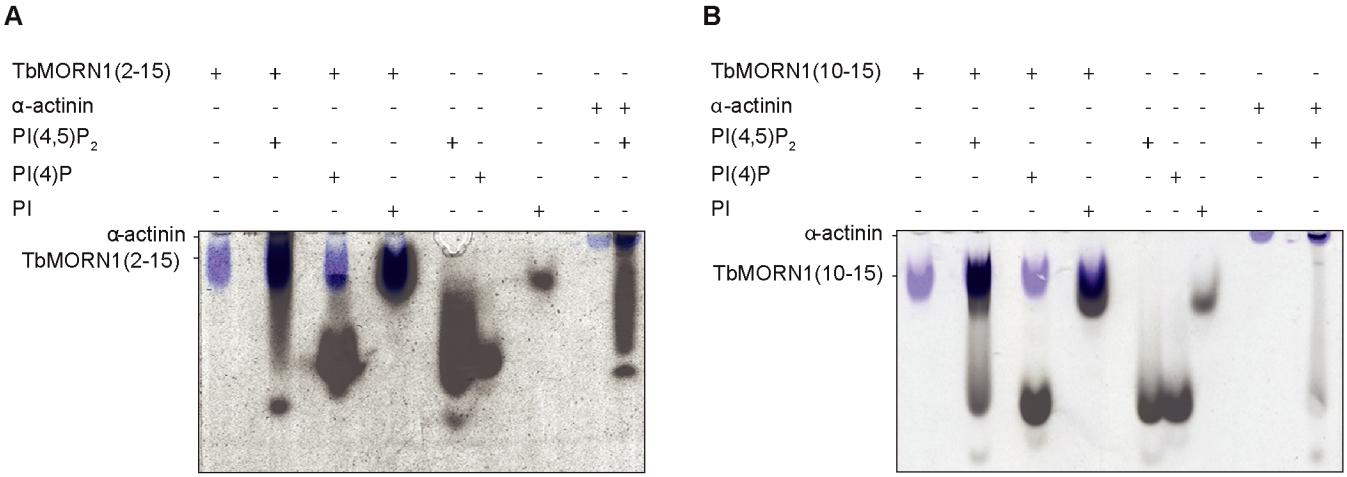

Figure S2. TbMORN1 interacts with PI(4,5)P_2 in native gel bandshift assays. (A) Native gel electrophoresis of TbMORN1(2-15) and (B) TbMORN1(10-15) in the presence and absence of PI(4,5)P_2, PI(4)P and PI, all labelled with Bodipy TMR fluorescent dye. α-actinin served as a positive control of PI(4,5)P_2 binding. Data obtained from two independent experiments, each using a different biological replicates.

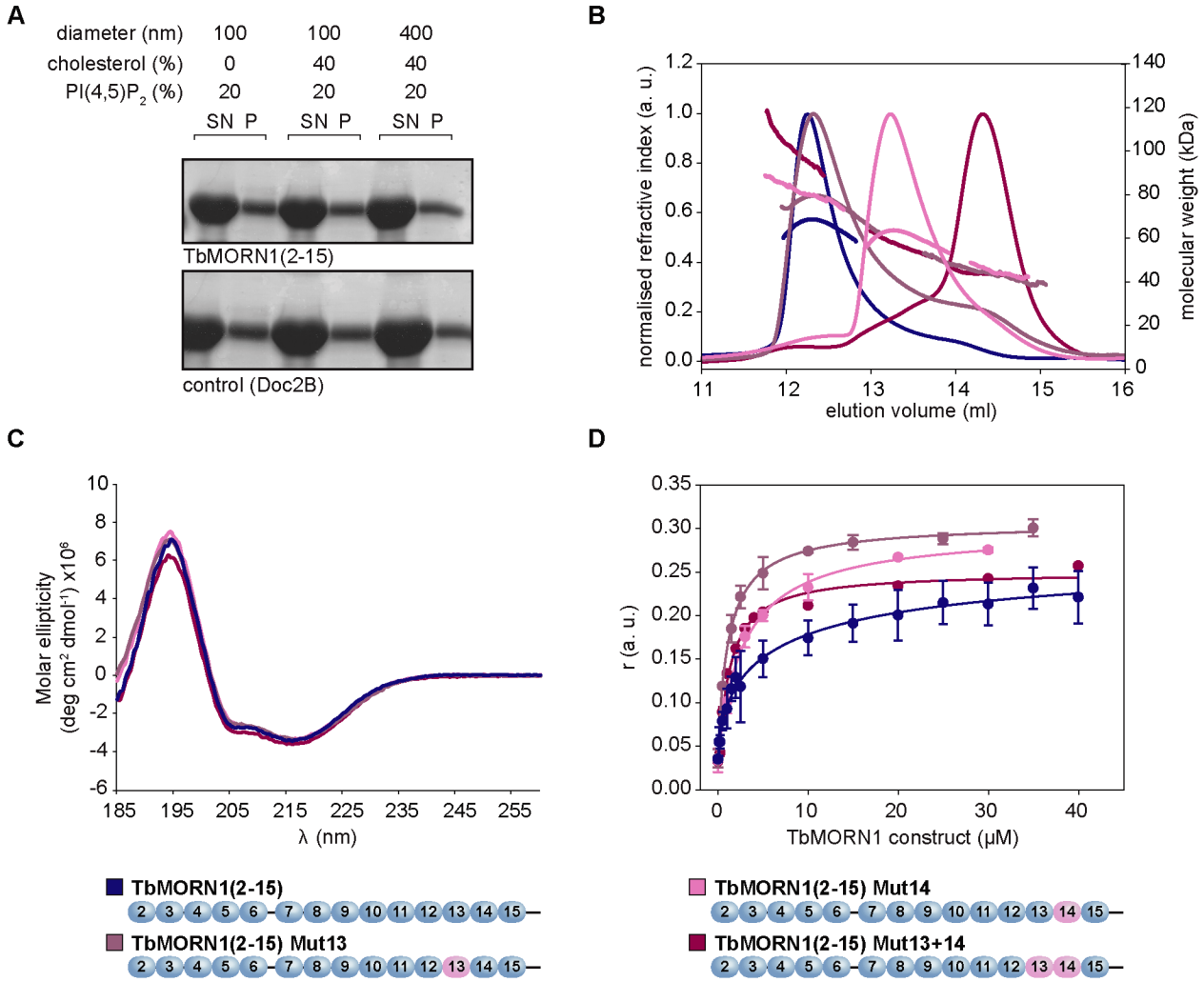

Figure S3. Mutagenesis of putative PI(4,5)P_2 binding sites in TbMORN1 has no effect on binding. (A) Liposome co-sedimentation assay performed on TbMORN1(2-15) in the presence of POPC liposomes containing 20% of porcine brain PI(4,5)P_2 and 0 or 40% cholesterol. The excess cholesterol was expected to promote local high concentrations of PI(4,5)P_2 on the surface of the liposomes. To assay for the effect of curvature, two batches of liposomes containing 20% PI(4,5)P_2 and 40% of cholesterol were tested, with the diameter of the liposomes being either 100 or 400 nm. No significant co-sedimentation of TbMORN1(2-15) and PI(4,5)P_2-containing liposomes was observed. The positive control, 10 μM Doc2B was predominantly found in the pellet (P) fractions. (B) SEC-MALS profiles of TbMORN1(2-15) and its mutagenised variants. Residues comprising the putative PI(4,5)P_2-binding sites in MORN repeats 13 and 14 were mutated to alanines. Mutagenesis of repeat 13 (Mut13) did not result in any change to the dimeric status of the protein. However, mutagenesis of repeat 14 (Mut14) resulted in a mixture of monomers and dimers being eluted, while mutagenesis of both repeats (Mut13+14) resulted in monomeric protein. (C) Far-UV CD profiles of TbMORN1(2-15) and its putative PI(4,5)P_2-binding mutants. The constructs remained β-proteins despite the site-directed mutagenesis. (D) Fluorescence anisotropy measurements of TbMORN1(2-15) and its putative PI(4,5)P_2-binding mutants, measured in the presence of 0.1 μM BODIPY TMR-PI(4,5)P_2. All constructs showed good interaction with the fluorophore-conjugated PI(4,5)P_2.

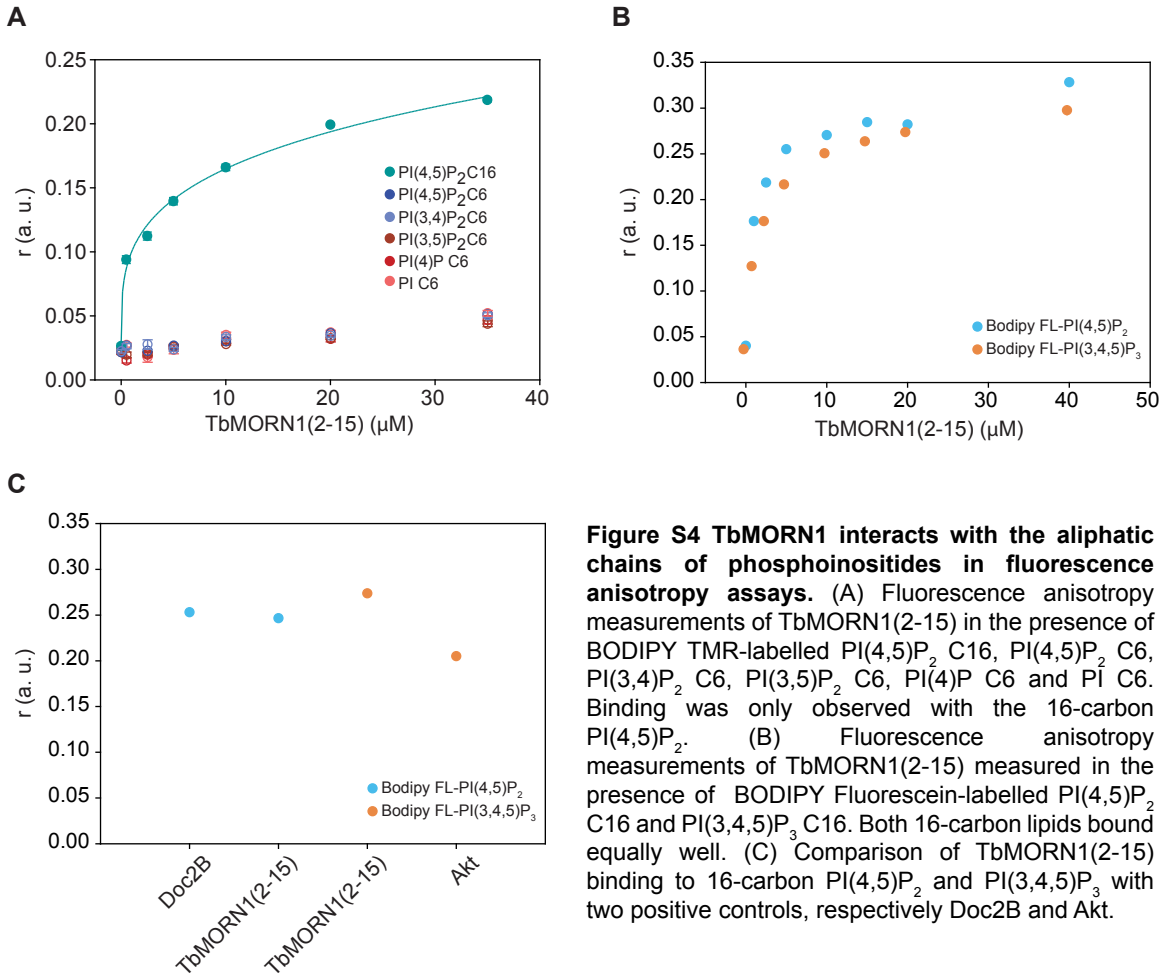

Figure S4 TbMORN1 interacts with the aliphatic chains of phosphoinositides in fluorescence anisotropy assays. (A) Fluorescence anisotropy measurements of TbMORN1(2-15) in the presence of BODIPY TMR-labelled PI(4,5)P_2 C16, PI(4,5)P_2 C6, PI(3,4)P_2 C6, PI(3,5)P_2 C6, PI(4)P C6 and PI C6. Binding was only observed with the 16-carbon PI(4,5)P_2. (B) Fluorescence anisotropy measurements of TbMORN1(2-15) measured in the presence of BODIPY Fluorescein-labelled PI(4,5)P_2 C16 and PI(3,4,5)P_3 C16. Both 16-carbon lipids bound equally well. (C) Comparison of TbMORN1(2-15) binding to 16-carbon PI(4,5)P_2 and PI(3,4,5)P_3 with two positive controls, respectively Doc2B and Akt.

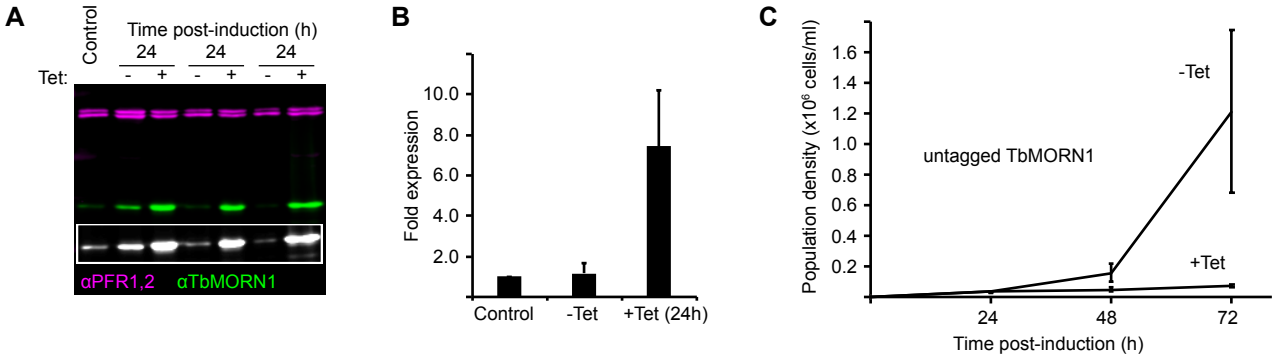

Figure S5. Overexpression of untagged TbMORN1 causes a dominant negative phenotype. (A) Inducible overexpression of untagged TbMORN1. Immunoblot of whole-cell lysates from three separate clones overexpressing untagged TbMORN1 from an ectopic locus. TbMORN1 was detected using anti-TbMORN1 antibodies; anti-PFR1,2 antibodies were used as a loading control. Inset shows a greyscale image of the TbMORN1 channel with enhanced levels so the endogenous protein is visible. Three separate clones were assayed, each in three independent experiments; an exemplary blot is shown. One of the three clones appeared to have slightly leaky expression, with TbMORN1 levels in the -Tet condition being higher than controls. (B) Quantification of overexpression. TbMORN1 levels in control, uninduced (-Tet) and induced (+Tet) were normalised relative to the loading control and expressed relative to the control cells. Approximately 7-fold overexpression was achieved relative to control cells. Data were obtained from blots using 3 separate clones, each induced in 3 independent experiments. Bars show mean + SD. (C) Overexpression of untagged TbMORN1 is deleterious. Uninduced (-Tet) and TbMORN1 overexpressing (+Tet) cells were assayed at 24 h intervals in a 3-day timecourse. Data were obtained from blots using 3 separate clones, each induced in 3 independent experiments. Mean +/- SD.

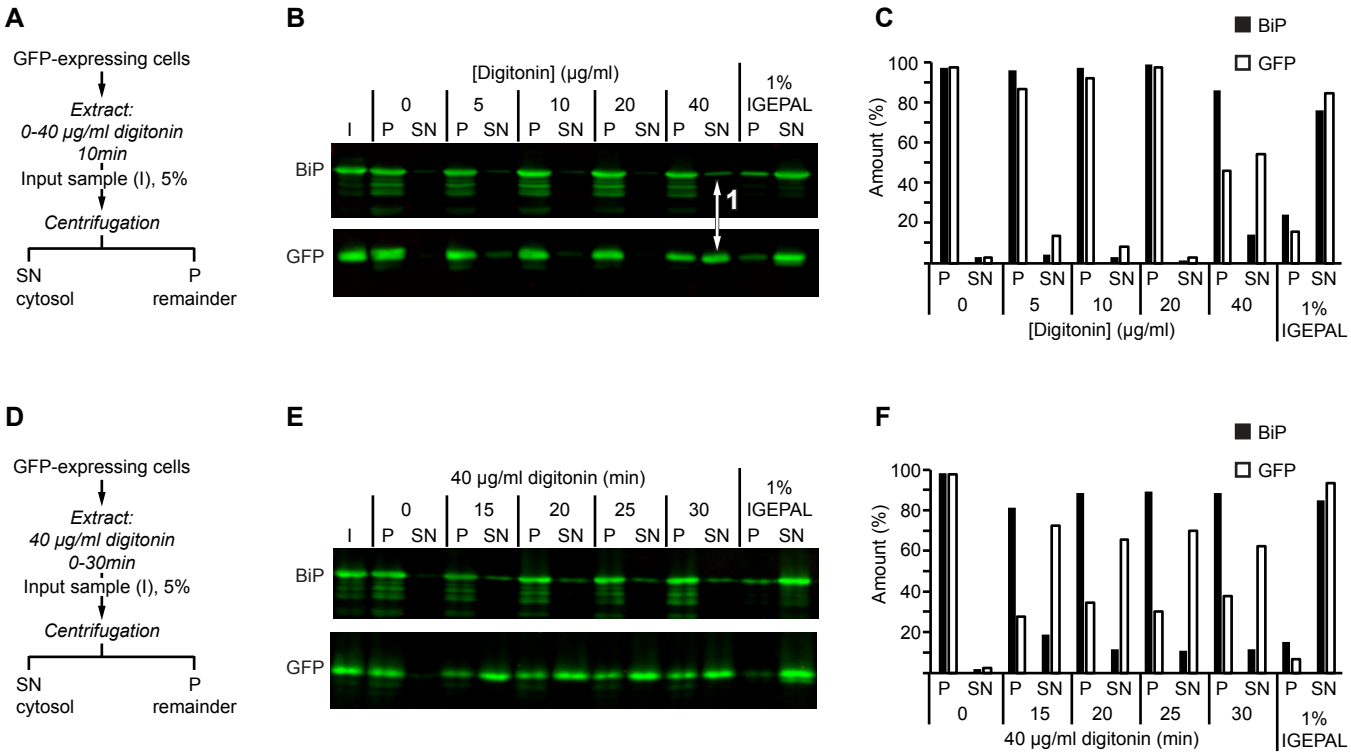

Figure S6. Optimisation of digitonin fractionation. (A) Schematic of the one-step fractionation scheme. Cell expressing cytosolic GFP were incubated in increasing concentrations of digitonin for 10 min prior to separation of fractions by centrifugation. Equal fractions (5%) were then blotted with antibodies specific for GFP and the endoplasmic reticulum chaperone BiP. (B) At 40 µg/ml digitonin, good solubilisation of GFP is achieved with only negligible solubilisation of BiP (arrow 1). Both proteins are efficiently solubilised using 1% IGEPAL as a positive control. Multiple independent experiments were carried out; an exemplary blot is shown. Note that the membrane was cut into strips prior to blotting, but the samples shown are from the same experiment. (C) Quantification of the immunoblot shown in B. (D, E, F) As per panels A-C, but with a constant 40 µg/ml digitonin concentration and considering the effect of varying incubation time (0-30 min).

A

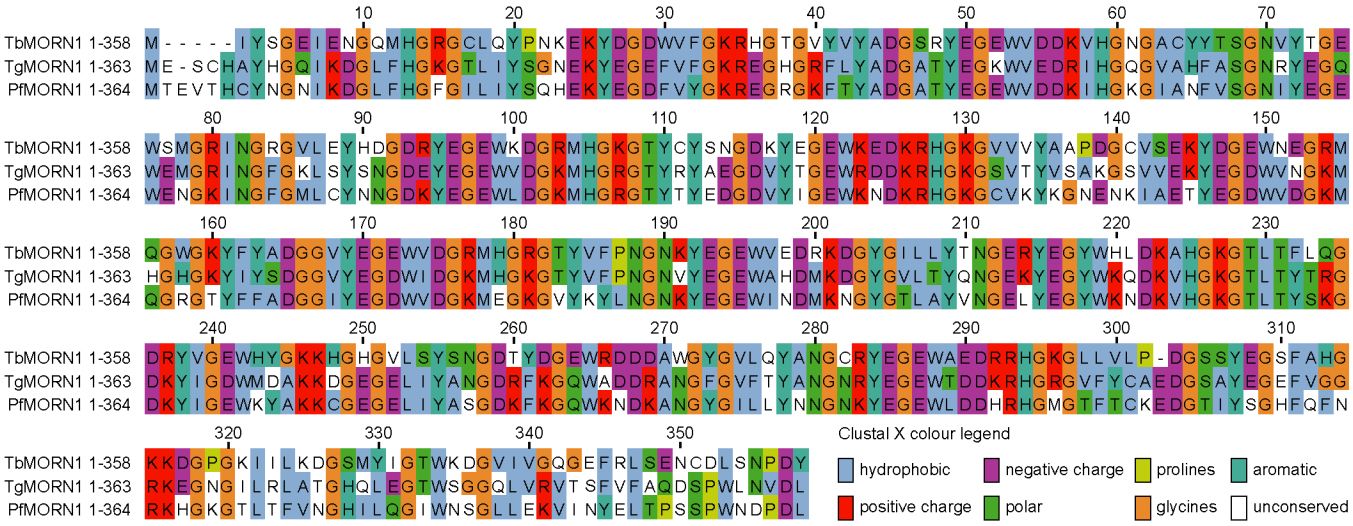

B

Comparison of MORN1 proteins and % of their sequence identity	
T. brucei / P. falciparum	54
T. brucei / T. gondi	57
P. falciparum / T. gondii	65

C

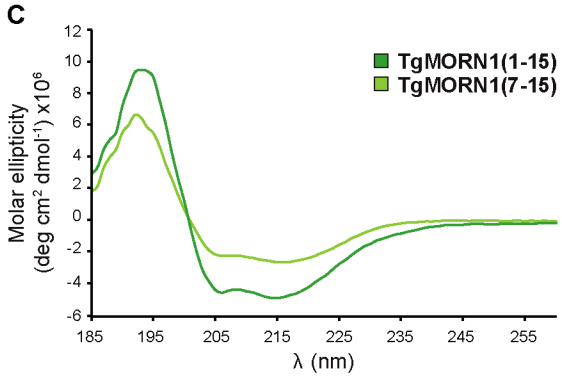

Secondary structure, calculated from CD (%)

TgMORN1	α	β, anti	β, para	turn	other
(1-15)	5.3	30.8	0.8	13.0	50.1
(7-15)	4.8	42.3	-	11.8	41.1

D

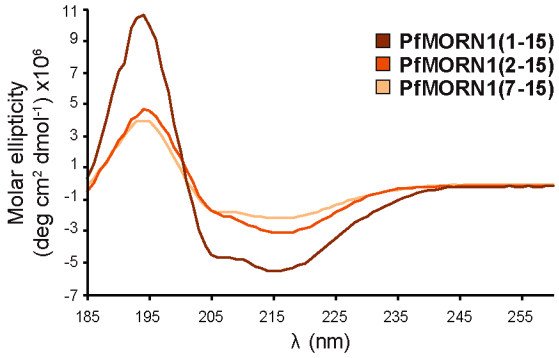

Secondary structure, calculated from CD (%)

PfMORN1	α	β, anti	β, para	turn	other
(1-15)	6.4	29.8	1.9	13.8	48.1
(2-15)	6.2	35.7	-	13.4	44.7
(7-15)	6.6	32.6	1.0	12.0	47.8

Figure S7. Comparison of MORN1 proteins, and secondary structure analysis of apicomplexan MORN1s. (A) Amino acid sequence alignment of MORN1 proteins from *Trypanosoma brucei, Toxoplasma gondii* and *Plasmodium falciparum*. The number of amino acids in each protein is indicated, amino acid numbers in the alignment are those for TbMORN1. The alignment is coloured according to the amino acid properties. (B) Pairwise comparison of percentage sequence identity between the three proteins. (C) Far-UV CD measurements obtained for TgMORN1(1-15) and TgMORN1(7-15). The secondary structure content predictions for each of the measured proteins were calculated in BeStSel and are shown below the CD graph. (D) As (C), but PfMORN1(1-15), (2-15) and (7-15). Like TbMORN1, TgMORN1 and PfMORN1 are also all-β proteins.

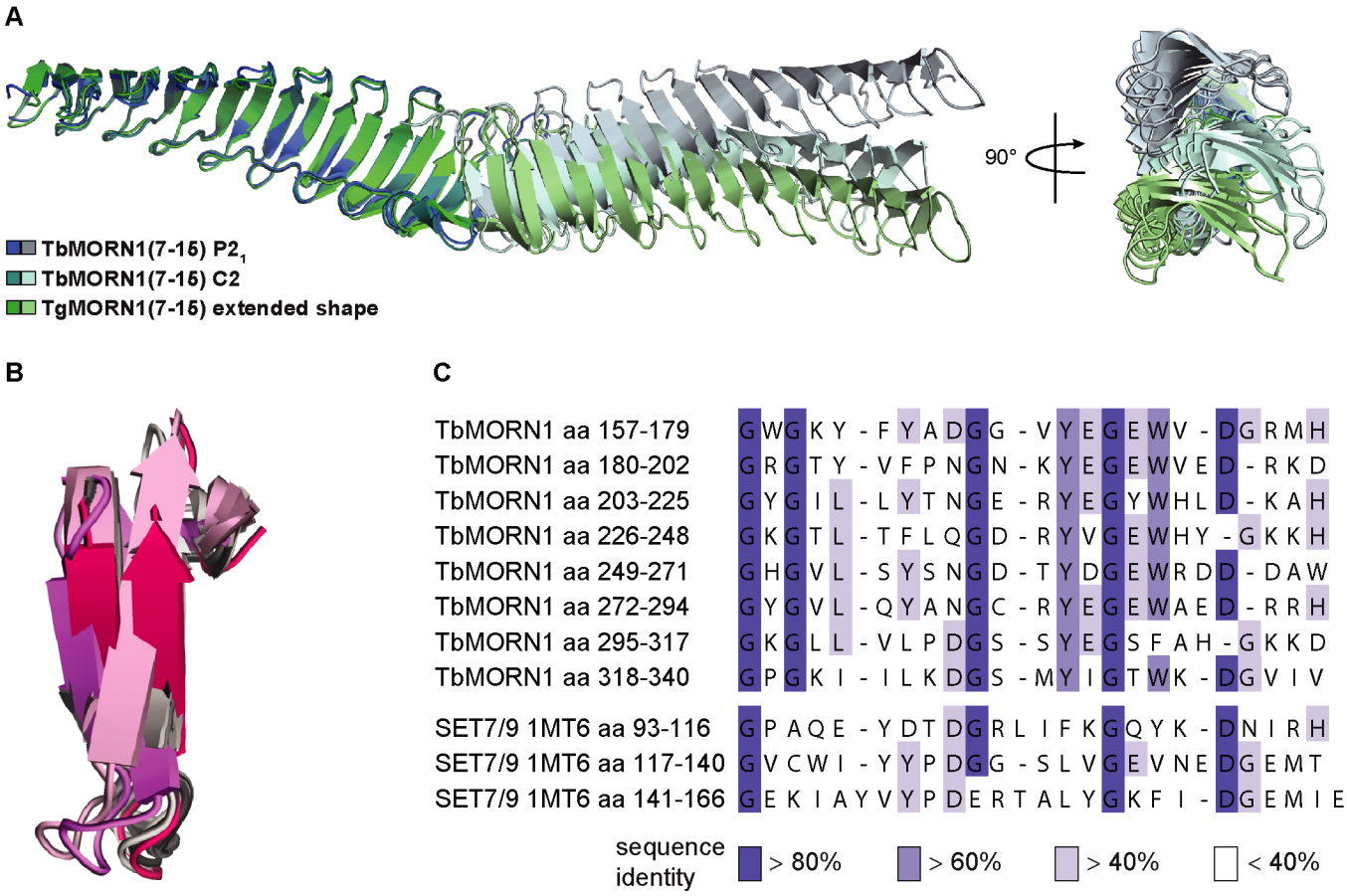

Figure S8. Comparision of MORN1 extended dimers, and with SETD7. (A) TbMORN1(7-15) P2$_1$, TbMORN1(7-15) C2, and TgMORN1(7-15) extended dimers superimposed on each other, and displayed in two orientations. In contrast to the other two proteins, the P2$_1$ crystal structure of TbMORN1(7-15) displays a bend of approximately 30° among the subunits. (B) TbMORN1(7-15) MORN repeats superimposed on three MORN repeats from SETD7 (SET7/9). Alignment of the three MORN repeats from SETD7 with MORN repeat 7 from the TbMORN1(7-15) crystal structure over 22-23 aligned C-atoms yielded rmsd values of 2.3, 1.5 and 1.9 Å respectively. (C) Sequence alignment of MORN repeats from the TbMORN1(7-15) crystal structure with three MORN repeats from SETD7. The first Gly residue is conserved in all MORN repeats of TbMORN1(7-15) and SETD7 structures.

A TbMORN1(7-15) C2

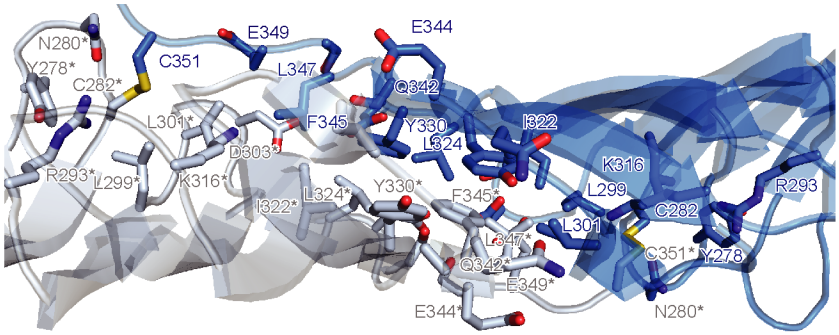

B TgMORN1(7-15)

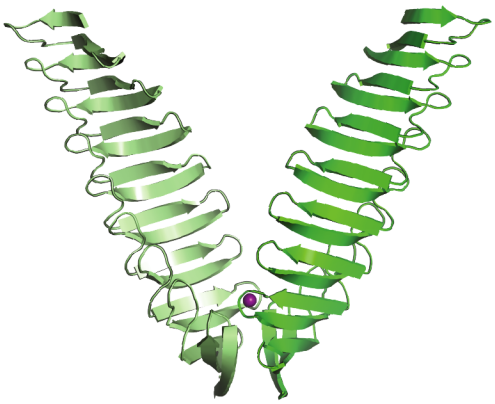

C TgMORN1(7-15) extended dimer

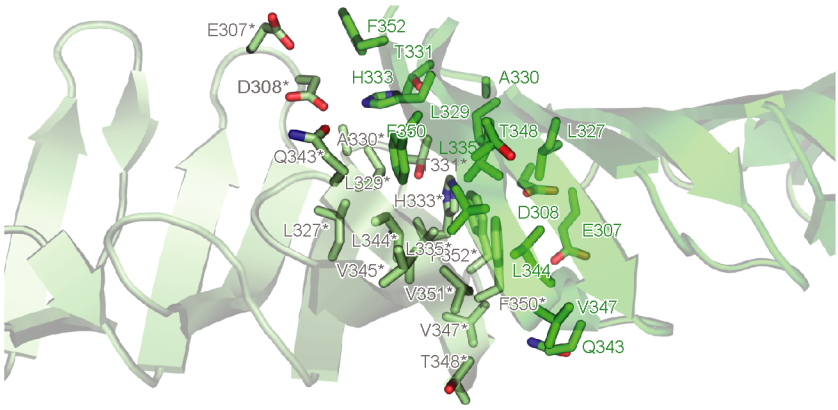

D TgMORN1(7-15) V-shaped dimer

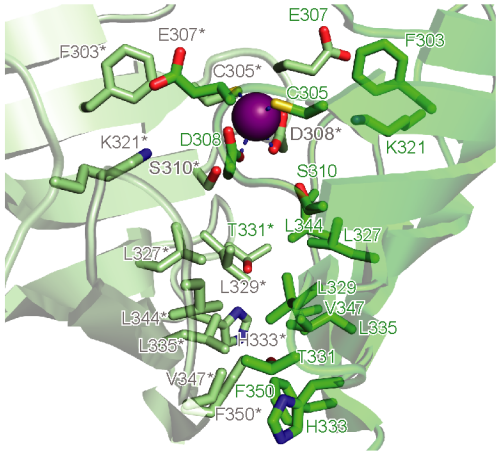

E SAXS - Kratky plots

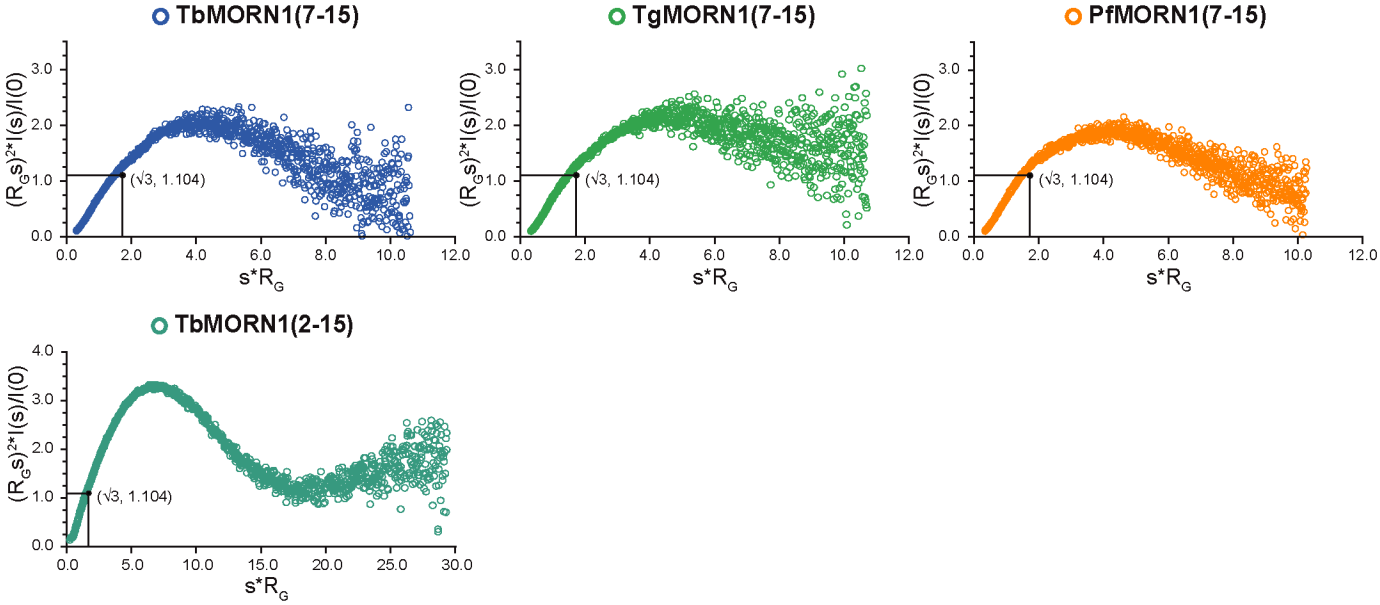

Figure S9. MORN dimer interfaces and SAXS analysis of proteins in solution. (A) Dimer interface of TbMORN1(7-15) C2 crystal form. In comparison to the $P2_1$ form, the dimer interface of C2 structure is broader, and is additionally stabilised by two disulphide bridges formed between Cys351 at the C-terminus of repeat 15 and Cys282 from the **β**-hairpin loop of repeat 12. (B) Crystal structure of the TgMORN1(7-15) V-shaped dimer, incorporating Zn2+ in its dimerisation interface. (C) Dimer interface of the TgMORN1(7-15) extended dimer, which utilises residues from MORN repeats 13-15. In contrast to TbMORN1(7-15), where the dimerisation interface is centred around aromatic stacking, a hydrophobic core plays a crucial role in the dimer interface of extended TgMORN1(7-15). Leu327, Leu329, Leu335, Leu344, Val345, Val347, Phe350 and Phe352 are part of this hydrophobic core. The dimer is stabilised by a single salt bridge formed between Asp308 of one, and His333 of the second subunit. This salt bridge is further stabilised by two hydrogen bonds between the main-chain nitrogen of Val345 and a carbonyl oxygen of Val347 of respective subunits. (D) Dimer interface of the TgMORN1(7-15) V-shaped dimer. Cys305 and Asp308 incorporate a structural Zn2+ ion, which stabilises the somewhat smaller dimerisation interface of this protein. Although its dimerisation interface is very similar to that of PfMORN1(7-15), it lacks the aromatic core of PfMORN1(7-15). The latter is replaced by a series of unique aromatic stacking interactions at the protein´s vertex, these being contributed by a pair of Phe350 residues, sandwiched between a pair of His333 residues. (E) Kratky plots derived from SAXS analysis of TbMORN1(7-15), TgMORN1(7-15), PfMORN1(7-15), and TbMORN1(2-15). The shape of the plots suggests an elongated shape of the dimers in solution.

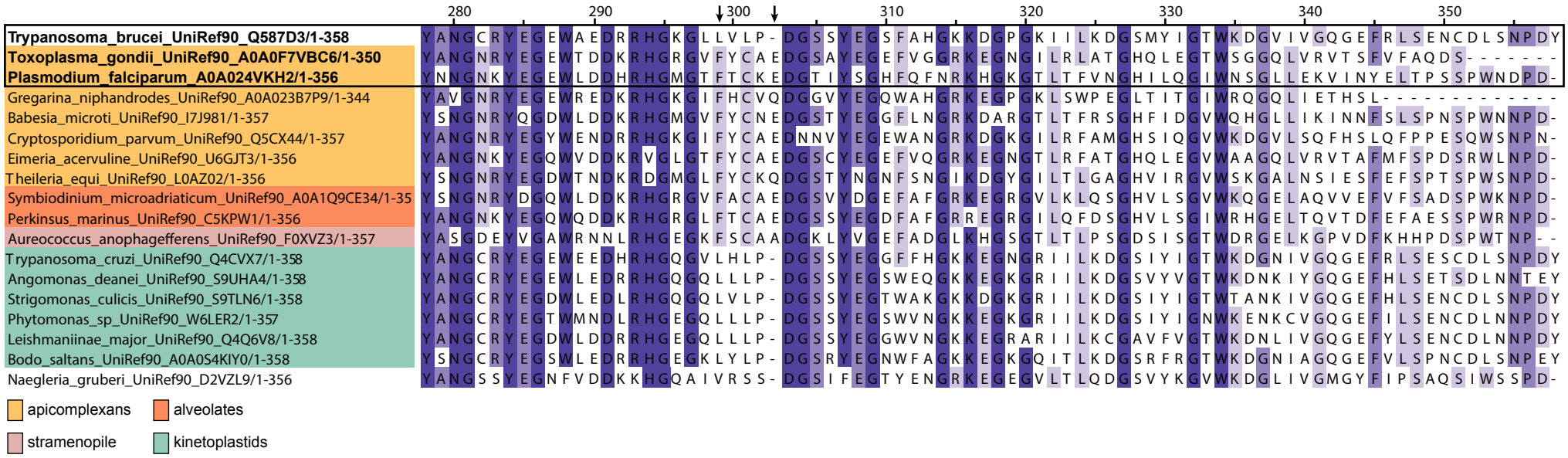

Figure S10. Conservation of residues for formation of V-shaped dimers in Apicomplexa and related clades. Amino acid sequence alignment of the C-termini of TbMORN1, TgMORN1, PfMORN1, and fifteen other MORN repeat-containing proteins from related taxa. Amino acid numbers are given according to the TbMORN1 protein, and the three proteins with experimentally-determined high-resolution structures are shown in bold within the black box. Essential for formation of a V-shaped dimer are a coordinating Cys residues and an anion-π interaction pair. In TbMORN1, the coordinating Cys residue has been substituted for Leu (Leu 301). Similarly the Phe and Glu residues of the anion-π interaction pair (indicated with black arrows) have been substituted for Leu (Leu299) and are not present (deletion after Pro302) respectively. This supports the conclusion that TbMORN1 exists only in the extended form, while the apicomplexan proteins and those from related clades are probably capable of adopting both extended and V-shaped conformations.

Table 1. X-ray data collection statistics

	PfMORN (SMet)	**PfMORN**	**TbMORN**	**TbMORN**	**TgMORN**	**TgMORN (V-shape)**
Source	ID29	ID29	ESRF ID23-1	ESRF ID23-1	ESRF ID30B	ESRF ID30B
Wavelength (Å)	0.979	0.976	0.979	1.89	0.967	1.0
Resolution (Å)	47.47-2.5 (2.59-2.5)	46.3-2.14 (2.2-2.14)	48.28-2.35 (2.43-2.35)	48.14-2.53 (2.65-2.53)	48.92-2.90 (3.08-2.90)	49.45-2.50 (2.60-2.50)
Space group	*C222*$_1$	*C222*$_1$	*P*2$_1$	*C2*	*P*4$_3$2$_1$2	*P*6$_2$22
Unit cell (Å, º)	a=57.33, b= 79.18, c= 94.42	a=57.33, b= 79.18, c= 94.42	a=69.04, b=27.63, c=114.54; β=101.83	a=192.88, b=49.74, c=41.98	a=b=53.92, c=348.85	a=b=205.86, c=40.58
Molecules (a.u.)	1	1	2	2	2	1
Unique reflections	7832(762)	12148 (974)	17460 (1247)	12419(975)	12331 (1819)	18162 (1960)
Completeness (%)	99.5(98.3)	99.6(98.1)	95.4 (71.5)	93.1(60.0)	99.1 (95.4)	99.7 (97.9)
R_{merge}[b]	0.059(0.301)	0.037 (1.283)	0.092 (0.466)	0.116 (1.365)	0.140 (2.252)	0.198 (2.116)
R_{meas}[c]	0.062(0.314)	0.042 (1.510)	0.100 (0.532)	0.146 (1.893)	0.158 (2.536)	0.204 (2.177)
CC(1/2)	0.999(0.983)	1.000 (0.467)	0.998 (0.897)	0.995 (0.303)	0.999 (0.772)	0.999 (0.426)
Multiplicity	13.0 (12.9)	4.2 (3.2)	6.1 (4.1)	6.2 (3.7)	8.4 (8.0)	17.9 (18.1)
I/sig(I)	30.3 (8.1)	17.5 (0.8)	13.4 (2.8)	9.3 (0.9)	11.8 (0.5)	14.6 (1.6)
B_{Wilson} (Å^2)	57.3	58.0	18.74	36.7	22.97	42.3
R_{work}[e]/R_{free}[f]		23.0/26.4	23.2/25.6	22.5/28.2	31.8/33.8	20.1/23.9
r.m.s.d. bonds (Å)		0.003	0.004	0.011	0.0084	0.007
r.m.s.d. angles (°)		0.6	1.24	1.612	1.417	0.811

[a] Values in parentheses are for the highest resolution shell.

[b] $$R_{merge} = \frac{\sum_{hkl}\sum_{i=1}^{N}\left|I_{i(hkl)} - \bar{I}_{(hkl)}\right|}{\sum_{hkl}\sum_{i=1}^{N} I_{i(hkl)}}$$

[c] $$R_{meas} = \frac{\sum_{hkl}\sqrt{N/(N-1)}\sum_{i=1}^{N}\left|I_{i(hkl)} - \bar{I}_{(hkl)}\right|}{\sum_{hkl}\sum_{i=1}^{N} I_{i(hkl)}}$$

where $\bar{I}_{(hkl)}$ is the mean intensity of multiple $I_{i(hkl)}$ observations of the symmetry-related reflections, N is the redundancy

[e] $$R_{work} = \frac{\sum\left||F_{obs}| - |F_{calc}|\right|}{\sum|F_{obs}|}$$

[f] R_{free} is the cross-validation R_{factor} computed for the test set of reflections (5%) which are omitted in the refinement process.

Intermolecular cross-links in TbMORN1

chemical cross-linking agent	cross-linked amino acids and respective MORN repeats	best e-value	number of PSMs in the dimer
BS^3 (spacer arm length 11.4 Å)	aa 100 x aa 123 (repeat 5 x repeat 6)	7.5×10^{-13}	4
	aa 223 x aa 246 (repeat 10 x repeat 11)	5.7×10^{-22}	7
	aa 296 x aa 321 (repeat 13 x repeat 14)	1.8×10^{-11}	56
	aa 321 x aa 321 (repeat 14 x repeat 14)	6.4×10^{-5}	1
EDC (spacer arm length 0 Å)	aa 308 x aa 321 (repeat 14 x repeat 14)	1.1×10^{-8}	5
	aa 321 x aa 326 (repeat 14 x repeat 15)	1.9×10^{-9}	3

Table S1. Intermolecular contacts in TbMORN1. A summary of intermolecular cross-links in the TbMORN1 dimer as a result of chemical cross-linking with either BS^3 or EDC followed by mass spectrometry analysis. To remove low quality peptide-spectrum matches (PSMs), an additional e-Value cutoff of < 0.001 was applied. In order to distinguish intra- from inter-molecular chemical cross-links, results from monomers and dimers were compared. Cross-links were scored as intermolecular when there were: (1) minimally 3 peptide PSMs in dimer and (2) minimally 3-times more PSMs in dimer than in monomer. Results compiled from two independent experiments.

TbMORN1 construct	Thermostability T_m (°C) (DSF)
2-15	44.2 ± 0.3
$2\text{-}15^{Mut13}$	43.8 ± 0.3
$2\text{-}15^{Mut14}$	41.4 ± 0.5
$2\text{-}15^{Mut13+14}$	41.7 ± 0.3

Table S2: Analysis of TbMORN1(2-15) mutagenesis constructs.
Thermostability of TbMORN1(2-15) and its mutagenised derivatives with mutations in MORN repeats 13 and 14 was measured by differential scanning fluorimetry (DSF), given here as melting temperature (T_m) values (°C).

Data collection parameters				
Radiation source	Petra III (DESY, Hamburg, Germany)			ESRF (Grenoble, France)
Beamline	EMBL P12			BM29
Detector	Pilatus 2M			Pilatus 1M
Beam geometry (mm, FWHM)	0.12 x 0.20			0.10 x 0.20
Wavelength (nm)	0.12			0.099
Sample-detector distance (m)	3.1			2.867
Momentum transfer *s* range (nm^{-1})	0.01 – 4.0			0.04 – 5.0
Exposure time (s)	1 sec (SEC-SAXS mode) 0.05 sec (Batch mode)			1 sec (SEC-SAXS mode)
Overall Parameters				
	TbMORN1 (7-15)	**TgMORN1 (7-15)**	**PfMORN1 (7-15)**	**TbMORN1 (2-15)**
Buffer	Buffer 1*	Buffer 2**	Buffer 2**	Buffer 2**
Temperature (°C)	20	20	10	20
Working concentration (mg/ml) Concentration range measured	n.a.	n.a.	1 1-8	n.a.
R_g from Guinier approximation (nm)	4.1±0.04	4.0±0.03	3.8±0.1	6.5±0.6
R_g from PDDF (nm)	4.4±0.02	4.3±0.04	4.2±0.03	7.2±0.05
D_{max} (nm)	155	17.0	16.0	260
Molecular weight, I(0) (kDa)	n.a.	n.a.	52 ±5	n.a.
Molecular weight, offline RALS (kDa)	46±5	50±5	32±5	74±5
Molecular weight from DATMOV, (kDa)	60±5	58±5	46±5	71±5
Molecular weight from sequence (dimer, kDa)	52	49	46	70
Software employed				
Primary data reduction	SASFLOW			ESRF EDNA pipeline
Data processing	PRIMUS/Chromixs			
Calculation of theoretical data	Crysol			
Ab initio modelling	DAMMIN		DAMMIF	
SASBDB accession code	SASDGA7	SASDGB7	SASDGC7	SASDG97

Buffer 1* 20 mM Tris, 200 mM NaCl, 2% glycerol, 0.5 mM DTT
Buffer 2** 20 mM Tris-HCl pH 7.5, 100 mM NaCl

Table S3. SAXS data collection summary.